2009

Reachability and model prediction based system protection schemes for power systems

Licheng Jin
Iowa State University

Reachability and model prediction based system protection schemes for power systems

by

Licheng Jin

A dissertation submitted to the graduate faculty

in partial fulfillment of the requirements for the degree of

DOCTOR OF PHILOSOPHY

Major: Electrical Engineering

Program of Study Committee:
Ratnesh Kumar, Major Professor
Nicola Elia
Chen-Ching Liu
Venkataramana Ajjarapu
Ron M. Nelson

Iowa State University

Ames, Iowa

2009

DEDICATION

To my parents Miaoyuan Jin and Lanyin Chen

TABLE OF CONTENTS

LIST OF TABLES

LIST OF FIGURES

ABSTRACT

Interconnected power systems have been disrupted by unforeseen disturbances from time to time when millions of consumers lose power supply at a very expensive cost. System protection and emergency control to counteract power system instability play an important role in power system operation. Motivated by the industry need to mitigate the effect of disturbances on system operation and improve power system security, this dissertation develops a general framework for system protection scheme based on reachability analysis and Model Predictive Control.

A systematic framework to determine switching control strategies is proposed to stabilize the system following a disturbance based on reachability analysis. The computation of the stability region of a stable equilibrium point with the purpose of power system stability analysis is proposed and the validity of discrete controls in transient stability design is studied.

Model Predictive Control (MPC) is also adopted to design system protection scheme. A control strategy for maintaining voltage stability following the occurrence of a contingency is presented. Based on economic consideration and control effectiveness, a control switching strategy consisting of a sequence and amounts of shunt capacitors to switch is identified for voltage restoration. The effect of the capacitive control on voltage recovery is measured via trajectory sensitivity. In addition, voltage stability margin is an indication of how far the post-transient operating point is from the voltage collapse point. It is an index of system security. A control scheme to restore voltage following a contingency and to maintain a pre-specified amount of post-transient voltage stability margin is proposed. Moreover, dissimilar controls exist in power system for voltage control. A mixed integer programming based algorithm is presented to study the optimal coordination of the dissimilar controls to improve voltage

performance following large disturbances. The developed algorithms are implemented with MATLAB and tested on the WECC system to enhance the performance of voltage and the 39 bus New England system for preventing voltage collapse.

CHAPTER 1. Overview

1.1 Background

Electricity holds a unique place in the world's infrastructure. It is a commodity, a technology and a necessity (26). The electric power industry started with Edison Electric Illuminating Company and operated from 1882. Since then, the power industry has been evolving from none compatible, isolated multiple electric power companies, to interconnected bulk power systems (41). This evolution is motivated by the pursuit of cheap and reliable electric power supply. The recent major change of power industry from its vertically integrated monopolistic structure to a deregulated competitive electric market structure was stimulated with the issuance of the landmark orders 888 and 889 in 1996 by the US Federal Energy Regulatory Commission (FERC). The major consequence of the restructuring is the emergence of independent entities for generation, transmission, and distribution. A market structure for trading electrical energy has been developed based on the criteria of efficiency and reliability. According to the North American Electric Reliability Corporation (NERC), reliability has two aspects - adequacy and security. Security is the ability of the electric systems to withstand sudden disturbances such as electric short circuits or unanticipated loss of system elements. Therefore, to be reliable, the power system must be secure at most of time.

1.1.1 Power system operating states

Based on the security level of a power system, its operating states are classified into normal state, alert state, emergency state, in extremis state and restorative state (65) as shown in Figure 1.1. This definition helps operators to design appropriate control actions for different operating conditions.

- **Normal state**. In normal state, the power balance between generation and load is satisfied and no equipment is overloaded. All the voltages are within limits. In addition, the system has sufficient security margin to withstand any of the credible contingencies.

- **Alert state**. Under this state, the power balance between generation and load is still met. No equipment is overloaded. No voltage is out of its limits. However, when a severe contingency occurs, the system will either have overloaded equipments or have voltage violations.

- **Emergency state**. The power balance between generation and load is still satisfied. However, either overload or voltage violation happens in emergency state. If suitable corrective control actions are taken, the state can still be restored to normal state or at least alert state.

- **In extremis state**. Under this state, the power balance between generation and load is lost. Voltage violation may happen and some equipments are overloaded. There are cascading outages. Load shedding may be taken to save as much of the system as possible.

- **Restorative state**. Under this state, the operator performs control actions to restore all system load. Depending on different cases, the system can reach either normal or alert state.

1.1.2 Security assessment

The operation of a power system requires nearly strict synchronism of the rotational speed of many thousands of large interconnected generating units. Such operation requires not just the functioning of machine governors, but also all equipments operating within physical capabilities regardless of changes in customer demands or sudden disconnection of equipments from the system. Also due to economic consideration, a power system is operated close to its design limits, with smaller security margin and greater exposure to unsatisfactory conditions following disturbances. Security assessment plays an important role in system operation. It

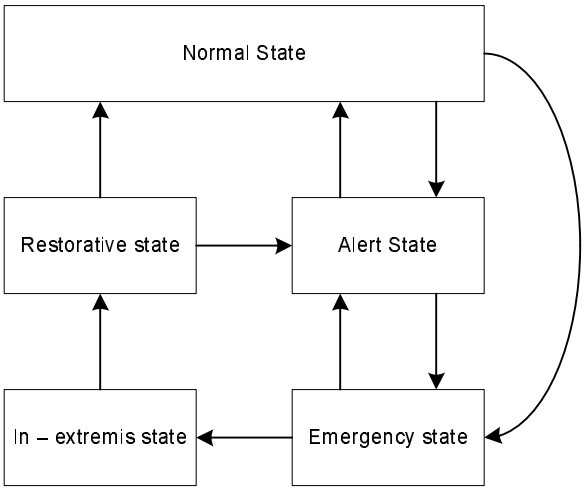

Figure 1.1 Power system operating state transition maps

involves the evaluation of available data to estimate the relative security level of present state or some near future state. According to (32), there are three levels of security assessment:

- Security monitoring. Using measurements provided by the supervisory control and data acquisition system (SCADA) and state estimation, identify whether the system is in normal state or not.
- Security analysis. Security analysis is used to check the system's ability to withstand disturbances. If the system is in the normal state, contingency analysis is used to test the security of the system. If one or more operation constraints is violated in the contingency analysis, the system is insecure. Otherwise, it is secure.
- Security margin determination. For a given operating condition, the determination of a security margin using some selected variables is used to assess the security level of a system. These margins are particularly needed in market environment. In this case, operators know how much load increase can be acceptable before the system becomes insecure.

Security assessment methods can be classified into two categories based on the different analysis methods: static security assessment (SSA) and dynamic security assessment (DSA).

- Static security assessment (SSA). Static security can be seen as the ability of a power system, after a disturbance, to reach steady-state operating conditions without violating system constraints, which include limits on bus voltages and the thermal bounds of the line (28). This analysis is usually based on power flow analysis. If operating conditions are not satisfactory with system constraints violation, preventive control or corrective control needs to be proposed to realize the following operation conditions:

  1.) No transmission line or other electric devices is overloaded.

  2.) Bus voltages should be within their limits. Usually 5% deviation from the normal value is allowed.

- Dynamic security assessment (DSA). Dynamic security analysis evaluates the power system's ability to withstand a set of severe but credible contingencies and to survive transition to an acceptable steady-state condition (86). This involves the dynamic performance of generator models, dynamic load models, etc. A number of approaches to study dynamic stability have been developed, such as time domain simulation (66), direct method of transient stability analysis (4; 19). Besides dynamic security assessment study, different control strategies have also been proposed to improve the dynamic performances of power systems through load shedding actions, load tap changer actions, reactive power compensators and generator reference voltage settings.

1.1.3 Stability analysis

In dynamic security assessment, power system stability analysis plays an important role. According to (61), power system stability is the ability of an electric power system, given initial operating condition, to regain a state of operating equilibrium after being subjected to a physical disturbance, with most system variables bounded so that practically the entire system remains intact. The power system is a highly nonlinear system and its stability is essentially a single problem. However, analysis of stability as well as devising methods to improve system operation performance can be greatly facilitated by classification of stability into appropriate categories.

The classification of power system stability is based on the following considerations (60):

- The physical nature of the resulting mode of instability: rotor angle stability, frequency stability and voltage stability.
- The size of the disturbance: small disturbance stability and large disturbance stability.
- The time span: short-term stability and long term stability.

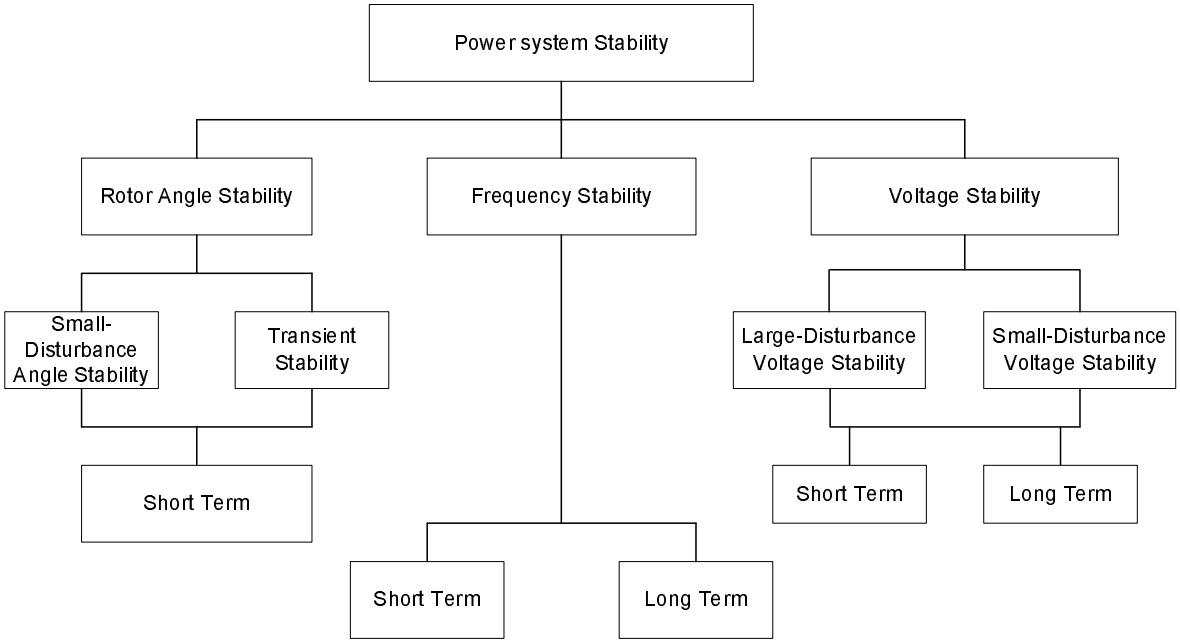

Figure 1.2 Classification of power system stability

Figure 1.2 shows the classification of power system stability (61).

- Rotor angle stability refers to the ability of synchronous machines to remain synchronism after a disturbance. The time frame of rotor angle stability analysis is from several seconds to 20 seconds.
  - Small-disturbance rotor angle stability is the ability of a power system to remain synchronism under small disturbances. In today's power system, small-distance rotor angle stability results from the insufficient damping of oscillations. The anal-

ysis is based on the linearization of the nonlinear system equations at the steady operation point (60; 21; 50).

- Large-disturbance rotor angle stability is the ability of the power system to remain synchronism when subject to a severe disturbance. Under a large disturbance, linearization of the system equation is not appropriate. The stability depends on the initial operating state of the system as well as the severity of the disturbance. The most common way to analyze system performance with a given initial point is time domain simulation, where a set of differential algebraic equations (DAEs) is solved.

- Voltage stability refers to the ability of a power system to maintain steady voltages at all buses after a disturbance with a given initial operating condition.

  - Large-disturbance voltage stability is the ability that a power system maintains steady voltages following large disturbances such as system faults, loss of transmission lines. The study of large-disturbance voltage stability is based on the nonlinear equations of generator models, load models, under load tap changer models, etc.

  - Small-disturbance voltage stability is the ability that a power system maintains steady voltages following small disturbances such as the fluctuation of loads. Under some assumptions, small-disturbance voltage stability can be analyzed by linearization of the nonlinear system equations. However, some nonlinear effect such as dead bands of tap changer controls can not be taken into consideration. A combination of linear and nonlinear analyzes is used in voltage stability analysis (77; 35).

  - Short-term voltage stability involves dynamics of induction motors. The time span for this analysis is several seconds.

  - Long-term voltage stability involves models such as under load tap changer, generator current limiters. The time span for the study ranges from several to many minutes (27; 77; 43).

- Frequency stability refers to the ability of a power system to maintain steady frequency after a severe system disturbance with a significant imbalance between generation and load. The period of time of interest for frequency ranges from fraction of seconds to several minutes. For a short-term phenomenon (22), the devices used for analysis are under frequency load shedding and generator controls and protections. The time span is fraction of seconds. For a long-term frequency stability (20; 59), the devices involve automatic generator regulators (AGC). The time span ranges from tens of seconds to several minutes.

1.2 Motivation

1.2.1 Traditional system protection scheme

A system protection scheme (SPS) is designed to detect abnormal system conditions and take predetermined, corrective action (other than the isolation of faulted elements) to preserve system integrity and provide acceptable system performance (53). System protection schemes came up as a trade off between investments, operation cost and customer service quality. They are attractive mechanisms to improve system performance (stability, safety and security) due to their low economic costs and environmental friendliness when compared to the alternatives such as building new power plants and transmission lines. Doudna et. al. (29) presented the design of a remedial action in Nebraska Public Power District which is a good example of SPS. Gerald Gentleman substation was built to supply around 1200 MW power to the system by two 230 kV transmission lines and one 345 kV line. Study indicated that any of the three lines was out of service, the system was subject to instability and post-disturbance overloads. It was not economical to construct a new transmission line to mitigate this situation. Therefore, the design and implementation of a fast valving and generator tripping schemes was carried out to relieve the instability and overload system condition. Traditional system protection scheme is designed in off-line planning studies. It is implemented automatically when it is triggered by some specific system operation condition. It consists of three main parts:

- Inputs (transmission line overload, status of circuits breakers, etc)

- A decision-making system that initiates certain actions based on the inputs
- Actions (such as generator or load tripping, capacitor switching, etc)

According to input variables, SPS can be subdivided into two categories: response-based SPS and event-based SPS. Response-based SPS uses power system operation condition (voltages, frequencies, etc) to initiate control actions after the disturbance has caused the input variables significantly degraded. Undervoltage load shedding and under frequency load shedding are two examples of this type of SPS. Event-based SPS is designed to trigger control actions by the direct detection of a particular combination of events. This type of SPS is rule-based. Rules are developed from off-line simulation. Examples of event-based SPS are load shedding or generator rejection by the tripping of a transmission line. Currently, these off-line designed system protection schemes are widely used in power industries all over the world. An overview of existing SPS in power industry is presented in (53). Table 1.1 is a summary of the SPSs introduced in (53).

Country	SPS examples
Australia	under frequency load shedding, controlled opening of interconnection, contingency arming scheme
Brazil	reginal load shedding, generator tripping, concentrated load-shedding
Canada	Under frequency load shedding system, generation rejection and remote load shedding, 735 kV shunt reactors automatic switching system
France	out of step relays against losses of synchronism, generation rejection, on-load tap changers blocking, under frequency load shedding
Ireland	Under frequency load shedding, automatic frequency restoration
Italy	Automatic load/unit disconnection system
Scandinavia	automatic grid separation within Nordel
Sweden	Generation disconnection system, SPS against voltage collapse in South part of Sweden
Thailand	Generator shedding, udner voltage load shedding, under frequency load shedding

Table 1.1 An overview of existing SPS

1.2.2 Real time system protection scheme

System protection schemes to cope with load fluctuations and disturbances caused by faults are a vital part of a power system. Contrast to the predetermined traditional SPS, the objective of a real time SPS is to carry out the control actions to mitigate the effects of potential instability or a safety/security degradation of a power system (such as a partial shutdown or a total collapse) detected by an online dynamic security assessment program. Based on measurements received at control centers through high-speed communication channels and a system model, real time SPSs compute the necessary control decisions such as generator trippings, capacitor/reactor bank switchings, transformer tap adjustments, and load-shedding for insecure contingencies. Recent advances in dynamic security assessment, monitoring, communication, and computing technologies have greatly facilitated the implementation of real time SPSs.

The functional structure of a real time SPS is shown in Figure 1.3. Line flow measurements, bus voltage information, switch status measured by phase measurement units (PMUs) and collected by Phasor Data Concentrators (PDCs) are sent to a control center through communication channels. These measurements plus a network model are used by the state estimator (SE) for filtering out the noise and estimating the auxiliary (also known as static state) variables. The results from the state estimator are used for power flow analysis. A power flow solution is then used by an on-line dynamic security assessment program to initialize the state variables of the dynamic models. Further, it uses system models and disturbance information to perform the contingency analysis to evaluate the security margin of the power system. If a contingency is identified where the system will become unstable, a real time system protection scheme should be designed to mitigate and relieve this situation.

Traditionally *static analysis* based approaches have been employed for security against large disturbances (faults and loadings). For example several prior work such as (100; 12; 37; 69; 70), has studied the problem of determining locations and amounts of reactive power compensation devices to maintain voltage stability while minimizing the cost. The above work, however, is based on *static analysis*. It is assumed that a post-contingency stable equilibrium point can be reached. However, if disturbances are severe, a power system may not reach a post-contingency

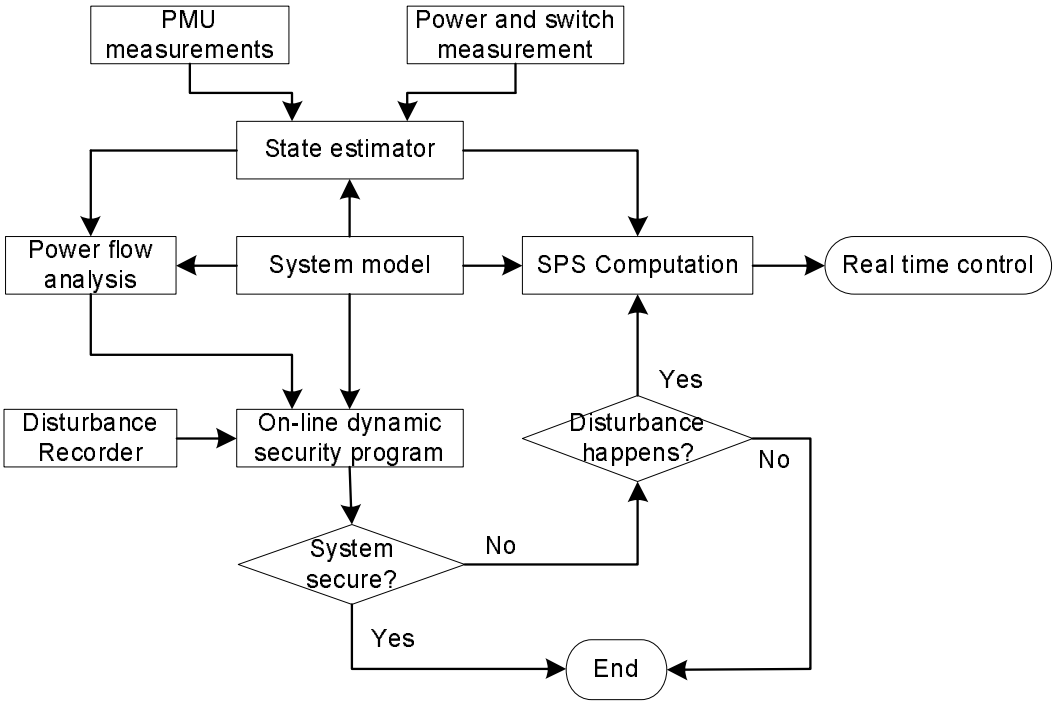

Figure 1.3 Structure of a real time system protection scheme

stable equilibrium point since the post-contingency trajectory may deviate out of the stability region. In this case, *dynamic analysis* is needed to ensure stable post-contingency trajectories.

1.3 Dissertation organization

The rest of the dissertation is organized as follows.

Chapter 2 is a brief introduction of mathematical representation of power system models used in this dissertation.

Chapter 3 provides reachability analysis based system protection scheme design. A novel method to compute the stability region of a stable equilibrium point with the purpose of power system stability analysis is proposed and the validity of discrete controls in transient stability design is studied.

Chapter 4 presents Model Predictive Control (MPC) based system protection scheme design. A control strategy for maintaining voltage stability following the occurrence of a contingency is presented. Based on economic consideration and control effectiveness, a control switching strategy consisting of a sequence and amounts of shunt capacitors to switch is identified for voltage restoration. The effect of the capacitive control on voltage recovery is measured via trajectory sensitivity. In addition, voltage stability margin is an indication of how far the post-transient operating point is from the voltage collapse point. It is an index of system security. A control scheme to restore voltage following a contingency and to maintain a pre-specified amount of post-transient voltage stability margin is proposed. Moreover, dissimilar controls exist in power system for voltage control. A mixed integer programming based algorithm is presented to study the optimal coordination of the dissimilar controls to improve voltage performance following large disturbances. The developed algorithms are implemented with MATLAB and tested on the WECC system to enhance the performance of voltage and the 39 bus New England system for preventing voltage collapse.

Chapter 5 mainly introduces the software realization of the MPC based control design.

The conclusion is given in Chapter 6.

CHAPTER 2. Power System Models

2.1 Power system network model

The purpose of a power system is to deliver the power required by customers in real time with an acceptable quality. Power flow is used to analyze the steady state power system operation condition (6). The analysis is based on real and reactive power balance at each bus of a power grid. At bus i, the network model is described as follows:

$$0 = P_{Gi} - P_{Li} - P_{Ni} \tag{2.1}$$

$$0 = Q_{Gi} - Q_{Li} - Q_{Ni} \tag{2.2}$$

where

P_{Gi}: real power generation injection at bus i

Q_{Gi}: reactive power generation injection at bus i

P_{Li}: real power load consumption at bus i

Q_{Li}: reactive power load consumption at bus i

P_{Ni}: net real power injection at bus i

Q_{Ni}: net reactive power injection at bus i

The output of real and reactive power of a generator is determined by the characteristics of the unit. The real and reactive power consumptions of a load are determined by the load characteristics. The net real and reactive power injections are constrained by the physical

characteristics of a power grid, which are represented as:

$$P_{Ni} = \sum_{k=1}^{n} V_i V_k (G_{ik} \cos\theta_{ik} + B_{ik} \sin\theta_{ik}) \tag{2.3}$$

$$Q_{Ni} = \sum_{k=1}^{n} V_i V_k (G_{ik} \sin\theta_{ik} - B_{ik} \cos\theta_{ik}) \tag{2.4}$$

where

V_i: voltage magnitude of bus i

V_k: voltage magnitude of bus k which is connected with bus i

G_{ik}: conductance of the line from bus i to bus k

B_{ik}: susceptance of the line from bus i to bus k

θ_{ik}: voltage phase angular difference between bus i and bus k

Operational considerations indicate that the active power P_{Gi} and the voltage magnitude V_i of a generator bus may be specified. For a load at bus i, the P_{Li} and Q_{Li} are also known. The power grid parameters G_{ik}, B_{ik} can be obtained by the network model. Therefore, power flow basically solves the nonlinear equation (2.3), (2.4) to obtain the steady states such as unknown bus voltage magnitude and phase angles of the power grid.

2.2 Synchronous generator model

The complete mathematical description of synchronous generators is too complicated to be used for system analysis and control design. Different degrees of approximations are used to simplify the generator model. In this dissertation, two kinds of generator models are used. One is the classical model (Chapter 3), the other is the two-axis model (Chapter 4).

2.2.1 Classical Model

The classical model is the simplest model for generators (6). Following assumptions are adopted:

- Mechanical power input is constant
- q-axis transient voltage is constant

The differential equations for the classical model for generator i are as follows:

$$\dot{\delta}_i = \omega_i - \omega_s \tag{2.5}$$

$$M_i\dot{\omega}_i = P_{mi} - P_{ei} - D_i(\omega_i - \omega_s) \tag{2.6}$$

where,

$$P_{ei} = \sum_{j=1}^{n}[E_iE_jB_{ij}\sin(\delta_i - \delta_j) + E_iE_jG_{ij}\cos(\delta_i - \delta_j)]$$

and

δ_i: electrical rotor angle of generator i

ω_i: rotor speed of generator i with respect to the synchronous frame

ω_s: synchronous speed

M_i: inertial constant of generator i

P_{mi}: mechanical power input of generator i

P_{ei}: electrical power output of generator i which is determined by interface equations between the generator i and power system network.

D_i: damping coefficient

2.2.2 Two-axis model

The two-axis generator model accounts for the transient effects (80). The mathematical formulation of generator i with this model is given by

$$\dot{\delta}_i = \omega_i - \omega_s \tag{2.7}$$

$$M_i\dot{\omega}_i = P_{mi} - (I_{di}E'_{di} + I_{qi}E'_{qi}) + (x'_{qi} - x'_{di})I_{qi}I_{di} - D_i(\omega_i - \omega_s) \tag{2.8}$$

$$T'_{d0i}\dot{E}'_{qi} = E_{fdi} - E'_{qi} - (x_{di} - x'_{di})I_{di} \tag{2.9}$$

$$T'_{q0i}\dot{E}'_{di} = -E'_{di} - (x_{qi} - x'_{qi})I_{qi} \tag{2.10}$$

where,

E'_d: direct axes (d axes) stator EMF corresponding to rotor transient flux components

$E_{qi'}$: quadrature axes (q axes) stator EMF corresponding to rotor transient flux components

I_d: the d axes stator current

I_q: the q axes stator current

T'_{d0}: open-circuit d axes transient time constant

T'_{q0}: open-circuit q axes transient time constant

x_d, x'_d: d axes synchronous and transient reactance

x_q, x'_q: q axes synchronous and transient reactance

E_{fd}: stator EMF corresponding to the field voltage

Interfaces of voltage equations to the power network are given by:

$$E'_{qi} = v_i \cos(\delta_i - \theta_i) + r_{ai} I_{qi} + x'_{di} I_{di} \tag{2.11}$$

$$E'_{di} = v_i \sin(\delta_i - \theta_i) + r_{ai} I_{di} + x'_{qi} I_{qi} \tag{2.12}$$

where v and θ are bus voltage and angle, r_a is the machine armature resistance.

2.3 Excitation system model

Different types of excitation system models used in power system are presented in (49). In this dissertation, we use the simplified IEEE type DC-1 excitation system as shown in Figure 2.1. The model is described by the following equations:

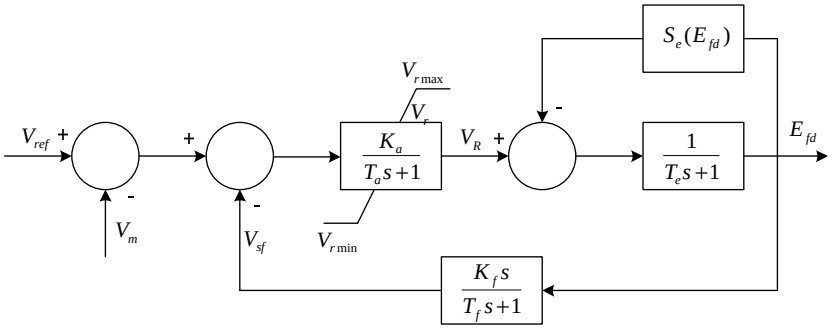

Figure 2.1 IEEE type DC-1 excitation system

$$T_a \dot{V}_r = (K_a(V_{ref} - V_m - V_{sf} - \frac{K_f}{T_f} E_{fd}) - V_r \tag{2.13}$$

$$T_f \dot{V}_{sf} = -(\frac{K_f}{T_f} E_{fd} + V_{sf}) \tag{2.14}$$

$$T_e \dot{E}_{fd} = -(E_{fd}(1 + S_e(E_{fd})) - V_R) \tag{2.15}$$

with

$$V_R = \begin{cases} V_r & \text{if } V_{rmin} \leq V_r \leq V_{rmax}, \\ V_{rmin} & \text{if } V_r < V_{rmin}, \\ V_{rmax} & \text{if } V_r > V_{rmax}. \end{cases}$$

where

V_m: the voltage measurement value of the bus regulated by the generator

V_{ref}: the reference voltage of the automatic voltage regulator (AVR)

V_{sf}: the output of exciter soft feedback

K_f: the gain of the exciter soft feedback

T_f: the time constant of the exciter soft feedback

K_a: the amplifier gain

T_a: the amplifier time constant

V_r: the non-windup output of AVR

V_R: the windup output of AVR

T_e: time constant of the exciter

S_e: exciter saturation function which is a function of exciter output voltage E_{fd}

2.4 Load model

Load dynamics has a significant effect on voltage performance following contingencies. A widely used dynamic load model, namely, exponential recovery load model, is presented in (52) and (42). This model captures the physically observed behavior at high voltage buses. Moreover, it has been verified in several field tests for a wide range of operating conditions. In dynamic analysis, the active power consumption, denoted by P, is composed of two parts: the active power recovery P_r and the transient real power absorption P_t. The load model is expressed as follows:

$$T_P \dot{P}_r = -P_r + P_s - P_t \tag{2.16}$$

$$P = P_r + P_t \tag{2.17}$$

Here, P_s and P_t are the static and transient real power absorptions, which depend on the load voltage:

$$P_s = P_0(V/V_0)^{\alpha_s} \tag{2.18}$$

$$P_t = P_0(V/V_0)^{\alpha_t} \tag{2.19}$$

T_P is the time taken for real power recovery to some specific value, which is also known as real power time constant.

Similar equations hold for the reactive power. Following a contingency, the reactive power consumption, denoted by Q, is composed of two parts: the reactive power recovery Q_r and the transient reactive power absorption Q_t.

$$T_Q\dot{Q}_r = -Q_r + Q_s - Q_t \tag{2.20}$$

$$Q = Q_r + Q_t \tag{2.21}$$

Here, Q_s and Q_t are the static and transient reactive power absorptions, which depend on the load voltage:

$$Q_s = Q_0(V/V_0)^{\beta_s} \tag{2.22}$$

$$Q_t = Q_0(V/V_0)^{\beta_t} \tag{2.23}$$

T_Q is the time taken for reactive power recovery to some specific value, which is also called reactive power time constant.

2.5 Under load tap changer

An under load tap changer (ULTC) transformer can be used to regulate a bus voltage. A continuous model is shown in Figure 2.2. The mathematical representation of this continuous version of ULTC is represented by

$$\dot{m} = -Hm + K(V_{reg} - V_{ref}) \tag{2.24}$$

where

m: Tap ratio of ULTC transformer bank

H: Integral deviation

K: Inverse time constant

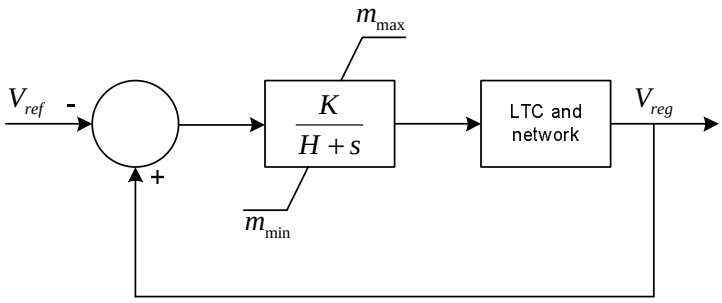

Figure 2.2 Under load tap changer: voltage control

A discrete model of a ULTC is described as follows:

$$m_{k+1} = m_k + \Delta m R \tag{2.25}$$

where

$$R = \begin{cases} 1 & \text{if } u - u_{ref} > \Delta u, \\ -1 & \text{if} u - u_{ref} < -\Delta u, \\ 0 & \text{if} \|u - u_{ref}\| \leq \Delta u \end{cases}$$

u: the voltage of the regulated bus

u_{ref}: the reference voltage value of the regulated bus

Δu: the error tolerance

2.6 Power system DAE model

Through the above discussions, a complete power system model includes both dynamic model and static model. They are described by both differential equations and algebraic equations. Therefore, power system model can be represented by a set Differential Algebraic Equations (DAE).

$$\dot{x} = f(x, y) \tag{2.26}$$

$$0 = g(x, y) \tag{2.27}$$

The differential variables x represent the dynamic states associated with generators, excitation systems, and dynamic loads. The algebraic equation g represents the network power balance of power systems. The algebraic states y include bus voltages magnitudes and bus phase angles.

In power system study, there also exists control variables and parameters. Therefore, Equation (2.26) and Equation (2.27) can also be written as Equation (2.28) and (2.29) to incorporate those variables. Vector u includes the control variables and parameters variable which may be used to control power system performance. In this dissertation, the under load tap changer is treated as a discrete control which has the characteristics described in section 2.5.

$$\dot{x} = f(x, y, u) \tag{2.28}$$

$$\dot{0} = g(x, y, u) \tag{2.29}$$

CHAPTER 3. An Application of Reachable Set Analysis in Power System Stability Assessment

3.1 Introduction

Power system transient stability (61) is related to the ability to maintain synchronism when subjected to a severe disturbance, such as a short circuit on a bus. The resulting system response involves large excursions of generator rotor angles and is governed by the nonlinear power-angle relationships. Transient stability assessment essentially determines whether or not the post-fault operating state can reach an acceptable steady-state operating point. The conventional method to determine transient stability is to integrate the system equations to obtain a time domain solution of the system variables, given system operating points and contingencies. An alternative method is to determine stability directly (83): The stability of a post-fault power system can be determined by checking the fault-on trajectory at clearing time. If it lies inside the stability region of a desired stable equilibrium point of the post-fault system, the system is stable.

The stability region is defined as a set of all points starting from which the trajectories eventually converge to the stable equilibrium point (SEP) of a general nonlinear autonomous system as time approaches infinity (54). In the last three decades numerous efforts have been undertaken to determine the stability region with the goal of power system transient stability analysis.

The studies of (94; 101; 17) provided the theoretical foundations for the geometric structure of the stability region. The authors in (17) proved that under certain conditions the stability boundary of a SEP is the union of the stable manifolds of the type one unstable equilibrium points and proposed a numerical algorithm to determine the stability region. Energy function

method has also been applied in transient stability assessment. (4) derived the energy function for machines based on a center of inertia frame of reference. A procedure for first swing transient stability assessment have been developed using the energy function of individual machines and groups of machines. Several techniques were proposed to determine the critical energy related to system's stability region. One is called the closest unstable equilibrium point (UEP) method (18). This corresponds to the smallest energy among all the UEPs. The controlling unstable equilibrium point method (15; 14) was carried out to provide a less conservative estimation of stability region. This corresponds to the energy at the UEP that is closest to the post-fault trajectory. PEBS (Potential Energy Boundary Surface) was also proposed to approximate the stability region. The energy at the crossing point of the post fault trajectory and the PEBS was the critical energy. (19) provided theoretical analysis of this approach.

Recently, some algorithms have been developed to approximate the stable manifold of an UEP. For example, in (95; 13) the Taylor expansion is used to get a quadratic approximation. In (88; 84), the stable manifolds around an UEP are approximated by the normal form technique. In (51), the authors apply the singular perturbation theory to decompose a particular power system into slow and fast subsystems based on the assumption that a power system can be perfectly separated in time-scale. Then the stability region of a SEP is obtained by numerical simulations.

Also controls are very commonly used to improve the transient stability and damping of a power system. The control of a power system can be continuous (generator exciter, governor control, etc) as well as discrete (line impedance control through series/shunt capacitors switch, tripping of generators/loads, etc.). Thus, power system control is hybrid, making a controlled power system a hybrid system. The application of hybrid systems based modeling and control techniques for power systems is a recent activity (44; 46; 38; 85; 33). The application of discrete switching control to stability of power networks has been reported in articles such as (39; 9; 7; 58; 11; 48; 57; 56). (67) provided a method to obtain voltage stability regions. (97) applied the stability region in studying the voltage collapse in power systems.

In this chapter, we propose a novel method to compute the stability region of a given power system with the purpose of assessing the transient stability. This method is then adopted to validate the effectiveness of discrete controls. This means, when the said control is switched on, following the clearance of a fault, we verify whether the system will reach a desired stable equilibrium point. We also suggest by which a sequence of discrete controls may be exercised to steer the system to a desired SEP.

This chapter is organized as following. Some fundamental concepts of reachable set analysis and the computation of a reachable set are introduced in section 3.2. In section 3.3 an algorithm to determine the stability region of a SEP is presented. In section 3.4 an algorithm is developed to determine the validity of an existing control in power system transient stability assessment. Section 3.5 presents an illustrative example . Section 3.6 provides discussions and the conclusion.

3.2 Reachable set and its computation

3.2.1 Reachable set

Reachable sets are a way of capturing the safety and stability properties of entire groups of trajectories at once. There are two basic types of reachable sets depending on whether an initial or a final condition is specified. The forward reachable set is defined as the set of all states that can be reached along trajectories that start in a specified initial set. On the other hand, the backward reachable set is the set of states starting from where trajectories can reach the specified target set. The forward and backward reachable sets are shown in Figure 3.1. In Section 3.3, we make use of backward reachable sets to compute the stability region of a stable equilibrium point of a nonlinear system. This is then used to validate a candidate discrete control.

A reachable set is a subset of state space. One way of describing a subset of states is via an implicit surface function representation. Consider a closed set $S \subseteq R^n$. An implicit surface representation of S would define a function ϕ: $R^n \rightarrow R$ such that $\phi(x) \leq 0$ if $x \in S$ and $\phi(x) > 0$ if $x \notin S$. On the boundary of S, it holds that $\phi(x) = 0$. For this reason, $\phi(x)$ is also

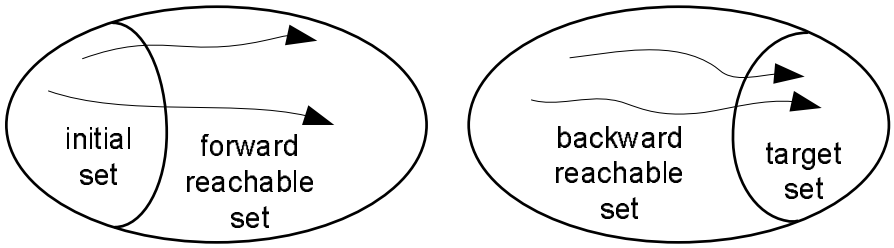

Figure 3.1 Illustration of forward and backward reachable sets

called surface function.

Consider an autonomous system described by an ordinary differential equation:

$$\frac{dx}{dt} = f(x), \tag{3.1}$$

where $x \in R^n$ is the state vector and $f(x)$ is the vector field.

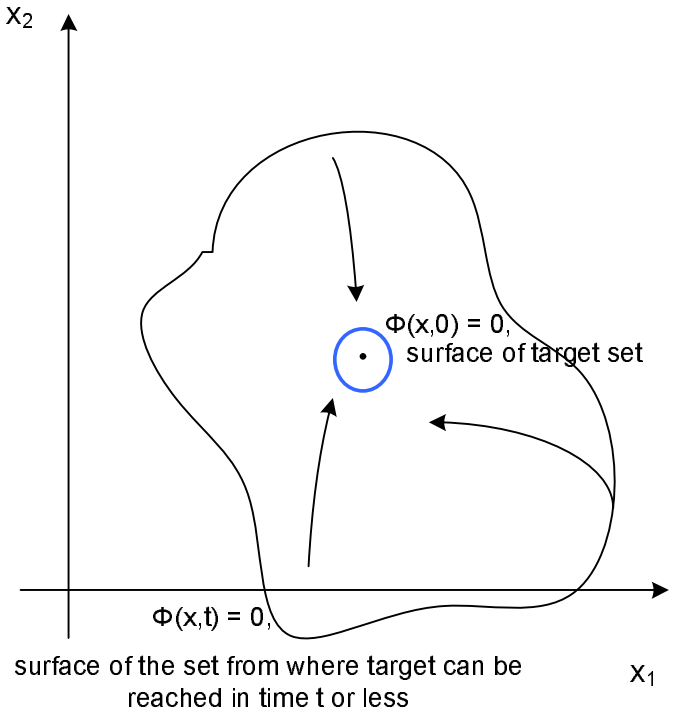

Figure 3.2 The representation of backward reachable sets

As shown in Figure 3.2, suppose $\phi(x,t)$ is the surface function representing the backward reachability set at time t starting from the level surface $\phi(x,0)$. $\phi(x,t) = 0$ is a moving surface

in $(n+1)$ dimensional space. It is the boundary of the set of all states $x \in R^n$ from where a target set can be reached in time t or less. The boundary of "target set" is represented by $\phi(x,0) = 0$. Note that if $\phi(x,0) \leq 0$ represents an ε neighborhood of an stable equilibrium point, then $\phi(x,\infty) \leq 0$ represents the region of stability of the equilibrium point. Consider the surface $\phi(x,t) = 0$ in the $(n+1)$ dimensional space. For every (x,t) on this surface, the ϕ value is zero.

3.2.2 The computation of a reachable set

Consider a small variation along this surface, i.e., moving (x,t) to a neighboring point $(x+dx, t+dt)$ on the surface, the variation in ϕ will be zero:

$$d\phi = \phi(x+dx, t+dt) - \phi(x,t) = 0 \ ,$$
$$d\phi = \frac{\partial\phi}{\partial x_1}dx_1 + ... + \frac{\partial\phi}{\partial x_n}dx_n + \frac{\partial\phi}{\partial t}dt \ .$$

From this it follows that,

$$\phi_x^T \frac{dx}{dt} + \phi_t = 0. \tag{3.2}$$

where $\phi_x = [\frac{\partial\phi}{\partial x_1}, ..., \frac{\partial\phi}{\partial x_n}]$, subscript T means transpose. Substituting (3.1) into (3.2), we can get

$$\phi_x^T f(x,t) + \phi_t = 0. \tag{3.3}$$

Thus we obtain the desired PDE and this PDE describes the propagation of the backward reachability set boundary as a function of time. The general Hamilton-Jocobi equations have the following formate:

$$\phi_t + H(\phi_x) = 0 \tag{3.4}$$

where H can be a function of both space and time. $\phi_x = [\frac{\partial\phi}{\partial x_1}, ..., \frac{\partial\phi}{\partial x_n}]$ is the gradient of the implicit function ϕ. Equation (3.4) defines the motion of the interface where $\phi(x,t) = 0$. Equation (3.3) is a special case of Equation (3.4). The viscosity solution $\phi(x,t)$ of the PDE is an implicit surface representation of the backward reachable set (76). A bounded, uniformly

continuous function $\phi(x,t)$ is a viscosity solution (31) to the Equation (3.4) if for any infinitely differentiable test function $\psi(x,t)$, the following conditions are satisfied:

- if $\phi(x_0,t_0)-\psi(x_0,t_0)$ is a local maximum of the function $\phi-\psi$, then

$$\psi_t(x_0,t_0)+H(\psi_x(x_0,t_0))\leq 0$$

- if $\phi(x_0,t_0)-\psi(x_0,t_0)$ is a local minimum of the function $\phi-\psi$, then

$$\psi_t(x_0,t_0)+H(\psi_x(x_0,t_0))\geq 0$$

This HJI PDE can be solved with the very accurate numerical methods drawn form the level set literature (78). Level set methods are a collection of numerical algorithms for computing the dynamics of moving curves and surfaces. For Equation (3.4), there are three terms that must be evaluated: the spacial derivative $\phi_x(x,t)$, the Hamiltonian $H(\phi_x(x,t))$ and the time derivative $\phi_t(x,t)$. The techniques for approximating each of these terms at each node can be separately decided using the values of ϕ at the node and its neighbors.

3.2.2.1 Spatial Derivative

Traditional finite difference approximations of order p for the spatial derivative of a function represented on a grid are based on the assumption that the function and at least its first $p-1$ derivatives are continuous. Convergent numerical approximations of ϕ_x were developed shortly after viscosity solutions were first proposed. A critical feature of all these schemes is their use of directional approximations. At a grid point x_i, a first-order accurate forward difference is defined as

$$\frac{\partial\phi}{\partial x}\approx\frac{\phi(x_{i+1},t)-\phi(x_i,t)}{x_{i+1}-x_i}$$

It is also denoted as a right approximation, with notation ϕ_x^+. A first-order accurate backward difference is defined as

$$\frac{\partial\phi}{\partial x}\approx\frac{\phi(x_i,t)-\phi(x_{i-1},t)}{x_i-x_{i-1}}$$

It is also called left approximation, denoted as ϕ_x^-. In order to get a more accurate approximation for ϕ_x^+ and ϕ_x^-, essentially nonoscillatory (ENO) polynomial interpolation of data is

introduced by Osher and Sethian (79) for the Hamilton-Jacobi equation. The basic idea is to extend first-order accurate differencing to higher-order spatial accuracy by making use of values from more than a grid point's immediate neighbors. Although several different approximations to the left and right are computed in ENO schemes, only the least oscillatory is chosen. (71) pointed out that the ENO philosophy of picking the least oscillatory approximation is overkill in smooth regions where data are well behaved. They proposed a weighted ENO (WENO) method that takes a convex combination of all the approximations in smooth regions of the solution to increase the order of accuracy. ENO and WENO discretize the spatial derivative terms in a higher accuracy than the first-order right and left approximation. Practical experience suggests that level set methods are sensitive to spatial accuracy. Therefore, WENO method is desirable in the implementation of level set methods.

3.2.2.2 Hamiltonian

One of the well studied numerical approximation of Hamiltonian $H(\phi_x)$ is Lax-Friedrichs (LF) scheme (25). Function $\hat{H}$ is called a numerical Hamiltonian under LF approximation if

$$\hat{H}(\phi_x^+, \phi_x^-) = H(\frac{\phi_x^+ + \phi_x^-}{2}) - \frac{1}{2}\alpha^T(\phi_x^+ - \phi_x^-)$$

where ϕ_x^+ and ϕ_x^- are the right and left approximations of ϕ_x respectively and $H(\phi_x)$ is in Equation 3.4. α^T is a vector of dissipation coefficients that control the amount of numerical viscosity to damp out spurious oscillations in the solution. The components of the vector α is defined based on the partial derivatives of H with respect to its parameter ϕ_x on the computational domain

$$\alpha_i = max|\frac{\partial H}{\partial \phi_x}| \tag{3.5}$$

The choice of the dissipation coefficient can be rather subtle. Too much dissipation will excessively smooth the approximate solution. However, too little dissipation will result in numerical instability. The amount defined in Equation 3.5 is sufficient to guarantee stability.

3.2.2.3 Time Derivative

Based on the computation of the spacial derivative ϕ_x and the numerical Hamiltonian $\hat{H}$, the value of ϕ becomes the solution of the ordinary differential equation (ODE)

$$\phi_t + \hat{H}(\phi_x^+, \phi_x^-) = 0$$

Total variation diminishing (TVD) Runge-Kutta (RK) methods are proposed in (90) to solve the ODE. Runge-Kutta integration is a clever extension of Euler integration that allows substantially improved accuracy, without imposing a severe computational burden. The idea is to step into the interval and evaluate derivatives. This is similar to shortening time step in Euler integration, but provides more accuracy with less increase in computation. The basic first-order accurate TVD RK scheme is just the forward Euler method. The second-order accurate TVD RK scheme is identical to the standard second-order accurate RK scheme. First, an Euler step is taken to advance the solution to time $t^n + \Delta t$,

$$\frac{\phi^{n+1} - \phi^n}{\Delta t} + \hat{H}^n = 0$$

A second Euler step is taken to advance the solution to time $t^n + 2\Delta t$.

$$\frac{\phi^{n+2} - \phi^{n+1}}{\Delta t} + \hat{H}^{n+1} = 0$$

Then the solution at time $t^n + \Delta$ is a convex combination of the initial data and the result of two Euler steps.

$$\phi^{n+1} = \frac{1}{2}\phi^n + \frac{1}{2}\phi^{n+2}$$

The third-order accurate TVD RK schme is made up of three Euler steps. First, an Euler step is taken to advance the solution to time $t^n + \Delta t$.

$$\frac{\phi^{n+1} - \phi^n}{\Delta t} + \hat{H}^n = 0$$

A second Euler step is taken to advance the solution to time $t^n + 2\Delta t$.

$$\frac{\phi^{n+2} - \phi^{n+1}}{\Delta t} + \hat{H}^{n+1} = 0$$

Then an approximation to ϕ at time $t^n + \frac{1}{2}\Delta t$ is obtained by

$$\phi^{n+\frac{1}{2}} = \frac{3}{4}\phi^n + \frac{1}{4}\phi^{n+2}$$

After that, the third Euler step is taken to advance the solution to time $t^n + \frac{3}{2}\Delta t$.

$$\frac{\phi^{n+\frac{3}{2}} - \phi^{n+\frac{1}{2}}}{\Delta t} + \hat{H}^{n+\frac{1}{2}} = 0$$

Then a third-order accurate approximation to the solution at time $t^n + \Delta t$ can be obtained by

$$\phi^{n+1} = \frac{1}{3}\phi^n + \frac{2}{3}\phi^{n+\frac{3}{2}}$$

Second order Runge-Kutta integration has an error that is proportional to time step cubed for an integration step and proportional to time step squared for the whole simulation. Fourth order Runge-Kutta integration has an error that is proportional to time step to the fifth power for an integration step and proportional to time step to the fourth power for the whole simulation. In standard Runge-Kutta (RK) schemes, the time step Δt is restricted by the Courant-Friedrichs-Lewy (CFL) condition to be some flow speed dependent multiple of the spatial grid size Δx. Applying standard RK schemes to the solution of HJ PDEs will result in a step size Δt proportional to Δx^2. However, the TVD Runge-Kutta schemes will not introduce oscillations into the solution if when Δt is proportional to Δx. Given a target set defined by an implicit surface function $\phi(x, t_0)$, we use level set methods to compute the propagation of the target set backwardly. By this means, the backward reachable set is obtained.

3.3 Computation of stability region

Section 3.2 introduces the concept of reachable sets and their computation using level set methods. Here we apply the reachable set analysis for the determination of the stability region for power system transient stability assessment. Given a post-fault stable equilibrium point (SEP), there exists an open neighborhood of the SEP that is contained in the stability region. We pick a sufficiently small ε ball around the SEP as the target set and propagate its surface function representation backward in time to compute the region of stability of the equilibrium point.

The following algorithm summarizes the procedure to determine the stability region of post-fault power system.

1.) Form the state space equations of the post-fault power system, $\frac{dx}{dt} = f(x)$.

2.) Find the stable equilibrium point of this autonomous nonlinear system, by solving $f(x) = 0$ and let $x^* \in R^n$ be a SEP.

3.) Specify a ε ball centered at the stable equilibrium point with sufficiently small radius ε. Define an implicit surface function at time $t = 0$ as,

$$\phi(x, 0) = \|x - x^*\| - \varepsilon. \tag{3.6}$$

Then the target set is the zero "sublevel" set of the function $\phi(x, 0)$, i.e, it is given by,

$$\{x \in R^n | \phi(x, 0) \leq 0\} = \{x \in R^n | \|x - x^*\| \leq \varepsilon\}. \tag{3.7}$$

Note that, a point x is inside the target set if $\phi(x, 0)$ is negative, outside the target set if $\phi(x, 0)$ is positive, and on the boundary of the target set if $\phi(x, 0) = 0$.

4.) Propagate in time the boundary of the backward reachable set of the target set by solving the following HJ PDE:

$$\phi_x^T f(x, t) + \phi_t = 0, \tag{3.8}$$

with terminal conditions $\|x - x^*\| - \varepsilon = 0$. The viscosity solution $\phi(x, t)$ to (3.8) is the backward reachable set of the target set at time t,

$$\{x \in R^n | \phi(x, t) \leq 0\}. \tag{3.9}$$

The above backward reachable set of the ε ball around the stable equilibrium point is computed using a software tool from (Mitchell). It is always contained in the stability

region of the stable equilibrium point. As t goes to infinity, the backward reachable set approaches the true stability region. If the stability region is bounded, the level set based numerical computation of the backward reachability set eventually converges to the stability region within a finite computation time.

Example 1 *For the nonlinear system (reverse of Van Der Pol Oscillator),*

$$\frac{dx_1}{dt} = -x_2,$$
$$\frac{dx_2}{dt} = x_1 + (x_1^2 - 1)x_2,$$

(0,0) is the only equilibrium point that is stable. So in this case we can not employ the manifold-based method (17) to find the stability region of the equilibrium point. Our backward reachability based method is applicable in all cases and using it we compute the stability region as shown in Figure 3.3.

In Figure 3.3, the region inside the dashed line is the stability region of the stable equilibrium point. We validate our result by drawing the phase portrait from which we can see that our computation is precise.

3.4 Application to control validation

Section 3.3 presents an algorithm to compute the stability region of a given power system. This can be used to validate effectiveness of any discrete control with regards to transient stability. After a fault occurs and is cleared, we need to examine the initial post-fault state. If the initial post-fault state is inside the stability region of the planned discrete control, the trajectory is stable. Otherwise, the trajectory is unstable. There may exist many discrete controls in the power system to improve the stability of the trajectory. When the post-fault trajectory becomes unstable, appropriate controls need to be switched on to stabilize it. Based on the algorithm of section 3.3, we can validate whether the existing control is effective or not.

Following is the algorithm for the control validation:

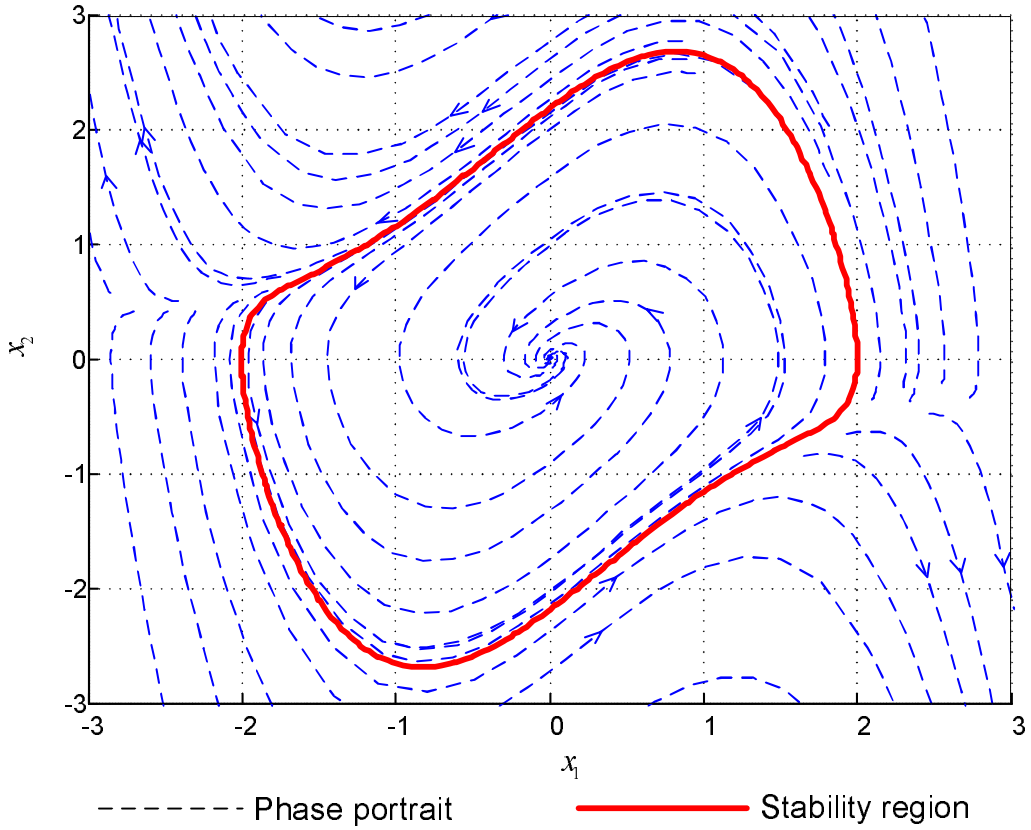

Figure 3.3 Stability region computed by level set methods

1.) Compute the stability region of a stable equilibrium point x_1 of the normal system with no controls on, referred as the mode 1.

2.) Check if the post-fault initial state x_0 is inside the stability region of mode 1, if yes, stop. The trajectory is stable without any controls on. Otherwise, the trajectory is unstable, go to next step.

3.) Compute the stability region of a stable equilibrium point x_i of the system with control i on, referred to as mode i.

4.) Check if the post-fault initial state x_0 is inside the stability region of control i. If yes, control i can be switched on, in which case, the system will eventually reach the equilibrium point x_i. Otherwise, control i can not prevent the instability of the trajectory.

5.) In case control i can stabilize the trajectory, but the SEP x_i is not a desired operating

point, the trajectory can be "steered" to another SEP x_j, whose stability region has a nonempty intersection with stability region of x_i. To achieve this, control j is switched on after switching on the control i and at a time when the system trajectory enters the intersection of two stability regions.

6.) Step 5 may be repeated to steer the trajectory further to yet another SEP if desired.

3.5 Example

In this section an example is presented to show how the stability region is computed and the control is validated.

3.5.1 A Single-Machine-Infinite-Bus Model

The classical single-machine-infinite-bus model of power system is shown in Figure 3.4. The system model is given as follows:

$$\begin{cases} \frac{d\delta}{dt} = \omega \\ \\ \frac{d\omega}{dt} = \frac{P_m - P_e^M \sin\delta - D\omega}{M} \end{cases} \tag{3.10}$$

Here, δ is the machine rotor angle and ω is the relative angular velocity of the rotor. Suppose the inertial constant $M = \frac{T_J}{\omega_0} = 0.026\ s^2/rad$, $P_m = 1.0\ per\ unit$, $P_e^M = \frac{EU}{x} = 1.35\ per\ unit$.

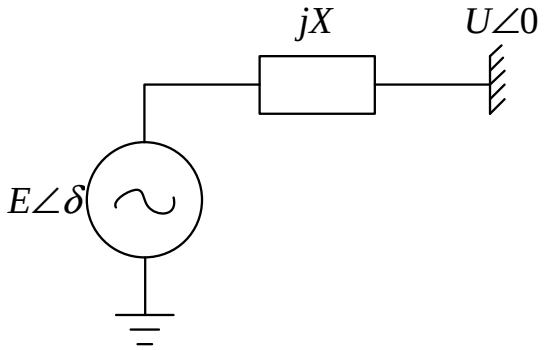

Figure 3.4 A single-machine-infinite-bus model

3.5.1.1 The computation of stability region of normal system

From the system equation (3.10) and the chosen parameter values, the point $(0.8324, 0)$ is identified to be a stable equilibrium point of this system. We define the target set as $\sqrt{(\delta - 0.8324)^2 + \omega^2} \leq 0.1$. The stability region computed using our algorithm lies inside the solid line drawn in Figure 3.5. From this figure we conclude that if the post-fault initial condition of the state variables is inside the stability region, the trajectories converge to the stable operating point. If the initial condition is outside the stability region, the trajectories will be unstable. We validate our result by drawing the corresponding phase portrait using time domain simulation of some sample trajectories from which we can see that our method can precisely compute the stability region.

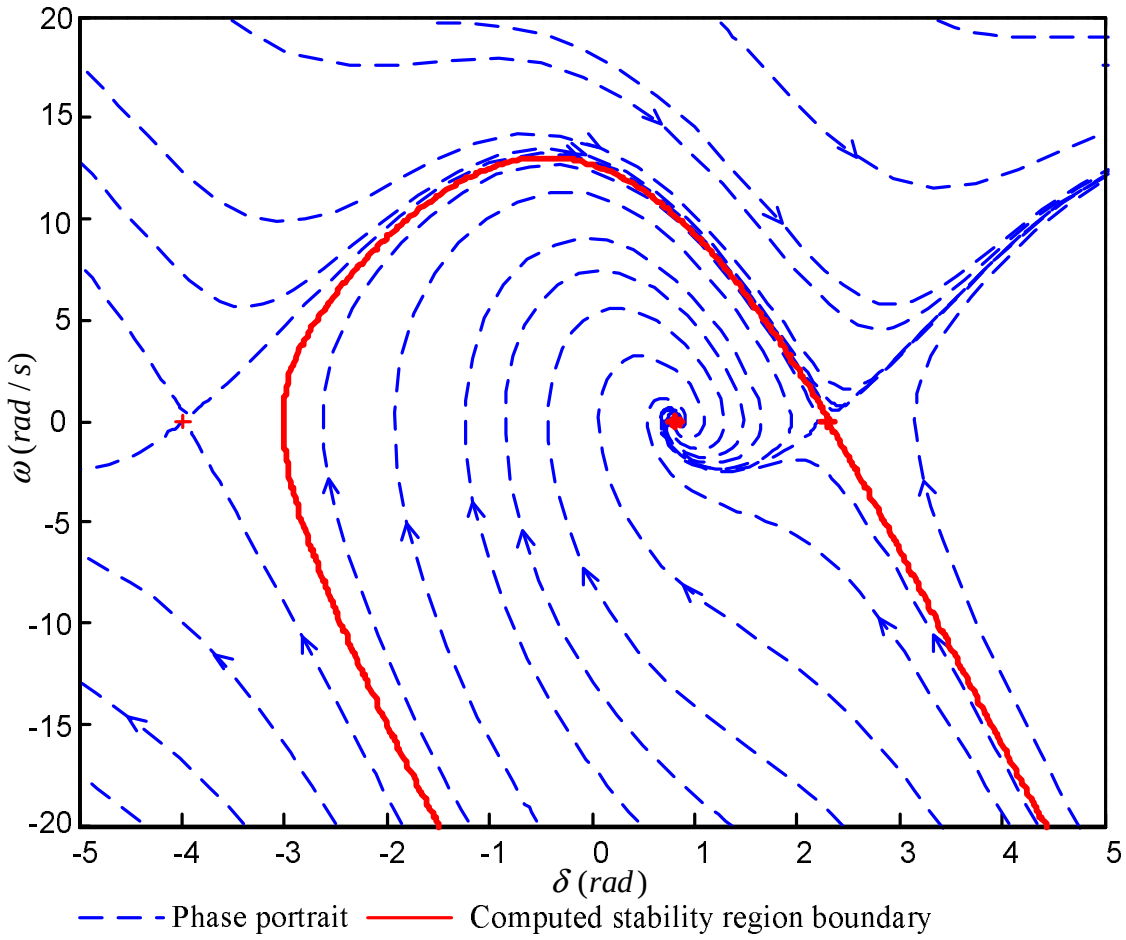

Figure 3.5 Stability region and phase portrait for $D = 0.12\ s/rad$

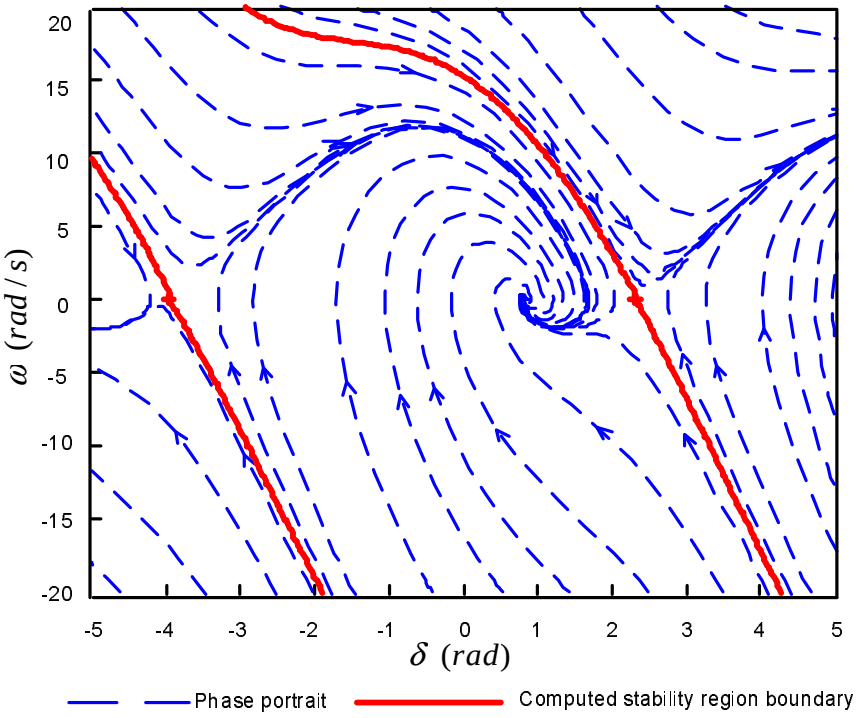

Figure 3.6 Stability region and phase portrait for $D = 0.15\ s/rad$

When the damping coefficient D is increased, the stable equilibrium point remains the same as $(0.8324, 0)$. For $D = 0.15$, we compute the stability region as shown in Figure 3.6. The figure clearly shows that when D is increased, the size of the stability region also increases. The observation is validated by time domain simulations. Figure 3.7 and Figure 3.8 give the time domain responses of the rotor angle and velocity for an initial condition $(\delta_0, \omega_0) = (-5, 15)$ when D equals 0.12 s/rad and 0.15 s/rad, respectively. Figure 3.8 shows that the trajectories eventually settle at the post-fault stable operating point. However, when D is 0.12 s/rad, the system loses stability for this initial condition as shown in Figure 3.7. This is not unexpected since a large D implies a larger stability region.

3.5.1.2 Transient stability design

Figure 3.9 shows a single-machine-infinite-bus system with provision for shunt and series controls. Define the system with no controls on as mode 1, with series control on as mode 2, with shunt control on as mode 3, and with both series control and shunt control on as mode 4.

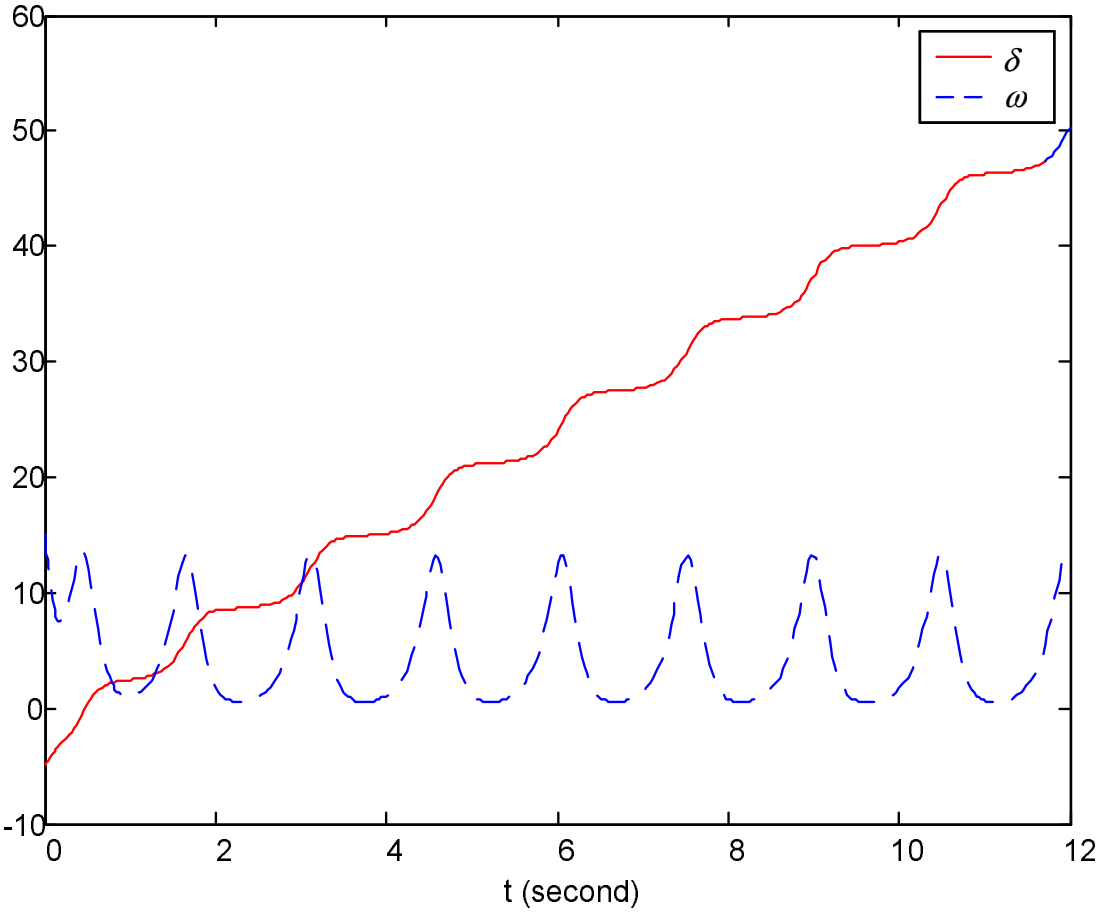

Figure 3.7 Time domain simulation when $D = 0.12\ s/rad$

When series capacitors are added, the system is switched from mode 1 to mode 2. The reactance of the transmission line becomes $X_1 + X_2 - X_{series}$. Suppose the existing series control compensation is 40%, then the maximum power transferred equals $P_e^M = EU/(X_1 + X_2 - X_{series}) = 2.25\ per\ unit$.

When shunts capacitors are added, the system is switched from mode 1 to mode 3. Assume $B_c = 0.5 p.u.$ Then according to the $Y-\Delta$ network transformation, $X_{12} = X_1+X_2-B_cX_1X_2 = 0.5 + 0.5 - 0.5 \times 0.25 = 0.875$. So the maximum power transferred equals $P_e^M = EU/X_{12} = 1.543\ per\ unit$.

When both the series and shunt capacitors are added, the system is switched from mode 1 to mode 4. In this mode $X_{12} = 0.475$ and the maximum power transferred equals $P_e^M = EU/X_{12} = 2.842\ per\ unit$.

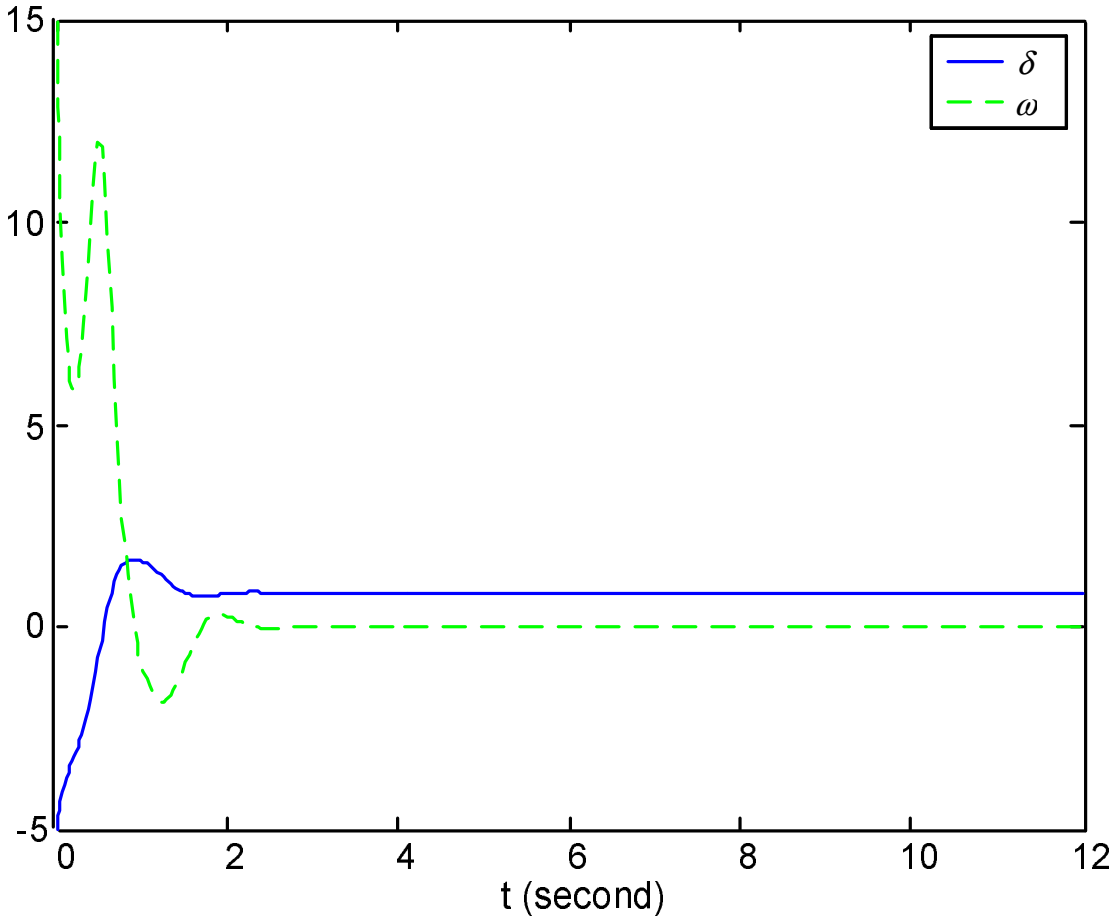

Figure 3.8 Time domain simulation when $D = 0.15\ s/rad$

The equilibrium points of these modes related with different controls are shown in Table 3.1.

The stability regions of these four modes are shown in Figure 3.10. The stability region of mode 1 is inside the dotted line, that of mode 2 is inside the dashed line, that of mode 3 is inside the dashed-dotted line, and that of mode 4 is inside the solid line.

Based on the stability region method, we can validate the effectiveness of different controls. When post-fault state is inside the stability region of mode 1, no control is needed because the state will finally reach the equilibrium point. When post fault state is out of the stability region of mode 1, we need to switch on some controls to ensure that the post fault state lies inside the stability region of one of the modes. For example, if the initial post-fault state is outside of the stability region of mode 2, we can judge that even if the series capacitors are

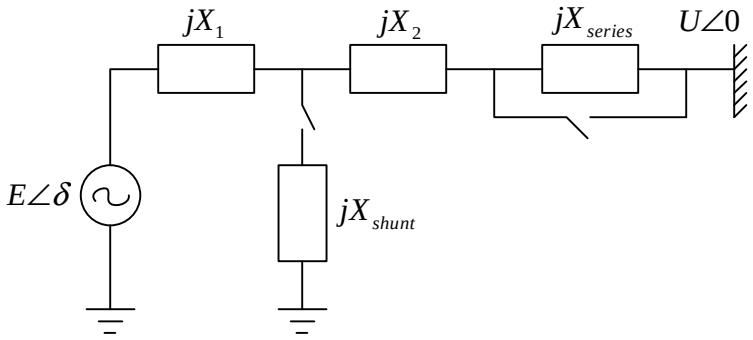

Figure 3.9 System model with shunt and series controls

Mode	Series Capacitor	Shunt Capacitor	X_i	P_e^M value	Equilibrium point
1	Off	Off	$X_1 + X_2$	1.35	$(0.8342, 0)$
2	On	Off	$X_1 + X_2 - X_{series}$	2.25	$(0.4603, 0)$
3	Off	On	$X_1 + X_2 - \frac{X_1 X_2}{X_{shunt}}$	1.543	$(0.7084, 0)$
4	On	On	$X_1 + (X_2 - X_{series})$ $- \frac{X_1(X_2 - X_{series})}{X_{shunt}}$	2.3478	$(0.4400, 0)$

Table 3.1 Four control modes and their certain parameters

switched on, the system will not maintain stability. That means in this case the series control is ineffective.

From Figure 3.10, we can also see that the equilibrium points of different modes are all inside the stability region of mode 1. *This means whenever a control is switched on and the system finally stabilizes at the equilibrium point of that mode, we can switch off the specific controls so that the system ultimately stabilizes at the equilibrium point of mode 1.* It follows that if a transient-fault causes the system state to deviate, then as long as this state lies in the union of 4 regions of stability, it is possible to switch the series/shunt capacitors "on" and eventually "off" to return the system to the equilibrium of normal configuration. The procedure that we outline establishes the methodology for system "recovery".

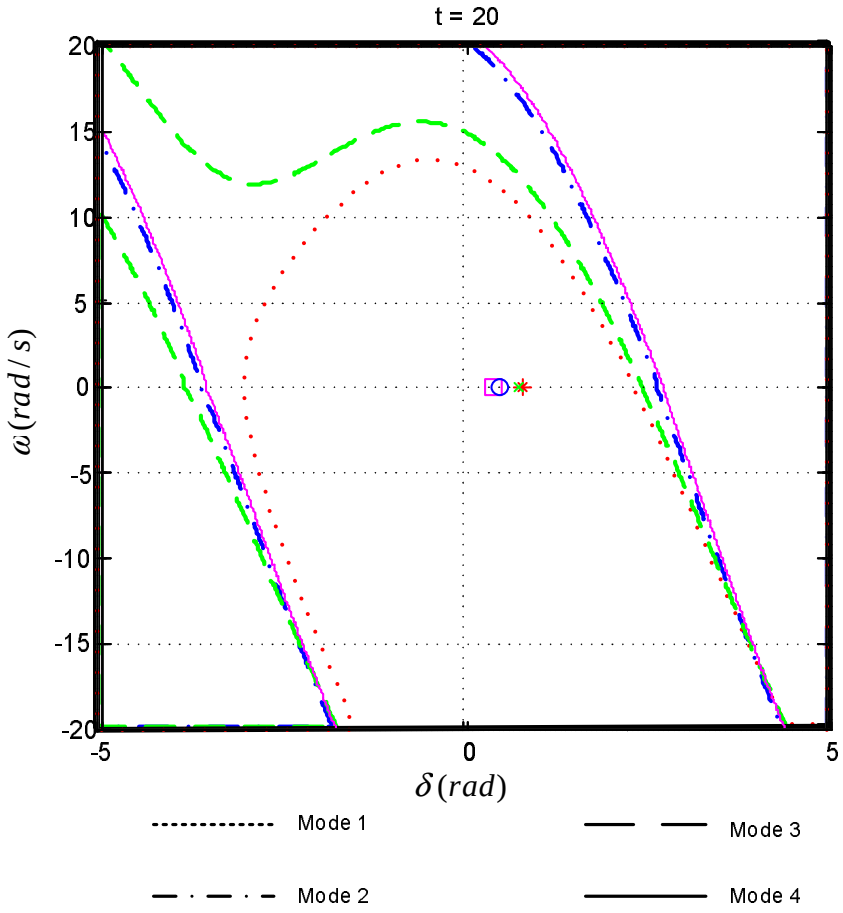

Figure 3.10 Stability region of four modes

3.6 Summary

A novel method for computing the stability region of a nonlinear system, such as a power system, is presented in this chapter. We also apply this method for power system transient stability design. The proposed method has the following advantages:

1. It computes the stability region accurately. For large systems, the computation may be stopped after a certain number of iterations to get a sub-region contained in the stability region in order to save the computation time.

2. It is easy to implement. We only need to form the mathematic model of the post-fault power system and identify the stable equilibrium point. After that, we can use level set methods to compute the stability region as a backward reachable set.

A limitation is that the complexity suffers from what is commonly known as "curse of dimensionality". This is because the propagation of implicit surface function utilizes a gridding of the state space and the number of grid points grow exponentially in the number of dimensions. As part of future research we plan to explore faster and/or approximate techniques for reachability computation. This includes possibility of parallelization, of hierarchical computation, etc.

CHAPTER 4. Application of Model Predictive Control in Voltage Stabilization

4.1 Overview

Voltage instability takes the form of a dramatic drop in bus voltages in a transmission system, which may result in system collapse. Nowadays, voltage stability has become a major concern in power system planning and operation. Several factors have contributed to this situation. First, building new transmission facilities are more and more difficult because of the high capital investment and little or no right-of-way. Second, the construction of large, remote power plants weakens the ability of voltage control and increases the electrical distance between load and generation. Third, the deregulation of power industry has created an economical incentive to operate power systems closer to their limits. Voltage instability can occur under certain severe disturbances. Therefore, it is imperative that schemes for power system protection be in place to mitigate the catastrophic effects such as large scale shutdowns and collapses caused by such disturbances. This chapter studies voltage control strategies based on a modified model predictive control with decreasing control horizon. The control design includes:

- A formulation of a model predictive control based system protection scheme for maintaining voltage stability under contingencies. The stabilizing control is achieved through the economic use of shunt capacitors.

- A formulation of a control strategy not only prevents voltage instability, but also maintains a desired amount of post-transient voltage stability margin. Voltage stability margin sensitivities are used to characterize the effect of control variables on stability margin

enhancement. Prior work involving dynamic analysis for voltage stabilization did not include voltage stability margin as part of the control objective. The control means is shunt capacitors.

- A formulation of an optimal coordination of static var compensators (SVCs), transformer under load tap changers (ULTCs) and load shedding to improve voltage performance following large disturbances.

The distinguishing features of our MPC formulation are as follows:

- Use of trajectory sensitivities for determining the effect of control on voltage stabilization, which is a more accurate way of determining the effectiveness of control (as opposed to the less accurate linearization around a single state or more time-consuming computations based on numerical simulations).

- Optimization is performed repeatedly at each sampling instant. Only the first control step is implemented. This feature corrects the errors brought by model approximation, such as a linearized relationship between the voltages and the control variables.

- A decreasing horizon MPC is used. The control horizon decreases from one iteration to the next. This modification not only reduces the computation time, but also helps the convergence of the optimization process. This feature of MPC has not been explored in prior work on stabilization of power systems.

- Optimization performed at each step involves a quadratic cost function together with linear constraints, which makes the formulation scalable to large-sized practical systems (as demonstrated by the application to the 39 bus New England system).

This chapter is organized as follows. Section 4.2 introduces methodologies which are used in the control design. Basic concepts and the application of the model predictive control and trajectory sensitivity are presented. Section 4.3 presents an effective and economic control strategy for controlling the shunt capacitors so as to eliminate voltage instability following any pre-identified contingency. Section 4.4 proposes an optimal capacitor switching sequence and

amounts given their locations and capacities to satisfy the requirements of voltage performance and voltage stability margin. Section 4.5 proposes an optimal coordinated control strategy consisting of continuous and discrete power system controls to improve voltage performance and prevent voltage instability. Section 4.6 discusses about implementation issues. Section 4.7 is a summary.

4.2 Methodology

4.2.1 Model predictive control

Model Predictive Control (MPC) is a class of algorithms that compute a sequence of control variable adjustments in order to optimize the future behavior of a plant (system). MPC was originally developed to meet the specialized control needs of petroleum refineries. Now it has been used in a wide variety of application areas including chemicals, food processing, automotive, aerospace, metallurgy, and power plants. An introduction to the basic concepts and formulations of MPC can be found in (87). The principle of MPC is graphically depicted in Figure 4.1. Here x represents the state variable that needs to be controlled to a specific range. The available control is represented by variable u.

At a current time t_k, the MPC solves an optimization problem over a finite prediction horizon $[t_k, t_k + T_p]$ with respect to a predetermined objective function such that the predicted state variable $\hat{x}(t_k + T_p)$ can optimally stay close to a reference trajectory. The control is computed over a control horizon $[t_k, t_k + T_c]$, which is smaller than the prediction horizon $(T_c \leq T_p)$. If there were no disturbances, no model-plant mismatch and the prediction horizon is infinite, one could apply the control strategy found at current time t_k for all times $t \geq t_k$. However, due to the disturbances, model-plant mismatch and finite prediction horizon, the true system behavior is different from the predicted behavior. In order to incorporate the feedback information about the true system state, the computed optimal control is implemented only until the next measurement instant $(t_k + T_s)$, at which point the entire computation is repeated.

In a MPC, the optimization problem to be solved at time t_k can be formulated as follows:

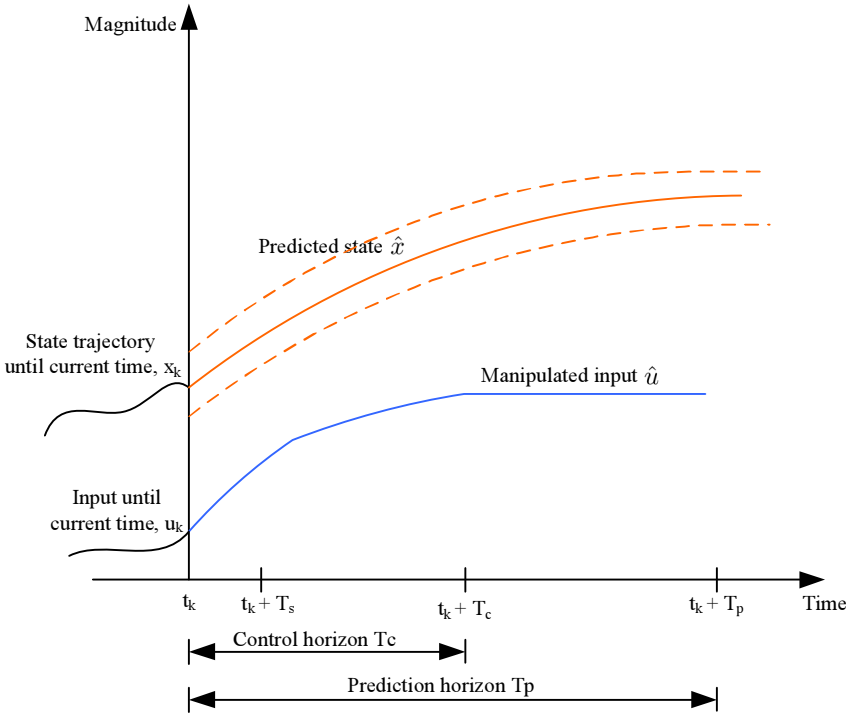

Figure 4.1 Principle of MPC

$$\min_{\hat{u}} \int_{t_k}^{t_k+T_p} F(\hat{x}(\tau), \hat{u}(\tau))d\tau \tag{4.1}$$

subject to

$$\dot{\hat{x}}(\tau) = f(\hat{x}(\tau), \hat{u}(\tau)), \quad \hat{x}(t_k) = x(t_k) \tag{4.2}$$

$$u_{min} \leq \hat{u}(\tau) \leq u_{max}, \quad \forall \tau \in [t_k, t_k + T_c] \tag{4.3}$$

$$\hat{u}(\tau) = \hat{u}(t_k + T_c), \quad \forall \tau \in [t_k + T_c, t_k + T_p] \tag{4.4}$$

$$x_{min}(\tau) \leq \hat{x}(\tau) \leq x_{max}(\tau), \quad \forall \tau \in [t_k, t_k + T_p] \tag{4.5}$$

Here, T_c and T_p are the control and prediction horizon with $T_c \leq T_p$. $\hat{x}$ denotes the estimated state and $\hat{u}$ represents "estimated" control (The true state may be different and the true control matches the estimated control only during the first sampling period).

Equation (4.1) represents the cost function of the MPC optimization. Equation (4.2) represents the dynamic system model with initial state $x(t_k)$. Equations (4.3) and (4.4) represent

the constraints on the control input during the prediction horizon. Equation (4.5) indicates the state operation requirement during the prediction horizon.

In the context of power systems, MPC has been applied mainly in two areas: voltage stabilization and frequency control.

An emergency voltage control using tree search and model predictive control is presented in (63). The emergency controls considered in the paper are: capacitor bank switching, tap changer operation and load shedding. The optimization objective is to minimize the deviation of the predicted voltage trajectory with respect to the reference trajectory as well as the weighted control cost. A special penalty is incurred when a constraint violation or a singularity induced bifurcation occurs. The paper mentions four different approaches to predict the system trajectory: nonlinear numerical simulation, Euler state prediction, off-equilibrium linearizations, and Euler state prediction linear output approximation. The model predictive control is solved by an exhaustive tree search to compute a discrete-only control strategy.

In (64), a coordinated system protection scheme (SPS) against voltage collapse based on model predictive control and tree search is presented. Dissimilar and discrete controls such as generator voltage set-points, load-shedding, and tap-changers are coordinated. The objective function of the optimization includes: output deviation together with control and constraint violation costs. The prediction of the output trajectory is based on the linearization of the nonlinear system. The optimization is solved by exhaustive tree search. A Nordic test system is used to test the effectiveness of the scheme.

Model predictive control is also employed in (99), where an optimal coordinated voltage control for power system voltage stability is proposed. The controls used in the paper include: shunt capacitor banks, load shedding, and tap changers. The prediction of the output trajectory is based on the Euler state prediction. The main difference with the work reported in (63) lies in the method used for solving the the MPC optimization problem. The optimization problem is solved by a pseudo gradient evolutionary programming (PGEP) technique, which allows computing optimal value for both discrete and continuous controls. The coordinated voltage control strategy based on MPC is tested on the 39-bus New England system.

A method to compute an emergency voltage control strategy based on model predictive control is presented in (104; 102; 103). The controls include tap changers, load shedding, and generator voltage set-points. The prediction of the output trajectories is based on trajectory sensitivity. While in the traditional model predictive control setting only the first control out of a sequence of computed control inputs is implemented, in the above papers the authors compute only an initial sequence of control inputs and implement it over the entire control horizon. The optimization problem is an instance of mixed integer linear programming.

A voltage stabilization control strategy is proposed in (45) that is based on model predictive control and trajectory sensitivity. The control is exercised in form of load shedding. The objective function of the model predictive control is to minimize the amount of load shedding required to restore the voltages. The effectiveness of the load shedding on voltage restoration is established through trajectory sensitivity. The approach proposed in this recent work is arguably the most comprehensive, and has inspired the approach taken in the dissertation.

Besides voltage stabilization, model predictive control has also been used for frequency stabilization, which requires control for managing the imbalance between load and generation in the system. An approach to realize load following and regulation based on model predictive control is presented in (5). The generators ramp up/down their generation to follow slow load fluctuations that are forecasted based on the time period of the day, day of week, season, weather, etc. On the other hand, fast fluctuation in the aggregate load, which is a random phenomenon, are counteracted by way of load-following.

4.2.2 Trajectory sensitivity

Consider differential algebraic equations (DAEs) of a system,

$$\dot{x} = f(x, y, u), \quad x(0) = x_0 \tag{4.6}$$

$$0 = g(x, y, u) \tag{4.7}$$

where x is a vector of state variables, y is a vector of algebraic variables, and u is a vector of control variables. Trajectory sensitivity considers the influence of small variations in the control u (and any other variable of interest) on the solution of the state equations (4.6) and

(4.7). Let u_0 be a nominal value of u, and assume that the nominal system in (4.8) and (4.9) has a unique solution $x(t, x_0, u_0)$ over $[t_0, t_1]$.

$$\dot{x} = f(x, y, u_0), \quad x(0) = x_0 \tag{4.8}$$

$$0 = g(x, y, u_0) \tag{4.9}$$

Then the system in Equations (4.6) and (4.7) has a unique solution $x(t, x_0, u)$ over $[t_0, t_1]$ that is related to $x(t, x_0, u_0)$ as:

$$\begin{aligned} x(t, x_0, u) &= x(t, x_0, u_0) + x_u(t)(u - u_0) + \text{high-order terms} \\ y(t, x_0, u) &= y(t, x_0, u_0) + y_u(t)(u - u_0) + \text{high-order terms} \end{aligned}$$

Here $x_u(t) = \frac{\partial x(t,x_0,u)}{\partial u}$ is called the trajectory sensitivities of state variables with respect to control variables u and $y_u(t) = \frac{\partial y(t,x_0,u)}{\partial u}$ is the trajectory sensitivities of algebraic variables with respect to control variables u.

The evolution of trajectory sensitivities can be obtained by differentiating Equations (4.6) and (4.7) with respect to the control variables u and is expressed as:

$$\dot{x}_u(t) = f_x(t)x_u(t) + f_y(t)y_u(t) + f_u(t) \tag{4.10}$$

$$0 = g_x(t)x_u(t) + g_y(t)y_u(t) + g_u(t) \tag{4.11}$$

The trajectory sensitivity can be solved numerically. An efficient methodology is presented in (46) for the computation of trajectory sensitivities for a system represented by DAE equations. If the time domain simulation of a system is performed by the trapezoidal numerical integration approach, the trajectory sensitivity of state variables with respect to the small variations in initial state variables x and control variable u can be calculated as a by product of the time domain simulation. The x_u and y_u in Equation (4.10) and Equation (4.11) are part of the solution matrix.

Let

$$\bar{x} = \begin{bmatrix} x \\ u \end{bmatrix}, \qquad \bar{f} = \begin{bmatrix} f \\ 0 \end{bmatrix}$$

The DAE model (4.6) and (4.7) can be expressed as

$$\dot{\bar{x}} = \bar{f}(\bar{x}, y) \tag{4.12}$$

$$0 = g(\bar{x}, y) \tag{4.13}$$

Trapezoidal approach is used to approximate Equation (4.12) with a set of algebraic difference equations coupled to the original algebraic Equation (4.13). The evolution of the states $\bar{x}$, and y from time instant t_i to the next time instant t_{i+1} can be described as

$$\bar{x}^{i+1} = \bar{x}^i + \frac{\eta}{2}(\bar{f}(\bar{x}^{i+1}, y^{i+1}) + \bar{f}(\bar{x}^i, y^i)) \tag{4.14}$$

$$0 = g(\bar{x}^{i+1}, y^{i+1}) \tag{4.15}$$

where superscript i is the time instant t_i, $i+1$ is the time instant t_{i+1} and $\eta = t_{i+1} - t_i$ is the integration time step. Rearrange Equation 4.14 and Equation 4.15 as follows:

$$F = \begin{bmatrix} \frac{\eta}{2}\bar{f}(\bar{x}^{i+1}, y^{i+1}) - \bar{x}^{i+1} + \frac{\eta}{2}\bar{f}(\bar{x}^i, y^i) + \bar{x}^i \\ g(\bar{x}^{i+1}, y^{i+1}) \end{bmatrix} = 0 \tag{4.16}$$

Equation (4.16) is a set of implicit nonlinear algebraic equations. The Newton iterative technique is commonly used to solve for $\bar{x}^{i+1}$ and y^{i+1}, given $\bar{x}^i$ and y^i

$$\begin{bmatrix} \bar{x}^{i+1} \\ y^{i+1} \end{bmatrix} = \begin{bmatrix} \bar{x}^i \\ y^i \end{bmatrix} - F_\chi^{-1} F$$

where, F_χ is the Jacobian of F with respect to $\bar{x}, y$.

$$F_\chi = \begin{bmatrix} \frac{\eta}{2}\bar{f}_{\bar{x}} - I & \frac{\eta}{2}\bar{f}_y \\ g_{\bar{x}} & g_y \end{bmatrix}$$

Now consider the trajectory sensitivity equations. Differentiating Equations (4.12) and (4.13) with respect to the initial conditions $\bar{x}_0$ results in the DAEs of trajectory sensitivities

$$\dot{\bar{x}}_{\bar{x}_0} = \bar{f}_{\bar{x}}\bar{x}_{\bar{x}_0} + \bar{f}_y y_{\bar{x}_0} \tag{4.17}$$

$$0 = g_{\bar{x}}\bar{x}_{\bar{x}_0} + g_y y_{\bar{x}_0} \tag{4.18}$$

The trajectory sensitivity can be approximated by trapezoidal integration as follows:

$$\begin{aligned} \bar{x}_{\bar{x}_0}^{i+1} &= \bar{x}_{\bar{x}_0}^{i} + \frac{\eta}{2}(\bar{f}_{\bar{x}}^{i}\bar{x}_{\bar{x}_0}^{i} + \bar{f}_{y}^{i}y_{\bar{x}_0}^{i} + \bar{f}_{\bar{x}}^{i+1}\bar{x}_{\bar{x}_0}^{i+1} + \bar{f}_{y}^{i+1}y_{\bar{x}_0}^{i+1}) \\ 0 &= g_{\bar{x}}^{i+1}\bar{x}_{\bar{x}_0}^{i+1} + g_{y}^{i+1}y_{\bar{x}_0}^{i+1} \end{aligned}$$

Rearranging the above equation results in

$$\begin{bmatrix} \frac{\eta}{2}\bar{f}_{\bar{x}}^{i+1} - I & \frac{\eta}{2}\bar{f}_{y}^{i+1} \\ g_{\bar{x}}^{i+1} & g_{y}^{i+1} \end{bmatrix} \begin{bmatrix} \bar{x}_{\bar{x}_0}^{i+1} \\ y_{\bar{x}_0}^{i+1} \end{bmatrix} = \begin{bmatrix} -\frac{\eta}{2}(\bar{f}_{\bar{x}}^{i}\bar{x}_{\bar{x}_0}^{i}, + \bar{f}_{y}^{i}y_{\bar{x}_0}^{i}) - \bar{x}_{\bar{x}_0}^{i} \\ 0 \end{bmatrix} \tag{4.19}$$

Therefore, the sensitivity matrix (4.20) can be obtained as a solution of a linear matrix equation. Notice that the coefficient matrix of Equation (4.19) is exactly the same as Jacobian matrix F_χ in solving the for $\bar{x}^{i+1}$ and y^{i+1}. In our work, we extended the Power System Analysis Tool (75) (a MATLAB based tool) to do trajectory sensitivity calculation and the MPC optimization.

$$\begin{bmatrix} \bar{x}_{\bar{x}_0}^{i+1} \\ y_{\bar{x}_0}^{i+1} \end{bmatrix} = \begin{bmatrix} x_{x_0} & x_{u_0} \\ u_{x_0} & u_{u_0} \\ y_{x_0} & y_{u_0} \end{bmatrix} \tag{4.20}$$

Figure 4.2 illustrates the application of trajectory sensitivity in evaluating the effect of controls on system behavior. The trajectory x_k of the nominal system represents the behavior under the control u_k. When the control is increased by Δu_1^k at time t_k, the change in predicted system behavior based on sensitivity analysis at time t_l, can be approximated as $\Delta x_1^{kl} = x_{u_1^k}^l \Delta u_1^k$. Here $x_{u_1^k}^l$ is the trajectory sensitivity of the state variable at time t_l with respect to the control at time t_k. Similarly if we increase the control by Δu_n^k at time $t_k + (n-1)T_s$, the change in the state variable at time t_l is represented by $\Delta x_n^{kl} = x_{u_n^k}^l \Delta u_n^k$. Here, $x_{u_n^k}^l$ is the trajectory sensitivity of the state variable at time t_l with respect to the control at time $t_k + (n-1)T_s$. Detailed information about trajectory sensitivity theory can be found in (54).

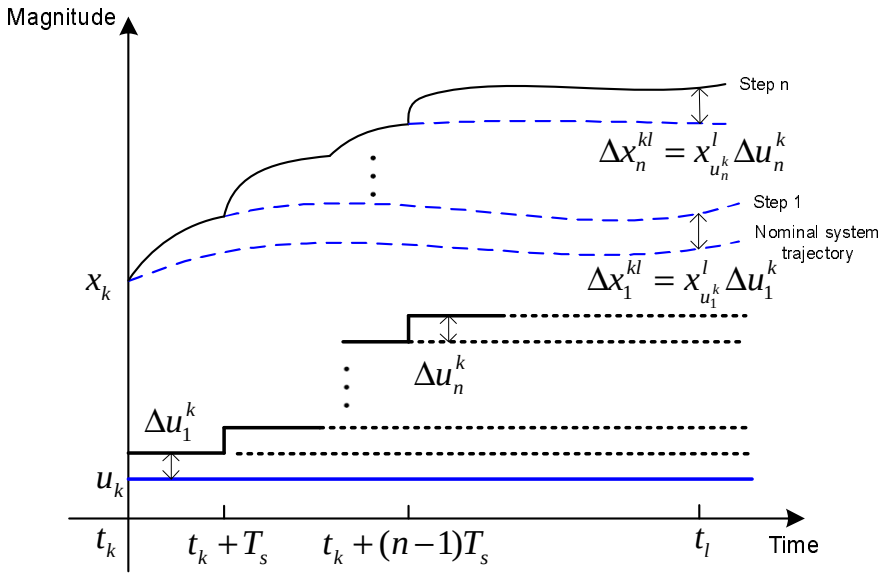

Figure 4.2 Application of trajectory sensitivity in system behavior prediction

4.3 Model predictive control based voltage control

4.3.1 Introduction

As a result of deregulation as well as demand increase, power systems operate close to their capacity. Although power systems are designed with proper planning and with proper stability margin, the instability can still occur under certain severe disturbances, and it is imperative that schemes for power system protection be in place to mitigate their catastrophic effects such as large scale shutdowns and collapses.

The control of voltage level is accomplished by controlling the production, absorption, and flow of reactive power at various locations in the system. With regard to a power system, sources and/or sinks of reactive power, such as shunt capacitors, shunt reactors, synchronous condensers, and static var compensators (SVCs) are used to control voltage level. In literature, many algorithms have been developed to maintain a satisfactory voltage profile. A detailed study of on-line voltage/var control performed on the Ontario Hydro system is presented in (30). The objective function is to minimize the transmission loss as well as the amount of controls. An optimal power flow (OPF) formulation is adopted to schedule generator voltages

and transformer tap positions in the bulk transmission system. In addition, the frequency of the generator voltages and transformer tap changers to be optimized is studied to achieve most of the possible transmission loss savings. An optimal power flow based real time voltage control method is proposed in (10). The primary goal is to remove voltage violations. However, under conditions where violations can not be removed, the objective is to minimize violations. Under the normal operating condition where all the voltages are satisfactory, the objective is to minimize system losses. The controls include transformer tap changers and generator voltage set-points. Besides the OPF based voltage control, Artificial Intelligence especially expert system has also been applied in the study. (68) develops an expert system to assist the decision-making of power system in presence of a voltage violation problem. Empirical rules are generated to mitigate voltage problem using tap changers, reactive injections, and generator voltage setting points. The proposed approach is composed of four steps: identification of the knowledge required to solve a selected problem, justification of the identified empirical rules, development of production rules and testing and modification. The sensitivity of voltage magnitude change with respect to various controllers is used to evaluate the maximum voltage increase with the available control. A rule-based approach for decentralized voltage control is presented in (98). A network decomposition technique is used to alleviate a bus voltage limit violation. Only the local information local to the bus with a voltage violation is adopted in control decision making. Network voltage sensitivity with respect to the available voltage controllers is calculated and a rule-based approach is developed to select the optimal set of control actions for alleviating voltage violations. The controls include generator voltage set-points, reactor switching and tap changers. Distributed expert systems are developed in (74) for voltage control. The controls is composed of load shedding, shunt capacitors, tap changers, static var compensator as well as load flow control. Each var compensating device is controlled by a dedicated computer. An expert system is designed in each computer. Communication exists among those computers. Contribution degree is defined to evaluate the ability of a control in restoring voltages. In (36) two rule-based techniques in a voltage control expert system are introduced. Reactive path concept is adopted to determine control regions of each

reactive power compensator and efficient controllers for each observed bus. The decision is based on two sets of rule-based techniques.

All the above work is based on *static analysis*, in which only the real and reactive power balance in each bus of a power system is considered. The power system is assumed to have a stable operating point. The voltage performance criteria could be met only if the system reaches a post-contingency stable operating point. However, if disturbances are sever, the power system may lose stability. Under this situation, the control strategy to restore the stable equilibrium point requires a *dynamic analysis*. The dynamic behavior of system components such as dynamic load characteristics, dynamic behavior of load tap changers need to be taken into account. In this section, we propose computation of the optimal strategies considering the dynamic behavior of a power system based on *model predictive control* (MPC). We utilize shunt capacitors for control purposes as they are effective means of voltage stabilization. The problem then becomes one of determining capacitor switching sequence and amounts given their locations and limits, together with the requirements on the magnitudes of voltages to stabilize a power system following a sever disturbance. This problem is solved utilizing a dynamic analysis. In our work, we simultaneously minimize the trajectory deviation and the cost of controls. Here, trajectory deviation refers to the deviation of a voltage trajectory from its nominal value. This is a multi-objective optimization and a positively weighted convex sum is chosen as the objective function. The dynamic voltage behavior includes the effects of aggregate exponential recovery dynamic loads. Trajectory sensitivities are used to estimate the effect of controls on the voltage behavior in a linear manner. Due to the use of model predictive approach, the influence of each optimization is limited to one step and the control gets recalculated and refined at each step, the overall control strategy turns out to be sound and robust.

4.3.2 Problem formulation

The purpose of this work is to find an effective and economic control strategy for controlling the shunt capacitors so as to eliminate voltage instability following any pre-identified

contingency. For analyzing voltage performance following disturbances, we model generator and automatic voltage regulator (AVR) as well as aggregated exponential dynamic load models (52; 42). The overall power system is represented by a set of differential algebraic equations (DAE) as in Equations (4.6) and (4.7). Here x is a vector of states including state variables in generator dynamic models, AVR models and dynamic load models such as, rotor angles and angular speeds of generators, outputs of AVRs, and active power recovery and reactive power recovery of dynamic load models. y is a vector of algebraic variables such as bus voltage magnitudes and phase angles. The vector u indicates the output of shunt capacitors. The computation is iterative over a finite control horizon, where in each step a quadratic programming problem is solved to compute the amounts of shunt capacitors to be added in that step. The quadratic programming formulation is valid when the capacitor control is continuous as in SVC. Even in the case where capacitor control is discrete, we can still proceed by assuming continuous control so as to compute an optimal control by solving a quadratic programming relaxation. Then for implementation, the nearest discrete control value can be applied. Any error will get propagated to a following control step, and where it will get corrected. The control is piecewise constant, changing only at the sampling times. Let T_p be the prediction horizon, T_c be the control horizon, T_s be the control sampling interval, and $N = \frac{T_c}{T_s}$ be the total number of control steps. The procedure to determine the control strategy at time t_k based on MPC is as follows:

Step 1: At time t_k (i.e. the $(k+1)^{th}$ sampling instant), an estimate of the current state $x(t_k)$ is obtained. The nominal power system evolves according to Equations (4.6) and (4.7). Here, $u = \{B_m^0 + \sum_{i=0}^{k-1} \Delta B_{m1}^i\}_{m=1}^{m=M}$ is the control variable (i.e. amounts of shunt capacitors currently in use). B_m^0 is the amounts of shunt capacitors that exist at time 0. $\sum_{i=0}^{k-1} \Delta B_{m1}^i$ is the amounts of shunt capacitors that were added over time $[0, t_k - T_s]$. Time domain simulation is used to obtain the trajectory of the nominal system (4.6) and (4.7), starting from the state $x(t_k)$ at time t_k to the end of prediction horizon $t_k + T_p$. At the same time, the trajectory sensitivity of bus voltages with respect to the shunt capacitors to be added at instants $t_k + (n-1)T_s, n = 1 \ldots N-k$ is obtained and denoted

as $V^{kj}_{B_{mn}}(t)$ (see below for the explanation of notation).

Step 2: At time t_k, solve the optimization problem over the prediction horizon $[t_k, t_k + T_p]$ and the control horizon $[t_k, t_k + T_c]$ as stated in (4.21)-(4.25). The objective function is composed of two parts. The first term is the trajectory deviation, the second term is the cost of controls. The combination of the deviation of voltages from nominal values and the control cost needs to be minimized. The number of candidate control locations and their upper limits are determined through a prior planning step (see for example (70)). The total number of control variables in the optimization is the number of candidate control locations times the number of control steps. The optimization is solved in Matlab, and it does converge to a global minimum.

Minimize (with respect to ΔB^k_{mn})

$$\int_{t_k}^{t_k+T_p} (\widehat{V}^k(t) - V_{ref})' R (\widehat{V}^k(t) - V_{ref}) dt + \sum_{m=1}^{M} \sum_{n=1}^{N-k} W_{mn} \Delta B^k_{mn} \tag{4.21}$$

Subject to

$$\Delta B^{min}_m \leq \Delta B^k_{mn} \leq \Delta B^{max}_m \tag{4.22}$$

$$B^{min}_m \leq B^0_m + \sum_{i=0}^{k-1} \Delta B^i_{m1} + \sum_{n=1}^{N} \Delta B^k_{mn} \leq B^{max}_m \tag{4.23}$$

$$V^{kj}_{min}(t) \leq V^{kj}(t) + \sum_{m=1}^{M} \sum_{n=1}^{N-k} V^{kj}_{B_{mn}}(t) \Delta B^k_{mn} \leq V^{kj}_{max}(t) \tag{4.24}$$

$$\Delta B^k_{mn} \geq 0 \tag{4.25}$$

- R is the weight matrix. $\widehat{V}^k(t)$ is the predicted voltage vector at the control sampling time t_k that contains all the bus voltages in the system at time t. ΔB^k is the control matrix calculated at time t_k.
- W_{mn} is the weighted cost of control m to be added at time $t_k + (n-1)T_s$.
- M is the total number of control variables, i.e. the number of shunt capacitor locations.

- N is the total number of control steps.
- ΔB_{mn}^{k} is the entry ΔB^{k}, which is the amount of control m to be added at time $t_k + (n-1)T_s$.
- $\Delta B_{m}^{min} \in \Re$ is the minimum amount of control m to be added at any step.
- $\Delta B_{m}^{max} \in \Re$ is the maximum amount of control m to be added at any step.
- ΔB_{m1}^{i} is the amount of control m implemented at the control sampling point $t_i, i = 0, ...k-1$.
- $B_{m}^{min} \in \Re$ is the minimum amount of control m that must be used, typically 0.
- $B_{m}^{max} \in \Re$ is the maximum available amount of control m.
- $V^{kj}(t) \in \Re$ is the voltage of bus j at time $t(t_k \leq t \leq t_k + T_p)$, of the nominal system of time t_k.
- $V_{min}^{kj}(t)$ is the minimum voltage at bus j desired at time $t_k \leq t \leq t_k + T_p$.
- $V_{max}^{kj}(t)$ is the maximum voltage at bus j desired at time $t_k \leq t \leq t_k + T_p$.
- $V_{B_{mn}}^{kj}(t)$ is the trajectory sensitivity of voltage at bus j at time $t_k \leq t \leq t_k + T_p$ with respect to control m added at time $t_k + (n-1)T_s$.

Step 3: At time t_k, a solution of the optimization problem (4.21)-(4.25) computes a sequence of controls ΔB_{mn}^{k}. Add only the first control ΔB_{m1}^{k} at time t_k and observe or estimate the system state $x(t_{k+1})$ at time $t_{k+1} = t_k + T_s$

Step 4: Increase k by $k+1$ and repeat steps (1)-(3) until the $k = N-1$.

4.3.3 Test case-application to WECC and to New England Systems

The proposed method has been applied to the WECC 9-bus system as well as to the New England 39-bus system. The exponential recovery load model is used in both cases. The parameters of the load model are as following:

$$T_p = T_q = 30, \alpha_s = 0, \alpha_t = 1, \beta_s = 0, \beta_t = 4.5.$$

The parameters in MPC optimization are determined based on the following considerations. Any voltage instability following a contingency must be stabilized in a certain time duration (typically the time in which voltage will decrease by 15%). This is the prediction horizon T_p. The control should be exercised on a time horizon T_c, which is shorter than the prediction horizon, typically the time in which voltage will decrease by 10% (if no control is applied). A discrete-time control must be applied within this duration T_c at a sample-rate high enough to adequately react to the changing voltage trajectory, as well as to allow accurate enough predictions of the voltage trajectory based on the linearization of the trajectory-sensitivity. This dictates the sampling duration T_s. The number of sampling point N is then determined as the ratio of T_c and the sampling duration T_s.

4.3.3.1 WECC 3-generator 9-bus test system

System description Figure 4.3 is a representation of the WECC 3-generator 9-bus system. A fourth-order model is used for modeling each of the three generators. The state variables include the rotor angle δ, the rotor speed ω, the q-axis transient voltage e'_q, and the d-axis transient voltage e'_d. Automatic Voltage Regulator (AVR) defines the primary voltage regulation for generator 1. The continuously acting regulator and exciter model (47) is employed in this study. It is represented by a four-dimensional state equation. The loads at buses 5, 6 and 8 are taken to be exponential recovery dynamic load and each load is described by a two-dimensional state equation. Therefore, the total dimension number of the state space is 22. At buses 5, 7 and 8, there exist shunt capacitors for voltage regulation. These are the control variables. Under normal conditions, all of the shunt capacitors are disconnected.

Fault scenario We consider a three-phase fault at bus 5 at $t = 1.0$ second, which is cleared at $t = 1.2$ seconds by the tripping of the line between bus 4 and bus 5. Based on the time domain simulation, the voltages at buses 5, 7 and 8 are shown in Figure 4.4 and are not satisfactory. At $t = 1.0$ second, the voltages begin to drop dramatically due to the three phase to ground fault. At $t = 1.2$ seconds, the voltages start to recover since the fault gets cleared. However, the voltages begin to oscillate. After 15 seconds, voltages begin to

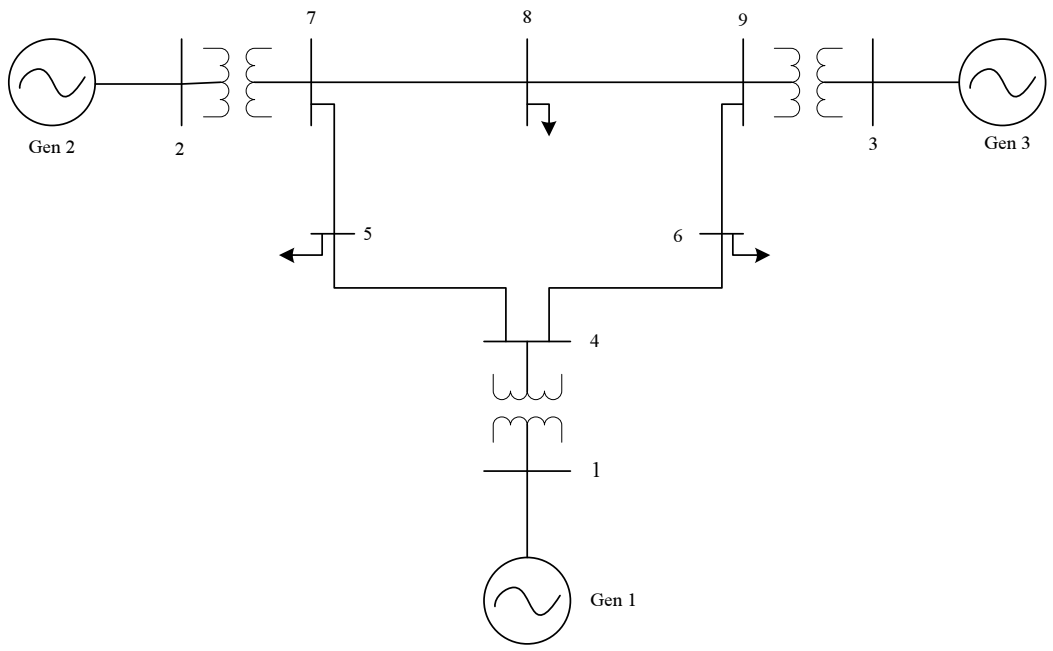

Figure 4.3 WECC 3-generator 9-bus test system

decline gradually. The dynamic load models result in slightly recovery load consumption, which deteriorate the voltage condition. These three voltages fall out of the lower limit 0.95 p.u eventually. According to the system's operational criteria, the load bus voltages must be above 0.95 p.u. Therefore, some control actions are required to satisfy the criterion that the voltages outlined above remain above 0.95 p.u.

Simulation result Model predictive control approach determines the amounts of shunt capacitors to be added at each sampling instant so as to recover the local voltages. Although the capacitors have a positive effect on low voltage problems, the maximum capacitor to be added at any step ΔB_m^{max} was set to be 0.1 p.u. This is because if large amounts of capacitors are added at one time, an over-voltage may occur, which has a bad effect on the electrical devices of the power system. During the optimization, we set the lower bound of all bus voltages to be 0.95 p.u. and upper bound of load bus voltages to be 1.05 p.u. For other buses, such as a generator bus, we set the maximum voltage magnitude to be 1.08 p.u., a bit higher than a load bus. These settings are practical. Fig. 4.5 shows the bus voltages after MPC

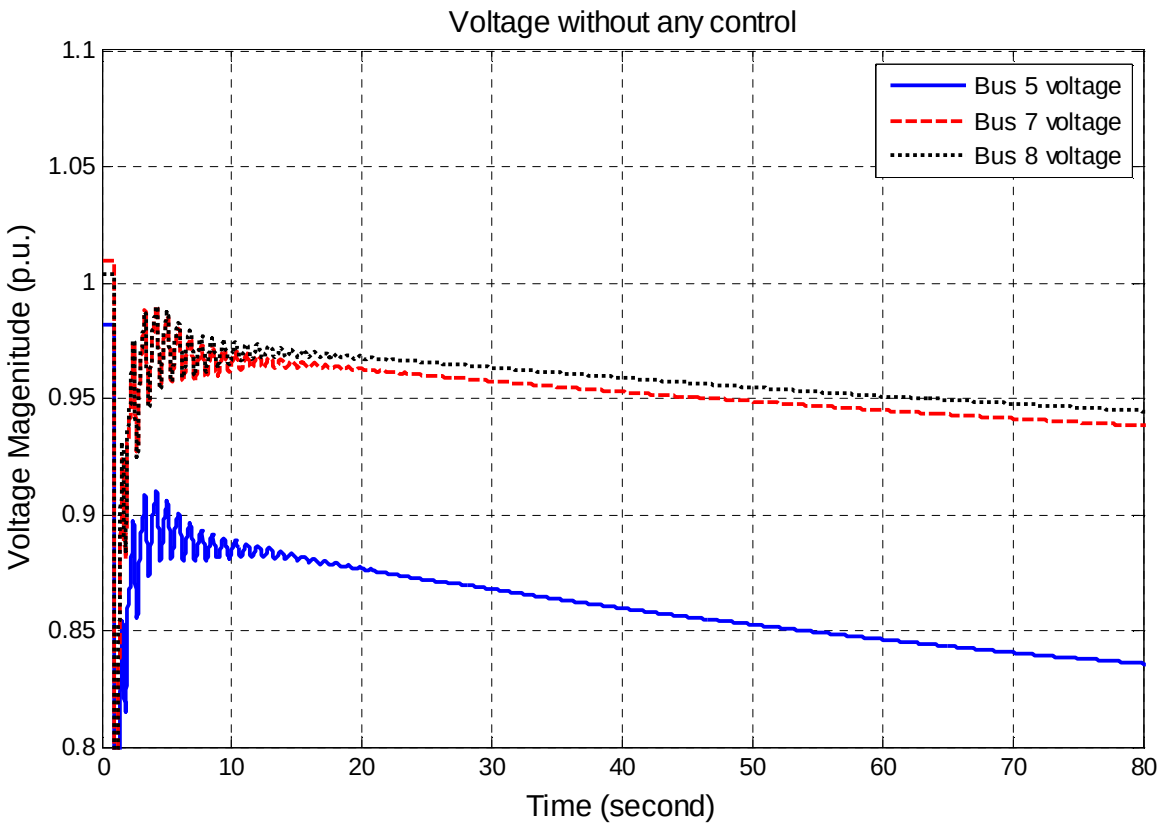

Figure 4.4 Voltage behavior of WECC system without MPC control

based control was implemented starting at time $t = 1.2$ seconds. From the figure, we can see that all the bus voltages were restored to above 0.95 p.u and the oscillations of the voltages disappeared within 35 seconds.

The control strategy is shown in Table 4.1. Suppose the control action starts right after the fault is cleared. The first control action happens at $t = 1.2$ seconds. 0.1 p.u. capacitors at bus 5 and bus 7 were added. 0.0648 p.u. capacitor at bus 8 was also added. The sample duration is 7 seconds as explained in the last paragraph. Therefore, the second control action happens at $t = 8.2$ seconds. The third, fourth and fifth control steps happen at 15.2 seconds, 22.2 seconds and 29.2 seconds respectively.

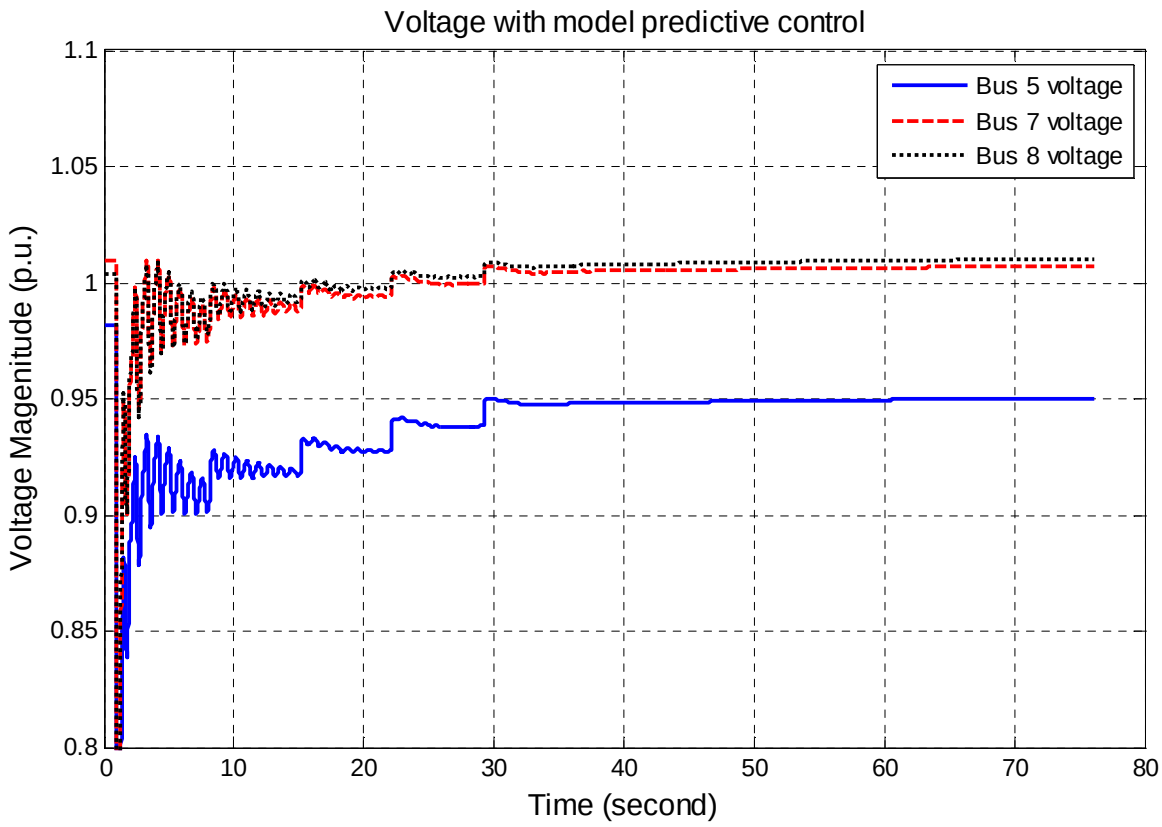

Figure 4.5 Voltage behavior of WECC system with MPC based control strategy

4.3.3.2 New England 10-generator 39-bus test system

System description Figure 4.6 represents the New England 10-generator 39-bus system. All the generator models have a fourth order state-space consisting of the rotor angle δ, the rotor speed ω, and the q-axis transient voltage e'_q and the d-axis transient voltage e'_d. The exception is the generator at bus 39 for which only a third-order model is used that does not include the d-axis transient voltage as part of the state-space. In addition, all the generators except generators at buses 34, 37 have automatic voltage regulators (AVRs), which are represented by fourth-order models. The load models used in the time domain simulation are exponential recovery dynamic loads. The total dimension of the state space is 131. The control variables include the shunt capacitors that are located at buses 16, 20, 22, 23 and 34. Under normal conditions, none of the shunt capacitors is in use.

Time(second)	1.2	8.2	15.2	22.2	29.2
Capacitor at bus 5 (p.u.)	0.1	0.1	0.1	0.1	0.0836
Capacitor at bus 7 (p.u.)	0.1	0	0	0	0
Capacitor at bus 8 (p.u.)	0.0648	0	0	0	0

Table 4.1 The resulting control strategy for WECC system

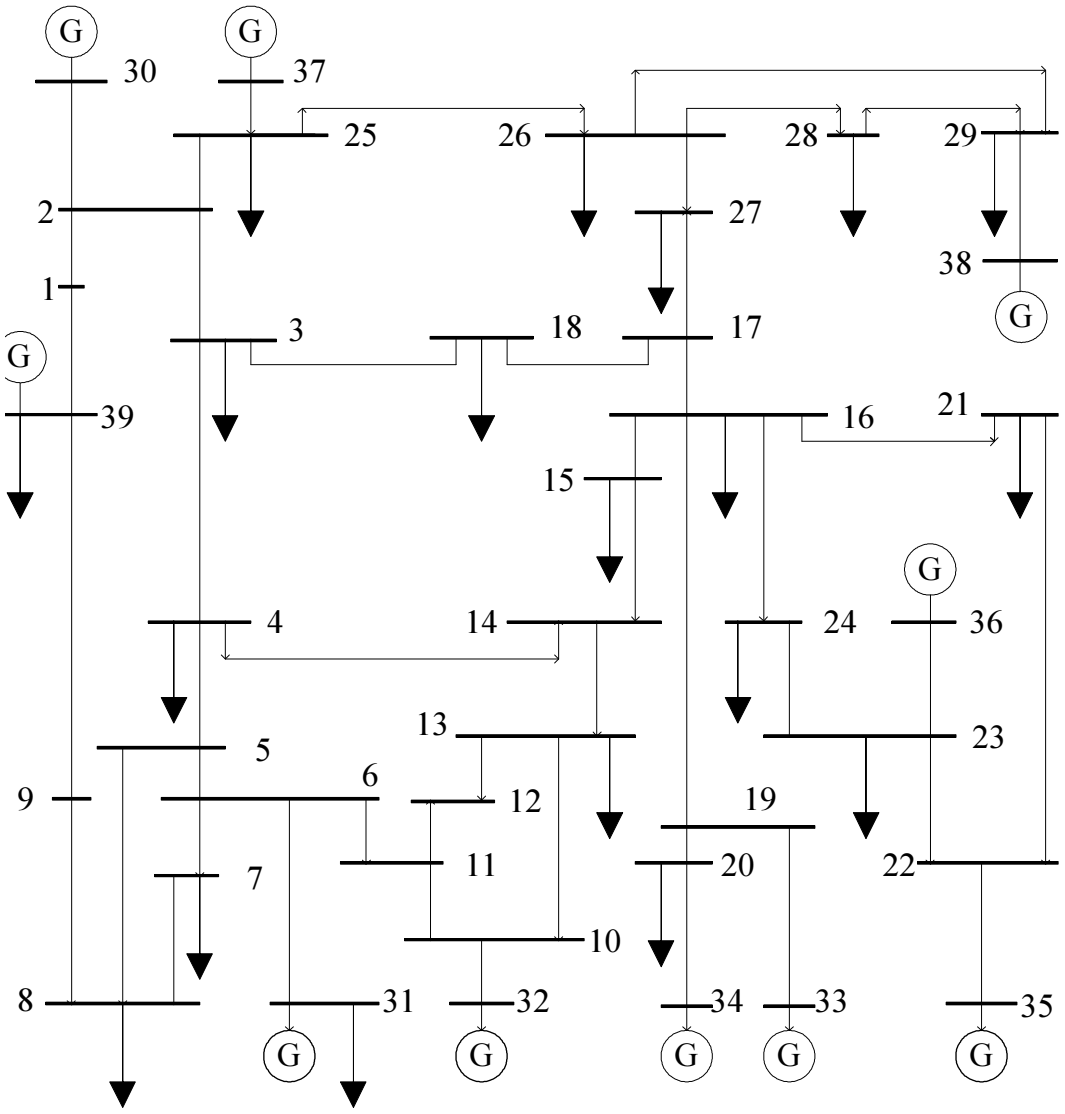

Figure 4.6 New England 10-generator 39-bus test system

Fault scenario The contingency considered here is a three-phase to ground fault at bus 21 at $t = 1.0$ second, which is cleared at $t = 1.1$ seconds and by tripping of the transmission line between bus 21 and bus 22. The voltage drops dramatically when the fault occurs as seen in Figure 4.7. After the fault is cleared at 1.1 seconds, the voltages recover around 0.95 p.u, although some oscillations proceed. About 30 seconds later, the oscillations disappear, but all the voltages start to decline very slowly. Then around 2 minutes later, the voltages collapse. One reason for the voltage recovery is the presence of generator automatic voltage regulators. When the system voltage drops following the fault, AVRs start to increase the generator excitation voltages so as to support the system voltage. However, AVRs have their upper limits. At the same time, the exponential recovery of the loads during the voltage disturbance worsens the operation of the system. The system can not fully recover from the contingency considering these two factors, which lead to the voltage collapse.

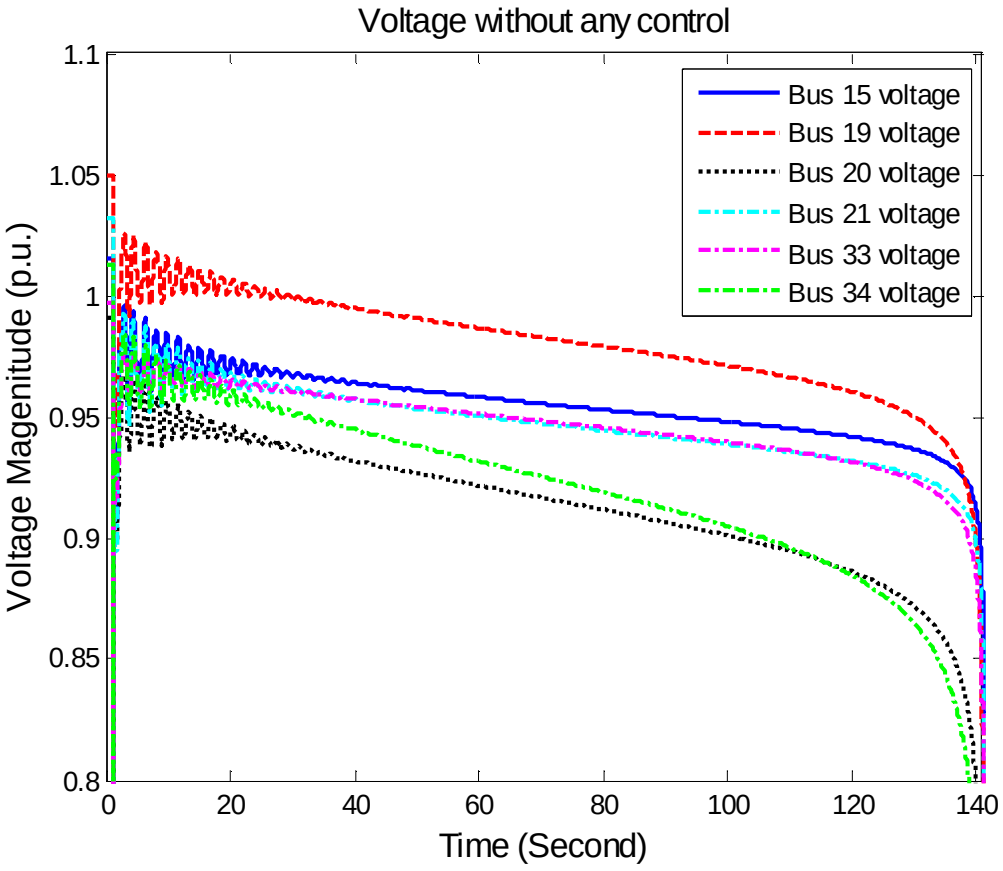

Figure 4.7 Voltage behavior of New England system without MPC control

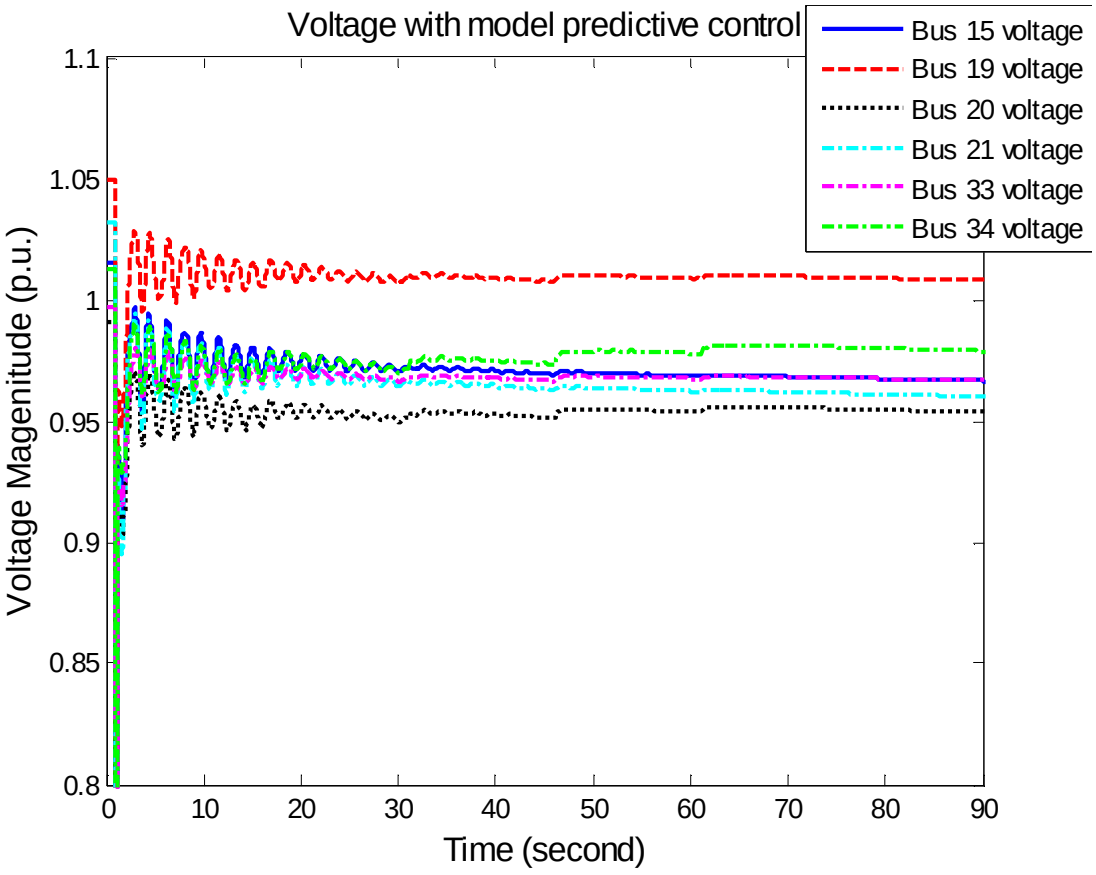

Figure 4.8 Voltage behavior of New England system with MPC control

Simulation result In this example, we have chosen prediction horizon T_p to be 80 seconds (the time in which voltage drops by nearly 10% at bus 20). T_c has been chosen to be 75 seconds. We found that a sample duration of $T_s = 15$ seconds works well for this example, and so we have the number of control steps: $N = \frac{T_c}{T_s} = \frac{75}{15} = 5$. The control strategy is determined by our model predictive control approach. The system response with MPC in place is shown in Fig. 4.8. The corresponding control strategy is shown in Table 4.2. The first control step happens right after the fault is cleared, i.e. 1.1 seconds. Since the sampling interval is 15 seconds, the second control happens at 16.1 seconds. The third, fourth and fifth control steps happen at 31.1 seconds, 46.1 seconds and 61.1 seconds respectively.

Time(second)	1.2	16.2	31.2	46.2	61.2
Capacitor at bus 16 (p.u.)	0	0	0	0	0
Capacitor at bus 20 (p.u.)	0	0	0	0	0
Capacitor at bus 22 (p.u.)	0	0	0	0	0
Capacitor at bus 23 (p.u.)	0	0	0	0	0
Capacitor at bus 34(p.u.)	0.1	0.1	0.1	0.1	0.0601

Table 4.2 The resulting control strategy for New England system

4.3.4 Comparison with traditional local feedback control

Shunt capacitors such as SVCs can also be used as in the setting of traditional local feedback control. The mathematical formulation of the local feedback control can be expressed as follows.

$$\dot{B} = \frac{1}{T_r}(K_r(V_{ref} - V) - B) \tag{4.26}$$

where K_r is regulation gain, V_{ref} is reference voltage, T_r is regulation time constant. V is the voltage magnitude of the regulated bus. B is the control amount. For the traditional local feedback control, shunt capacitor adjusts its output based on the voltage of the controlled bus.

Compared with traditional local feedback control, the proposed control scheme is more effective since it involves global state feedback and global control. The state of the entire power system is taken into consideration in deciding the global control. The WECC system discussed in subsection 4.3.3 can be used to illustrate this point. Suppose there are two shunt capacitors in the WECC system which are located at buses 5 and 6. Both SVCs have a capacity of 0.5 p.u.. The system data and fault scenario are the same as in subsection 4.3.3. Under no fault, the voltage magnitudes of buses 5 and 6 are 0.9819 p.u. and 0.9981 p.u. respectively. For local feedback control we set these values as the reference voltages at buses 5 and 6 respectively. Therefore, when there is no fault, the outputs of the shunt capacitors are zero. Suppose the regulation gain K_r is 100 and the regulation time constant T_r is 0.5 second. After the fault happens, Figure 4.9 depicts the dynamic behavior of voltage magnitudes at buses 5 and 6. Although the voltage at bus 6 is acceptable, the voltage at bus 5 is unsatisfactory (< 0.95 p.u.). Figure 4.10 shows the outputs of the SVCs at buses 5 and 6. Under no fault, the output

of the SVCs are zero. When fault happens, the voltage at bus 6 drops dramatically, and the output of SVC at bus 6 increases immediately based on the local feedback control to boost the voltage at bus 6. However, after around 5 seconds, the output of the SVC returns to zero since the voltage at bus 6 is greater than the reference value. The output of the SVC at bus 5 reaches its maximum value. Yet the voltage magnitude at bus 5 remains below the desired value. From this simulation, we can see that local feedback control based SVC only maintains the voltage of the regulated bus. It doesn't offer control for any unsatisfactory voltage behavior at other buses.

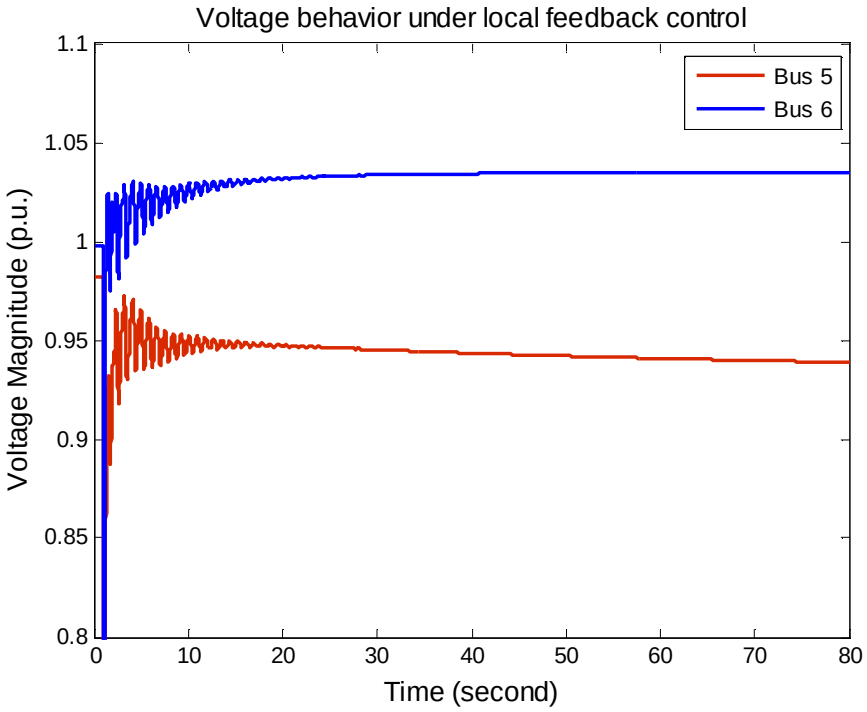

Figure 4.9 Voltage behavior of WECC system under local feedback control

For the case discussed above, we also use the proposed MPC-based method to design control. The parameters for the MPC control are the same as in subsection 4.3.3. The resulting control strategy is described as follows. At time 1.2 seconds, 0.5 p.u. of SVC control is added at bus 5 and 0.123 p.u. of SVC control is added at bus 6. At times 8.2 seconds and 15.2 seconds no control is added. At time 22.2 seconds, 0.0053 p.u. control is added at bus 6. At time 29.2 seconds, another 0.005 p.u. of SVC control is added at bus 6. The voltage behaviors at buses

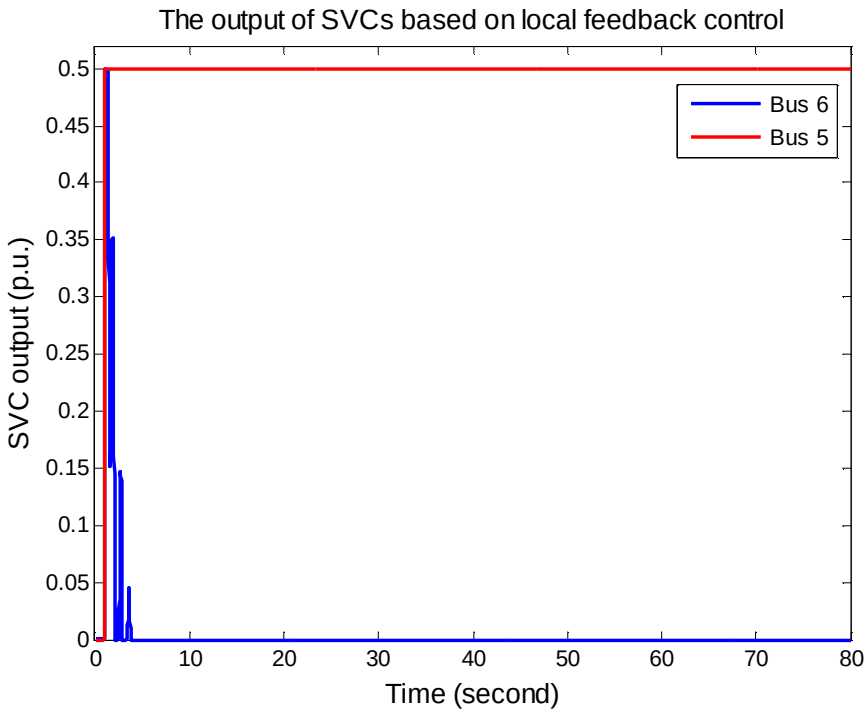

Figure 4.10 The output of SVC based on local feedback control

5 and 6 under the MPC based control design are shown in Figure 4.11. From this figure, we can see that voltage behavior at bus 5 under the proposed method is better than that under local feedback control. From this simulation, we can see that the main difference between the proposed method and the local feedback control is that the proposed method makes use of all the available controls in the system to improve voltage performance of all the buses. In contrast, the local feedback control based method makes use of only the local controls. (In the above example, control at bus 6 is not being used to compensate for performance at bus 5.)

4.3.5 Robustness study

The impact of data uncertainty on the performance of model based control methodologies is an important issue. In this subsection, the designed control is tested for robustness over different operating conditions using time domain simulation. Our study is based on the 9-bus 3-generator WECC example of subsection 4.3.3 for which the control scheme is as shown in Table 4.1. Since load plays an important role in voltage stability problem, our robustness

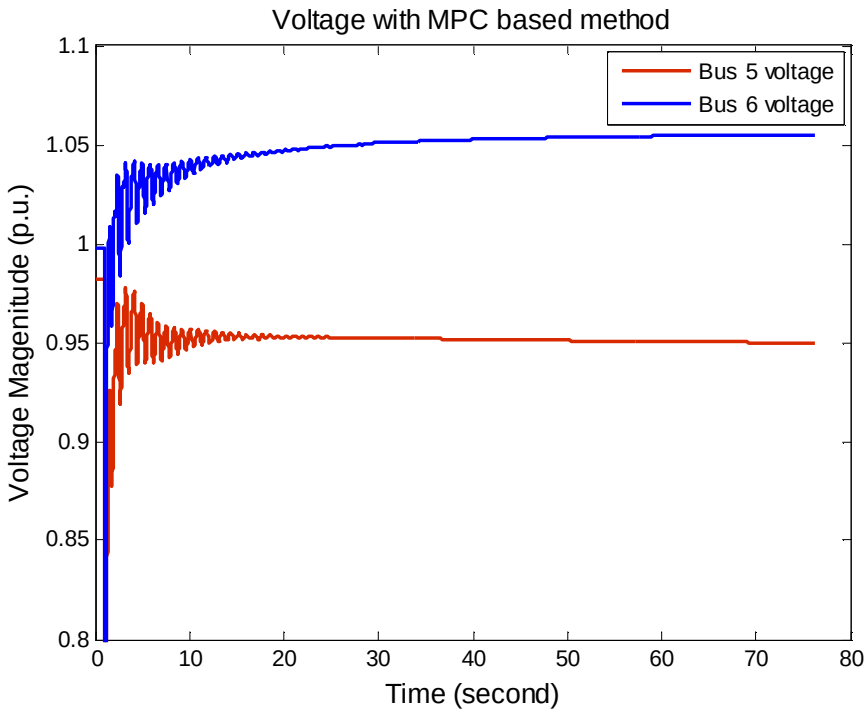

Figure 4.11 Voltage behavior of WECC system with MPC

study mainly focuses on the effect of load change, and consists of two parts. The first part is to study the effect of base case load variation on the robustness of the designed control. The second part studies the robustness of the designed control when random disturbances happen on the dynamic state variables of the load model.

4.3.5.1 Base case load increase

This part studies the robustness of the designed control when the total base case load increases. Figure 4.12 shows the voltage behavior of 1 % load increase. From this figure, we can see that the control scheme is still valid under the small load variation. Figure 4.13 indicates the voltage behavior of the same system with 3 % load increase. Although the voltages are stable, the voltage magnitude on bus 5 is lower than 0.95 p.u.. This study shows, under small load variation, the designed control is still valid. However, the case is not true under a larger disturbance. One way to improve the robustness of the designed control can be increased a little bit of the lower boundary of the vulnerable bus voltages in the constraints of

the optimization.

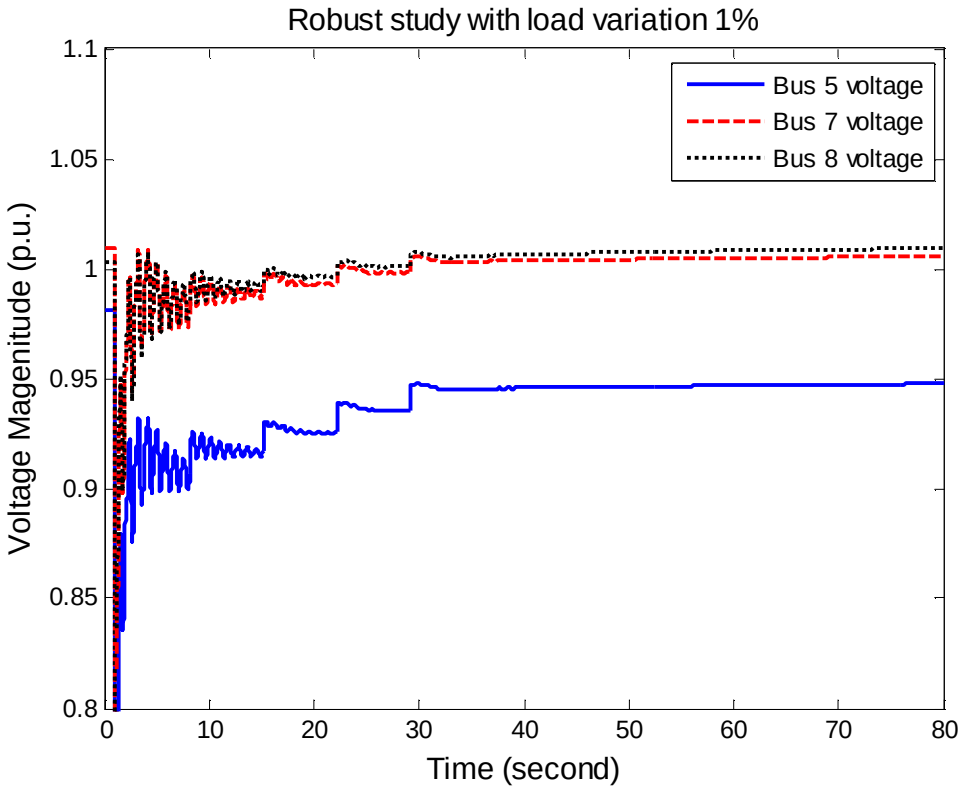

Figure 4.12 Voltage behavior with the designed control under 1% load increase

4.3.5.2 Random disturbance on an individual load

Besides the base case load change, we also study the effect of random disturbance on the dynamic state variable of an individual load. Assume the random disturbance is represented by a statistical variable with normal distribution whose mean is zero and variance is 1. In our study, a Matlab function *Normrnd* is used to generate the disturbance. The disturbance is imposed to the active power recovery P_r of the load at bus 6 at control sampling point 3. The first disturbance generated by the the Matlab program is 0.7258 increase of the dynamic state variable of the exponential recovery load model at bus 6. The voltage behavior under such disturbance is shown in Figure 4.14. The second disturbance is 0.5883 decrease of the same dynamic state variable. Figure 4.15 indicates the dynamic voltage behavior under the

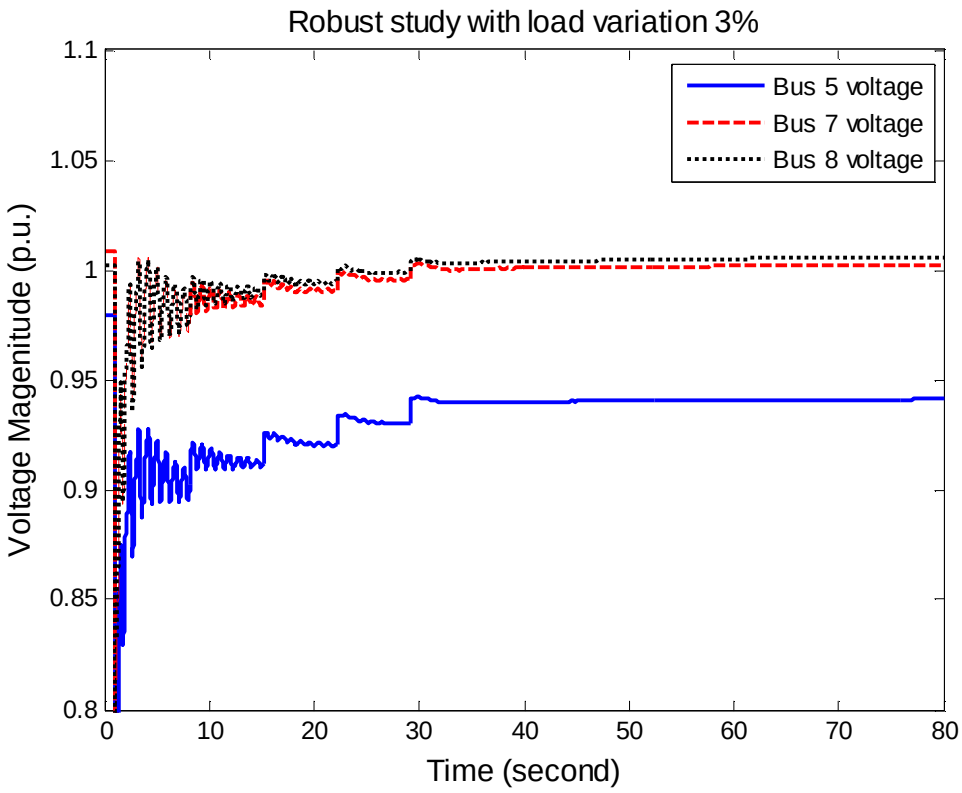

Figure 4.13 Voltage behavior with the designed control under 3% load increase

disturbance. These two figures show that the designed control has a certain robustness against random load disturbances.

4.4 Security constrained emergency voltage stabilization

4.4.1 Introduction

Power system security refers to the degree of risk of its ability to survive imminent disturbances (contingencies) without interruption of customer service (61). It is concerned with the robustness of the system to imminent disturbances. It depends on the severity of the disturbances as well as the system operating conditions. Many security indexes have been developed to study the degree of power system security. (1) and (2) propose a security performance index considering the overloads and voltage limit violations. The weighted value of the impact of overload of the network devices and voltage limits violations is used for classifica-

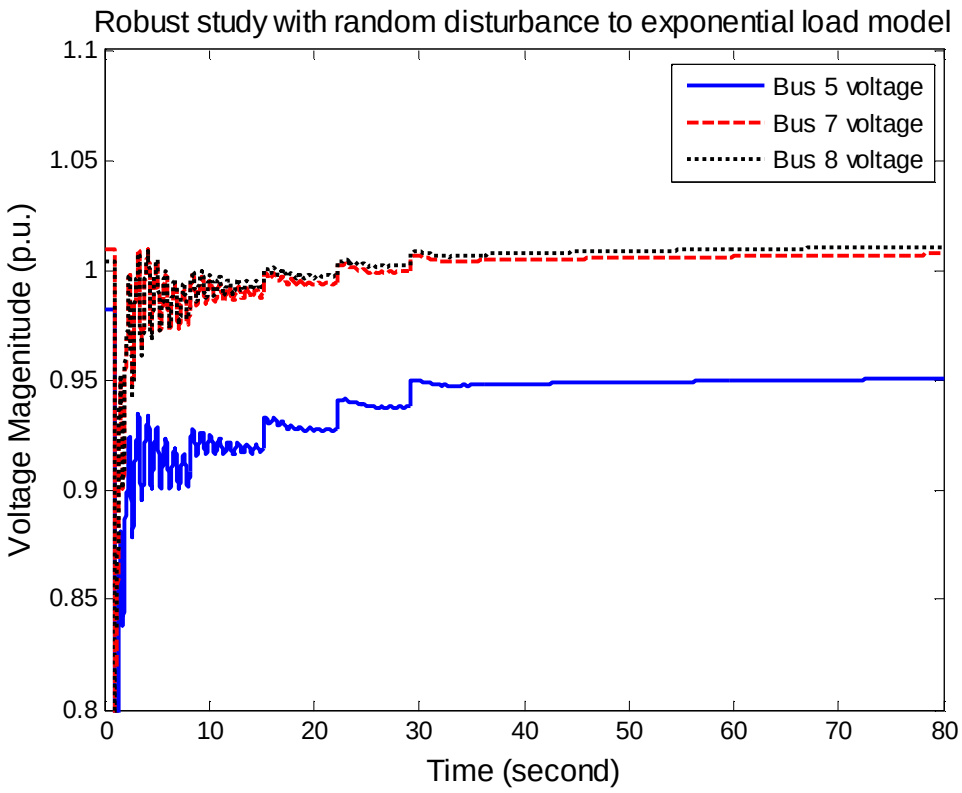

Figure 4.14 Voltage behavior with the designed control with 0.7258 increase for dynamic state variable 17

tion and screening of the contingencies. The computation is based on power flow analysis. A vulnerability index is proposed in (92) to give a comprehensive representation of power system security status. This comprehensive index takes account of generator real power and reactive power output status, voltage performance, individual loadability, branch flow and system loss. The larger the vulnerability index value is, the more vulnerable the system condition is. The calculation of the index is based on static analysis. A system margin is presented in (62) for evaluation of adequacy of a composite power system based on the concept of maximum load carrying ratio. The maximum load which the power system can supply without raising any system problems is calculated by a DC power flow and linear programming. Besides the static based security indices, many dynamic based security indices have also been studied. A fuzzy transient stability index is developed in (72). The index is based on the initial generator rotor accelerations after a particular disturbance incident which considers the power system oper-

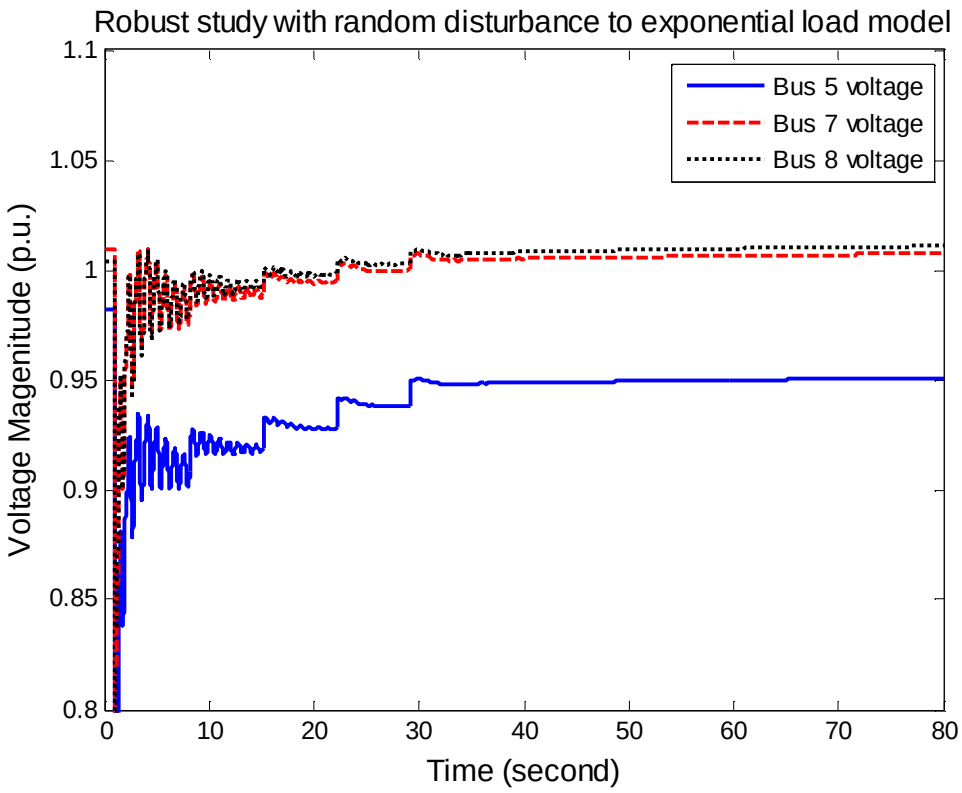

Figure 4.15 Voltage behavior with the designed control with 0.5883 decrease for dynamic state variable 17

ating state before the occurrence of the disturbance (loading, network configuration, capacity, etc) as well as the type and location of the fault. A pattern recognition method is used to assign an index of power system transient stability to the system operating states. In addition, a severity index consisting of coherency concept, transient energy conversion between kinetic energy and potential energy and three dot products of system variables is proposed in the dynamic security analysis (34).

The control strategy discussed in the previous section does not have a provision to include constraints on the security margin of a system. As a result, the security margin (voltage stability margin) of the computed optimal control strategy may not be satisfactory. In such a case, following the application of MPC based control, a small disturbance can result in a negative voltage stability margin and cause a voltage collapse. Hence there is a need to further extend the proposed design to account for the security margin (which must be greater than a

pre-specified lower bound). In our work, voltage stability margin is adopted to indicate how secure power systems are. The sensitivities of the voltage stability margin on the controls are used to indicate the effectiveness of the controls on system security.

4.4.2 Voltage stability margin

Voltage stability margin is an indication of how far the post-transient operating point is from the voltage collapse point. It is an index of system security. Consider a system with the DAE model

$$\dot{x} = f(x, y, u, \lambda)$$

$$0 = g(x, y, u, \lambda)$$

where x represents a vector of state variables, y represents a vector of algebraic variables, u is a vector of control variables and λ is a parameter.

Let $r(\lambda) \in \Re^{L\times 1}$ be a vector of variables which are parameterized by λ and a change in which (due to a change in λ) affects the system stability. (For the power system application, this will consist of load and generation power.) The l^{th} component of $r(\lambda)$ is denoted as $r_l(\lambda)$ which increases linearly with λ as:

$$r_l(\lambda) = (1 + K_l\lambda)r_l(0)$$

Here, K_l is a constant and $r_l(0)$ represents the base case value of the l^{th} component of $r(\lambda)$.

If λ increases slowly and continuously, a bifurcation point is reached beyond which the system loses stability. Let λ^* be the value of λ at this point, then this implies that

$$0 = f(x, y, u, \lambda), \quad 0 = g(x, y, u, \lambda)$$

has no solution when $\lambda > \lambda^*$. The stability margin is defined as

$$SM = \sum_{l=1}^{l=L}(r_l(\lambda^*) - r_l(0)) = \lambda^* \sum_{l=1}^{l=L} K_l r_l(0)$$

The rate change of stability margin with respect to the control variable u is known as the margin sensitivity with respect to u

$$SM_u = \frac{\partial SM}{\partial u} = \frac{\partial \lambda^*}{\partial u} \sum_{l=1}^{l=L} K_l r_l(0)$$

At the bifurcation point it holds that,

$$\frac{\partial \lambda^*}{\partial u} = -\frac{\omega^* F_u^*}{\omega^* F_\lambda^*}, \tag{4.27}$$

where ω^* is the left eigenvector corresponding to the zero eigenvalue of the system Jacobian $F_x^* = [f_x^*, f_y^*; g_x^*, g_y^*]$; $F_\lambda^* = [f_\lambda^*; g_\lambda^*]$ is the derivative of system equations with respect to the bifurcation parameter λ; and $F_u^* = [f_u^*; g_u^*]$ is the derivative of system equations to the control variable u. (A variable superscripted with * denotes the value of that variable at the bifurcation point.)

In a power system, the voltage stability margin can also be defined based on this concept. For this, the real power P_l at bus l corresponds to the l^{th} component of $r(\lambda)$ and satisfies:

$$P_l = (1 + K_{lp}\lambda)P_{l0}$$

where P_{l0} is the base case real power load at bus l and K_{lp} is the gain factor characterizing the real power increase pattern. λ is known as loading parameter. Then the *voltage stability margin*, defined as the distance between the current operating point and the bifurcation point, can be expressed as:

$$SM = \sum_{l=1}^{L} P_l^* - \sum_{l=1}^{L} P_l = \lambda^* \sum_{l=1}^{L} K_{lp} P_l$$

A continuation power flow method is presented in (3; 8; 16) to trace the bifurcation point, through which the voltage stability margin can be calculated. Figure 4.16 shows voltage stability margin of a nominal system. This figure shows the change of voltage with respect to the increase of total real power consumption when load increases gradually in the system. Suppose under normal condition, the system has a total system load indicated in Figure 4.16. The voltage stability margin SM is defined as the difference between the total load at the voltage collapse point and that of the nominal system.

The *voltage stability margin sensitivity* SM_u with respect to the control variable u is given by,

$$SM_u = \frac{\partial SM}{\partial u} = \frac{\partial \lambda^*}{\partial u} \sum_{l=1}^{L} K_{lp} P_{l0},$$

where $\frac{\partial \lambda^*}{\partial u}$ can be calculated by Equation (4.27). A detailed derivation of the sensitivity calculation is presented in (91) .

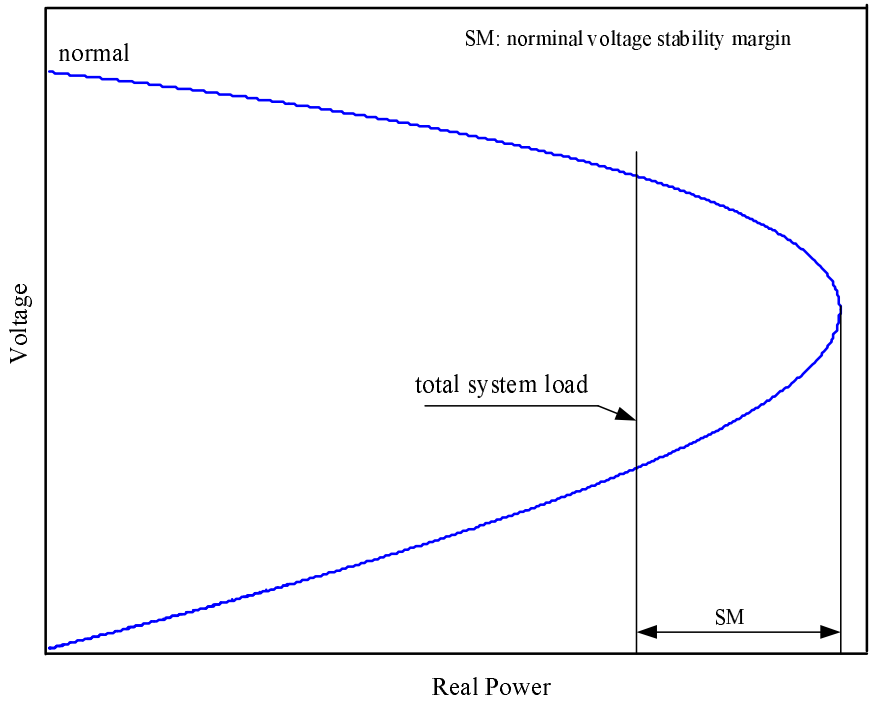

Figure 4.16 Voltage stability margin illustration

In order to design a protection scheme involving the system security requirement, voltage stability margin sensitivity will be used to determine the influence of control on voltage stability.

4.4.3 Problem formulation

The purpose of this work is to determine an optimal capacitor switching sequence and amounts given their locations and capacities to satisfy the requirements of voltage performance and voltage stability margin. Detect whether a certain pre-identified contingency has occurred (Note the approach can also work for contingencies that are not necessarily pre-identified, as long as they can be detected in real-time.). If the system performance is not satisfactory, for instance, voltages are out of the their limits or voltage collapse happens, an optimal control strategy is identified based on a decreasing horizon MPC algorithm consisting of the amount and sequence of shunt capacitor switching. This control strategy not only stabilizes system voltages within acceptable ranges following the contingency, but also ensures a desired voltage stability margin. The control changes only at the sampling instants. The procedure to

determine the control strategy at time t_k based on MPC is as follows:

(1) At time t_k (i.e. the $(k+1)^{th}$ sampling instant), an estimate of the current state $x(t_k)$ is acquired. Power system state estimators can provide an estimate of power flow states. The internal states of dynamic components, such as generators, AVRs, and speed governors can be estimated from those power flow states. The nominal power system evolves according to Equations (4.6) and (4.7). Here, $u = \{B_m^0 + \sum_{i=0}^{k-1} \Delta B_{m1}^i\}_{m=1}^{m=M}$ is the control variable (i.e. amounts of shunt capacitors currently in use). B_m^0 is the amounts of shunt capacitors that exist at time 0. $\sum_{i=0}^{k-1} \Delta B_{m1}^i$ is the amounts of shunt capacitors that were added over time $[0, t_k - T_s]$.

Time domain simulation is used to obtain the trajectory of the nominal system (4.6) and (4.7), starting from the state $x(t_k)$ at time t_k to the end of prediction horizon $t_k + T_p$. At the same time, the trajectory sensitivity of bus voltages with respect to the shunt capacitors to be added at instants $t_k + (n-1)T_s, n = 1 \ldots N-k$ is obtained and denoted as $V_{B_{mn}}^{kj}(t)$ (see below for the explanation of notation).

Also the sensitivity of voltage stability margin with respect to shunt capacitor at location m is calculated based on a continuation power flow program. It is expressed as $SM_{B_m}^k$ in the optimization.

(2) At time t_k, solve the optimization problem over the prediction horizon $[t_k, t_k + T_p]$ and a control horizon $[t_k, t_k + (N-k)T_s]$ as stated in (4.28)-(4.33). The objective of optimization is to minimize a weighted sum of the cumulative voltage deviations and the cumulative cost of capacitive controls as shown in Equation (4.28). Equation (4.29) constraints the amount of control m to be added at time $t_k + (n-1)T_s$. Equation (4.30) constraints the total amount of control m to be added over $[t_k, t_k + (N-k)T_s]$. Equation (4.31) constraints the voltage fluctuation at time $t \in [t_k, t_k + T_p]$. Equation (4.32) constraints the voltage stability margin.

Minimize

$$\int_{t_k}^{t_k+T_p} (\widehat{V}^k(t) - V_{ref})' R (\widehat{V}^k(t) - V_{ref}) dt + \sum_{mn} W_{mn} \Delta B_{mn}^k \tag{4.28}$$

Subject to

$$\Delta B_m^{min} \leq \Delta B_{mn}^k \leq \Delta B_m^{max} \tag{4.29}$$

$$B_m^{min} \leq B_m^0 + \sum_{i=0}^{k-1} \Delta B_{m1}^i + \sum_{n=1}^{N-k} \Delta B_{mn}^k \leq B_m^{max} \tag{4.30}$$

$$V_{min}^{kj}(t) \leq V^{kj}(t) + \sum_{m=1}^{M} \sum_{n=1}^{N-k} V_{B_{mn}}^{kj}(t) \Delta B_{mn}^k \leq V_{max}^{kj}(t) \tag{4.31}$$

$$SM^{k-1} + \sum_{m=1}^{M} SM_{B_m}^k (\sum_{n=1}^{N-k} \Delta B_{mn}^k) \geq SM_D \tag{4.32}$$

$$\Delta B_{mn}^k \geq 0 \tag{4.33}$$

Here,

- R is the weighting matrix. $\widehat{V}^k(t)$ is the voltage vector at time $t \in [t_k, t_k + T_P]$ as predicted at the sampling instant t_k.
- W_{mn} is the weight for the cost of control m to be added at time $t_k + (n-1)T_s$.
- M is the total number of control variables, i.e. the number of shunt capacitor locations.
- N is the total number of control steps.
- ΔB_{mn}^k is the amount of control m to be added at time $t_k + (n-1)T_s$ in iteration k.
- $\Delta B_m^{min} \in \Re$ is the minimum amount of control m to be added at any step, typically 0.
- $\Delta B_m^{max} \in \Re$ is the maximum amount of control m to be added at any step.
- ΔB_{m1}^i is the amount of control m implemented at the control sampling point $t_i, i = 0, ...k-1$.

- $B_m^{min} \in \Re$ is the minimum amount of control m that must be used, typically 0.
- $B_m^{max} \in \Re$ is the maximum available amount of control m.
- $V^{kj}(t) \in \Re$ is the voltage of bus j at time $t(t_k \leq t \leq t_k + T_p)$ of the nominal system at time t_k.
- $V_{min}^{kj}(t)$ is the minimum voltage at bus j desired at time $t_k \leq t \leq t_k + T_p$.
- $V_{max}^{kj}(t)$ is the maximum voltage at bus j desired at time $t_k \leq t \leq t_k + T_p$.
- $V_{B_{mn}}^{kj}(t)$ is the trajectory sensitivity of voltage at bus j at time $t_k \leq t \leq t_k + T_p$ with respect to control m added at time $t_k + (n-1)T_s$.
- SM^{k-1} is the voltage stability margin at time $t_k - T_s$.
- $SM_{B_m}^k$ is the stability margin sensitivity with respect to capacitor m at time t_k.
- SM_D is the desirable stability margin for the system.

(3) At time t_k, a solution of the optimization problem (4.28)-(4.32) computes a sequence of controls ΔB_{mn}^k. Add only the first control ΔB_{m1}^k at time t_k and observe or estimate the system state $x(t_{k+1})$ at time $t_{k+1} = t_k + T_s$.

(4) Increase k to $k+1$ and repeat steps (1)-(3) until $k = N-1$.

4.4.4 Application to New England 39 bus system

Figure 4.6 shows the New England 10-generator 39-bus system. A fourth-order generator model is used with the exception that a third-order model is used for the generator at bus 39. In addition, all generators excluding those at buses 34, 37 have automatic voltage regulators (AVRs), which are represented by fourth-order models. The loads are represented by the exponential recovery dynamic models. The control variables are the shunt capacitors at buses 16, 17, 19, 21 and 24. Under normal conditions, none of the shunt capacitors are in use.

4.4.4.1 Fault scenario

The contingency considered here is a three-phase-to-ground fault at bus 21 at $t = 1.0$ second, which is cleared at $t = 1.02$ seconds by tripping of the transmission line between buses

21 and 22. Bus voltages drop dramatically when the fault occurs as shown in Figure 4.17. After the fault is cleared at 1.02 seconds, the voltages recover around 0.95 p.u, although some oscillations follow. About 20 seconds later, the oscillations are damped out, but the voltages start to decline slowly because of the exponential recovery of the loads. Around 2 minutes later, the voltages collapse. According to a continuation power-flow based analysis, the post-fault power system has a voltage stability margin of 32.4%. However as can be seen from simulation (which considers the dynamic evolution), the system is unable to reach the associated post-fault equilibrium point. This illustrates the limitation of the control design based on a purely static analysis. Through our MPC based approach (which incorporates the dynamic analysis) we are able to ensure that the post-fault system has a desired voltage stability margin of 35%, and the system is able to reach the associated post-fault equilibrium point.

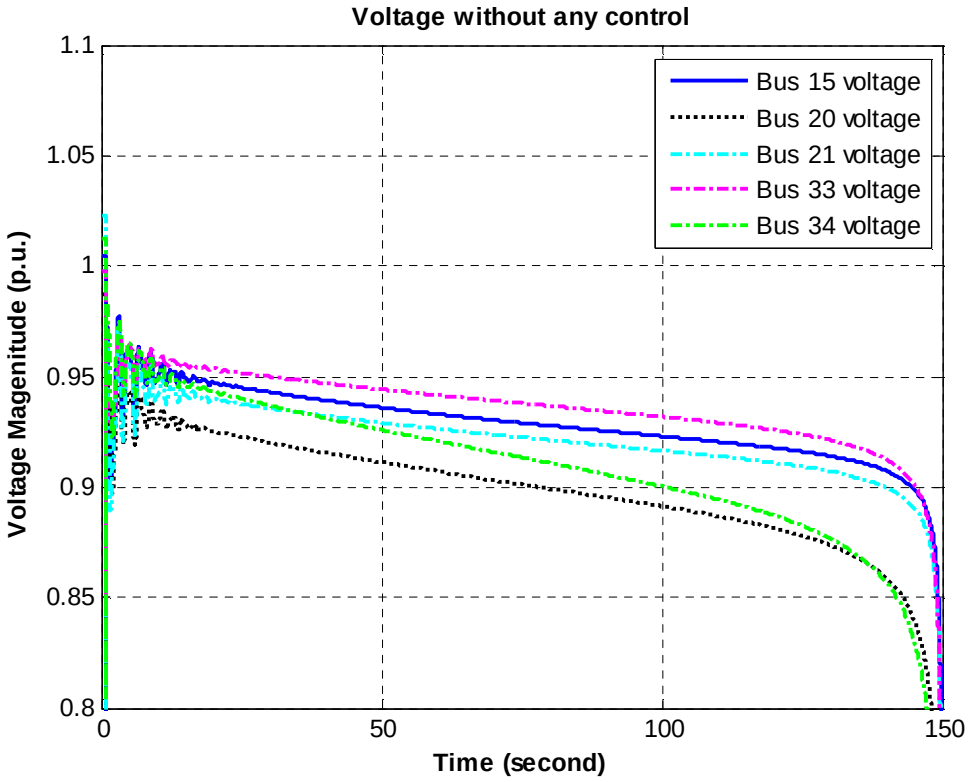

Figure 4.17 New England system voltage behavior without MPC control

4.4.4.2 Simulation result

After the fault is cleared, the shunt capacitors determined by MPC are applied to stabilize the voltage. The parameters for the MPC are as following: $T_p = 130$ seconds, $T_s = 20$ seconds, $N = 6$. An optimal control strategy that stabilizes voltage and ensures the security of post-transient power system is found based on the algorithm introduced in Section 4.4.3. The final control strategy is indicated in Table 4.3. Figure 4.18 shows the voltage response with the security constrained control strategy. As shown in the figure, the controls stabilize the system and bring voltages within limits. The post-fault power system has a voltage stability margin of 35.0%, which is the required value.

Time(second)	1.2	21.2	41.2	61.2	81.2	101.2
Capacitor at bus 16 (p.u.)	0	0.2	0.2	0	0.025	0.1
Capacitor at bus 17 (p.u.)	0.2	0	0	0	0.025	0
Capacitor at bus 19 (p.u.)	0	0.1919	0.0556	0	0.2	0
Capacitor at bus 21 (p.u.)	0.2	0.0200	0	0.2	0.025	0
Capacitor at bus 24(p.u.)	0.0333	0.2	0.15	0.1	0.025	0.2

Table 4.3 Control strategy for New England system

4.5 Model predictive control based coordinated dynamic voltage control

4.5.1 Introduction

The voltage problem is a local as well as a regional problem. One approach to study the coordinated voltage control is based on system response. In other words, direct telemetry of voltage at power system pivot nodes are used as feedback to design voltage control. This approach are popular in European countries and some south American countries. The coordinated control falls into three hierarchical levels: primary voltage control, secondary voltage control and tertiary voltage control according to the control response time and effective scale (96). The hierarchical levels are illustrated by Figure 4.19.

The primary control level basically is related with unit and plant control. The units in a

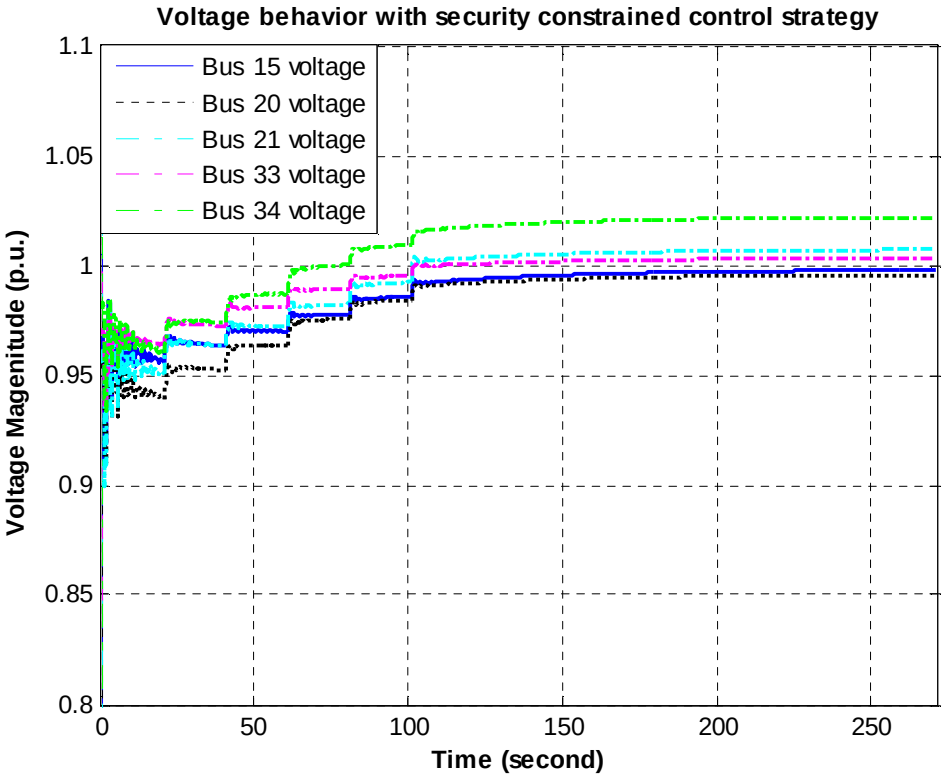

Figure 4.18 New England voltage behavior with security constrained MPC control

power plant usually are connected to a power grid through step-up transformers. Automatic voltage regulators (AVRs) directly installed on generators can be used to control generator terminal voltage. This control can also be applied to maintain the high-side voltage of step-up transformers equal to specific values to avoid reactive power interchange among plant units. Primary actions are very fast, in a time frame of few seconds. It is considered as a local control.

The secondary voltage control level is to adjust and to maintain the voltage profile inside a network area. Control actions in this level include var compensation devices like capacitors, inductors, synchronous or static voltage compensators and transformer load tap changers. Definition and implementation of secondary voltage control level are quite dependent on philosophy of each utility. The time frame for secondary control is from several seconds to minutes. It is considered a regional control.

The purpose of tertiary voltage control level is to increase the system's operating security

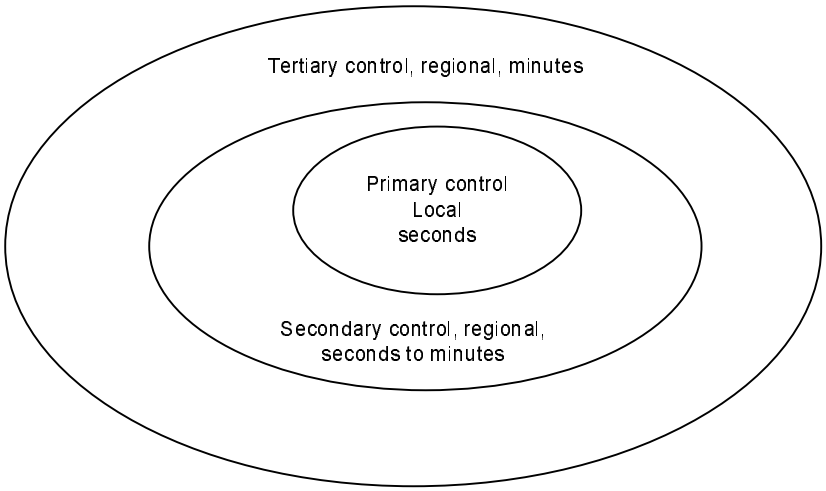

Figure 4.19 Hierarchical voltage control levels

and efficiency through centralized coordination of the decentralized secondary voltage controllers. The time scale of this control is several minutes or on demand.

The characteristics of the hierarchical coordinated voltage control system applied on the Italian transmission grid are introduced in (23; 24). The power plants adjust their reactive power output based on the voltage measured at pivot nodes. The hierarchical coordinated control scheme was studied on the French electrical system (96; 69). Spain (89), Belgium (40) as well as Brazil (93) have experiences to apply the secondary voltage control. Besides industry applications, some research work has been done on the response based coordinated voltage control. The work is based on static analysis. A knowledge based system for supervision and control of regional voltage profile and security using fuzzy logic is presented in (73). It involves the coordination of AVRs, shunt capacitors as well as the the high-side voltage set points at power plants.

Besides the response based control design, there also exists model based coordination control design. The motivation of model based coordination control design lies in the fact that local measurement sometime can not reflect the global system behavior. An example is provided in (45) to illustrate this situation. Paserba et. al. (82) discussed the coordination of distribution-level load tap changers (LTCs), mechanically-switched capacitors and static compensators (STATCOMs) to improve voltage profile and to reduce the mechanical switching

operations within the substation. Park et. al. (81) proposed a coordinated control method for LTCs and capacitors in distribution systems to reduce power loss and to improve the voltage profile during a day. Kim et. al. (55) presented an artificial neural network based coordination control scheme for LTCs and STATCOMs to minimize the amount of transformer tap changes and STATCOM outputs while maintaining acceptable voltage magnitudes at substation buses. The above work is based on power system steady state analysis. Some work has also been done to design a coordinated voltage control strategy by considering dynamic response of a power system. Larsson et. al. (63) presented a method of coordination of load shedding, capacitor switching and tap changers using model preventive control. The prediction of states is based on the numerical simulation of nonlinear differential algebraic equations (DAEs) directly and Euler state prediction. A tree search method is adopted to solve the optimization. Larsson et. al. (64) proposed a coordination of generator voltage set-points, load shedding and LTCs using a heuristic search and the predictive control. The prediction of states is based on the linearization of nonlinear DAEs. Wen et. al. (99) presented an optimal coordinated voltage control using model predictive control. The controls used include: shunt capacitors, load shedding, tap changers and generator voltage set-points. The prediction of voltage trajectory is based on the Euler state prediction. The optimization problem is solved by a pseudo gradient evolutionary programming (PGEP) technique. Zima et. al. (103) presented a coordinated voltage control by using tap changers, load shedding, and generator voltage setting points . The prediction of the voltage trajectories is based on trajectory sensitivity. The optimization is solved by a mixed integer program.

In this section, we design a coordinated control of SVCs, LTCs and load shedding to improve voltage performance following disturbances. Given the locations and capabilities of SVCs, LTCs and interruptible load, the control design problem is to determine the control sequences and the control amounts to satisfy voltage performance requirements. MPC with a decreasing control horizon is adopted in the control design. At each MPC iteration, a mixed integer quadratic programming (MIQP) problem is solved. The objective function is to minimize a weighted sum of the cumulative voltage deviations and the cumulative cost of the

coordinated controls. Trajectory sensitivities are used to estimate the effect of controls on voltage trajectories. The decreasing control horizon MPC not only reduces the computation time, but also greatly helps the convergence of the optimization process. The iterative optimization process of MPC helps ensure that errors introduced due to trajectory sensitivities and any model inaccuracies are minimized.

4.5.2 Problem formulation and solution

The purpose of this work is to determine an optimal coordinated control strategy consisting of continuous and discrete power system controls to improve voltage performance and prevent voltage instability. If the occurrence of a certain pre-identified contingency is detected and the system performance is not satisfactory, for instance, voltages are out of the their limits, an optimal coordinated control strategy is identified based on a decreasing horizon MPC algorithm consisting of the amount and sequence of dissimilar voltage control equipments such as SVCs, transformer tap changers and load shedding. The control changes only at the sampling instants. Let T_p be the prediction horizon, T_c be the control horizon, T_s be the control sampling interval, and $N = \frac{T_c}{T_s}$ be the total number of control steps. The procedure to determine the control strategy at the k^{th} sampling instant is as follows:

(1) At time t_k (i.e. the $(k+1)^{th}$ sampling instant), an estimate of the current state $x(t_k)$ is obtained. The nominal power system evolves according to Equations (4.21) and (4.22).

$$\dot{x} = f(x, y, u_c, u_d), \quad x(0) = x_0 \tag{4.34}$$

$$0 = g(x, y, u_c, u_d) \tag{4.35}$$

Here, $u_c = \{C_m^0 + \sum_{i=0}^{k-1} \Delta C_{m1}^i\}_{m=1}^{m=M_c}$ is the continuous control variable (e.g. amounts of SVC currently in use). C_m^0 is the amounts of continuous variables that exist at time 0. $\sum_{i=0}^{k-1} \Delta C_{m1}^i$ is the amounts of the continuous variable that were added over time $[0, t_k - T_s]$. $u_d = \{D_m^0 + \sum_{i=0}^{k-1} S_{m1}^i \Delta D_{m1}^i\}_{m=M_c+1}^{m=M_c+M_d}$ is the discrete control amount. D_m^0 is the amounts of discrete variables that exist at time 0. $\sum_{i=0}^{k-1} S_{m1}^i \Delta D_{m1}^i$ is the amount of the discrete control that were added over time $[0, t_k - T_s]$. Here S_{m1}^i is the step size

of the discrete actuator m at sampling point t_i, and ΔD^i_{m1} is the number of steps of the discrete actuator at time t_i.

Time domain simulation is used to obtain the trajectory of the nominal system (4.34) and (4.35), starting from the state $x(t_k)$ at time t_k to the end of prediction horizon t_k+T_p. At the same time, the trajectory sensitivities of bus voltages with respect to the continuous and discrete controls to be added at instants $t_k+(n-1)T_s, n=1\dots N-k$ are obtained and denoted as $V^{kj}_{C_{mn}}(t), V^{kj}_{D_{mn}}(t)$ (see below for the explanation of notation).

(2) At time t_k, solve the quadratic integer programming optimization problem over the prediction horizon $[t_k, t_k+T_p]$ and a control horizon $[t_k, t_k+(N-k)T_s]$ as stated in (4.36)-(4.43).

Minimize (with respect to ΔC^k_{mn} and ΔD^k_{mn})

$$\int_{t_k}^{t_k+T_p} (\widehat{V}^k(t)-V_{ref})' R (\widehat{V}^k(t)-V_{ref}) dt + \sum_{m=1}^{m=M_c}\sum_{n=1}^{n=N-k} W_{mn}\Delta C^k_{mn} + \sum_{m=M_c+1}^{m=M_c+M_d}\sum_{n=1}^{n=N-k} W_{mn} S^k_{mn}\Delta D^k_{mn} \quad (4.36)$$

Subject to

$$\Delta C^{min}_m \le \Delta C^k_{mn} \le \Delta C^{max}_m, \quad (4.37)$$

$$\Delta D^{min}_m \le \Delta D^k_{mn} \le \Delta D^{max}_m, \quad (4.38)$$

$$C^{min}_m \le C^0_m + \sum_{i=0}^{k-1}\Delta C^i_{m1} + \sum_{n=1}^{N-k}\Delta C^k_{mn} \le C^{max}_m \quad (4.39)$$

$$D^{min}_m \le D^0_m + \sum_{i=0}^{k-1} S^i_{m1}\Delta D^i_{m1} + \sum_{n=1}^{N-k} S^k_{mn}\Delta D^k_{mn} \le D^{max}_m \quad (4.40)$$

$$V^{kj}_{min}(t) \le V^{kj}(t) + \sum_{m=1}^{M_c}\sum_{n=1}^{N-k} V^{kj}_{C_{mn}}(t)\Delta C^k_{mn} + \sum_{m=M_c+1}^{M_c+M_d}\sum_{n=1}^{N-k} V^{kj}_{D_{mn}}(t) S^k_{mn}\Delta D^k_{mn} \le V^{kj}_{max}(t) \quad (4.41)$$

$$\Delta C^k_{mn} \ge 0, m=1,\cdots,M_c \quad (4.42)$$

$$\Delta D^k_{mn} \text{ is an integer, } m = M_c + 1, \cdots, M_c + M_d \tag{4.43}$$

Here,

- R is the weighting matrix.
- $\widehat{V}^k(t)$ is the voltage vector at time $t \in [t_k, t_k + T_P]$ as predicted at the sampling instant t_k.
- W_{mn} is the weight for the cost of control m to be added at time $t_k + (n-1)T_s$.
- M_c is the total number of continuous control variables, i.e. the number of available SVCs.
- M_d is the total number of discrete control variables, i.e. the number of available under load tap changer plus the number of load shedding candidate locations.
- N is the total number of control steps.
- ΔC^k_{mn} is the amount of continuous actuator m to be added at time $t_k + (n-1)T_s$ in iteration k.
- ΔD^k_{mn} is the number of steps of discrete actuator m to be added at time $t_k+(n-1)T_s$ in iteration k. It is an integer.
- S^k_{mn} is the step size of discrete actuator m at time $t_k + (n-1)T_s$ in iteration k.
- $\Delta C^{min}_m \in \Re$ is the minimum amount of continuous control m to be added at control sampling points, typically 0.
- $\Delta C^{max}_m \in \Re$ is the maximum amount of continuous control m to be added at control sampling points.
- $\Delta D^{min}_m \in \Re$ is the minimum number of steps of discrete control m to be added at control sampling points, typically 0.
- $\Delta D^{max}_m \in \Re$ is the maximum number of steps of discrete control m to be added at control sampling points.

- ΔC^i_{m1} is the amount of control m implemented at the control sampling point $t_i, i = 0, ..., k-1$.
- $C^{min}_m \in \Re$ is the minimum amount of continuous control m that must be used, typically 0.
- $C^{max}_m \in \Re$ is the maximum available amount of continuous control m.
- D^{min}_m is the minimum amount of discrete control m.
- D^{max}_m is the maximum available amount of discrete control$m$.
- $V^{kj}(t) \in \Re$ is the voltage of bus j at time $t(t_k \leq t \leq t_k + T_p)$ of the nominal system at time t_k.
- $V^{kj}_{min}(t)$ is the minimum voltage at bus j desired at time $t_k \leq t \leq t_k + T_p$.
- $V^{kj}_{max}(t)$ is the maximum voltage at bus j desired at time $t_k \leq t \leq t_k + T_p$.
- $V^{kj}_{C_{mn}}(t)$ is the trajectory sensitivity of the voltage at bus j at time $t_k \leq t \leq t_k + T_p$ with respect to the continuous control m added at time $t_k + (n-1)T_s$.
- $V^{kj}_{D_{mn}}(t)$ is the trajectory sensitivity of the voltage at bus j at time $t_k \leq t \leq t_k + T_p$ with respect to the discrete control m added at time $t_k + (n-1)T_s$.

The objective of the optimization is to minimize the voltage deviation and cumulative cost of continuous and discrete controls as shown in Equation (4.36). Equation (4.37) constraints the amount of the continuous control m to be added at time $t_k + (n-1)T_s$. Equation (4.38) is the control step constraints on discrete actuators. Equation (4.39) constraints the total amount of continuous control m to be added over $[t_k, t_k + (N - k)T_s]$. Equation (4.40) constraints the total amount of discrete control m to be added over $[t_k, t_k + (N - k)T_s]$. Equation (4.41) constraints the voltage fluctuation at time $t \in [t_k, t_k + T_p]$. The number of candidate control locations and their upper limits are determined through a prior planning step (see for example (70)). The total number of control variables in the optimization is the number of candidate control locations times the number of control steps. The optimization problem is solved in Matlab, and it does converge to a global minimum.

(3) At time t_k, the solution of the optimization problem (4.36)-(4.43) computes a sequence of controls $\Delta C^k_{mn}, \Delta D^k_{mn}$. Add only the first control $\Delta C^k_{m1}, S^k_{m1}\Delta D^k_{m1}$ at time t_k and obtain the system state $x(t_{k+1})$ at time $t_{k+1} = t_k + T_s$.

(4) Increase k to $k+1$ and repeat steps (1)-(3) until $k = N-1$.

4.5.3 Test case

The proposed method is illustrated using the modified WECC 9-bus system and New England 39-bus system. The exponential recovery load model is used in both cases. The parameters of the load model are as following:

$$T_P = T_Q = 30, \alpha_s = 0, \alpha_t = 1, \beta_s = 0, \beta_t = 4.5.$$

The parameters in MPC optimization are determined based on the following considerations. Any voltage instability following a contingency must be stabilized in a certain time duration (typically the time in which voltage will decrease by 15%). This is the prediction horizon T_p. The control should be exercised on a time horizon T_c, which is shorter than the prediction horizon, typically the time in which voltage will decrease by 10% (if no control is applied). A discrete-time control must be applied within this duration T_c at a sample-rate high enough to adequately react to the changing voltage trajectory, as well as to allow accurate enough predictions of the voltage trajectory based on the linearization of the trajectory-sensitivity. This dictates the sampling duration T_s. The number of sampling point N is then determined as the ratio of T_c and the sampling duration T_s.

The voltage control means in the test cases include SVCs, LTCs, and load shedding. To avoid over-voltage problems, the maximum amount of the controls is limited at each sampling point. For SVCs, the maximum control amount is 0.1 p.u.. The maximum number of load tap changer steps is 3. And the maximum load shedding at one sampling point is 10%. The step size of LTCs is 0.006 p.u.. The step size of load shedding is 5%.

4.5.4 Modified WECC 3-Generator Test System

4.5.4.1 System description

Figure 4.20 is a representation of the modified WECC 3-generator 9-bus system. Transformer banks with under load tap changers are connected to bus 6 and bus 8 to regulate the voltages of load buses 10 and 11. A fourth-order generator model is used. The state variables include rotor angle δ, rotor speed ω, q-axis transient voltage e'_q, and d-axis transient voltage e'_d. Generator 1 is equipped with an automatic Voltage Regulator (AVR). The continuously acting regulator and exciter model (47) are employed in the study. It is represented by a four-dimensional state equation. The loads at buses 5, 10 and 11 are represented by the exponential recovery dynamic model. Thus, each load is described by a two-dimensional state equation. Therefore, the total dimension of the state space is 22. The voltage control mechanisms include the followings:

- The SVCs at bus 5, bus 7, and bus 8;
- The under load tap changer of transformer banks connecting bus 8 and bus 11, bus 6 and bus 10;
- The load shedding at bus 5, bus 10, and bus 11.

4.5.4.2 Fault scenario

We consider a three-phase-to-ground fault at bus 5 at $t = 1.0$ second, which is cleared at $t = 1.2$ seconds by tripping of the line between bus 4 and bus 5. Based on the time domain simulation, the voltage performance is not satisfactory as shown in Figure 4.21. At $t = 1.0$ second, the voltages begin to drop dramatically due to the fault. At $t = 1.2$ seconds, the voltages start to recover since the fault is cleared. However, the voltages begin to oscillate. Fifteen seconds later, voltages begin to decline gradually. The dynamic load models result in slightly recovery of load consumption, which deteriorates the voltage condition. Assume that the post-transient load bus voltages must be above 0.95 p.u. Therefore, some control actions are required to satisfy the voltage performance requirement.

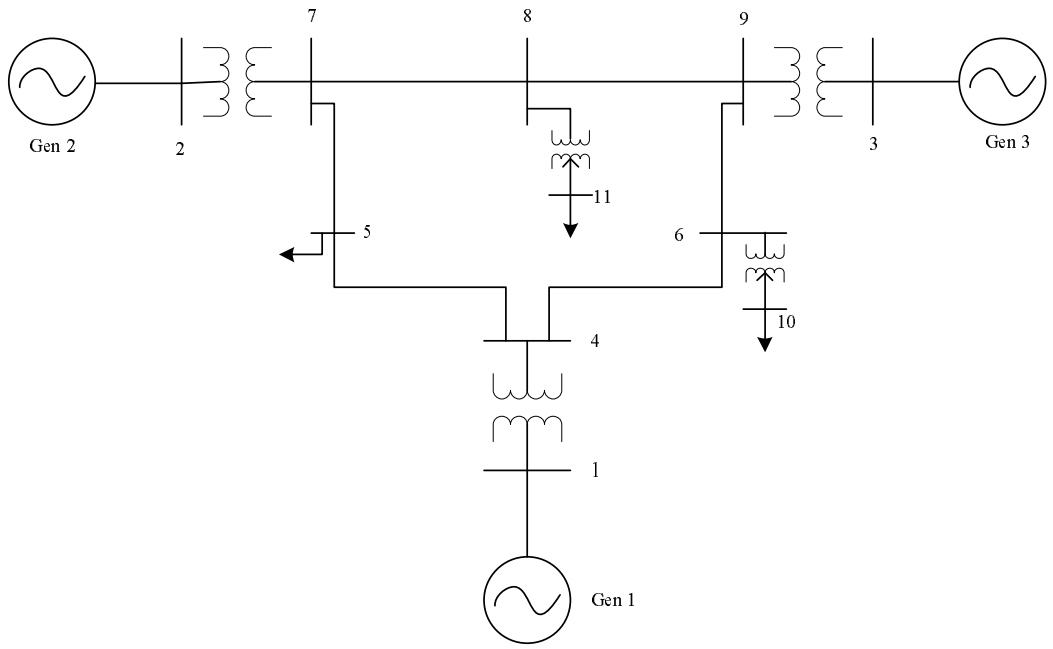

Figure 4.20 Modified WECC 3-generator 9-bus test system

4.5.4.3 Simulation result

n this example, we have chosen prediction horizon T_p to be 60 seconds (the time in which voltage drops by nearly 15% at bus 5). T_c has been chosen to be 50 seconds. We found that a sample duration of $T_s = 10$ seconds works well for this example, and so we have the number of control steps: $N = \frac{T_c}{T_s} = \frac{50}{10} = 5$. The model predictive control approach determines a coordinated control strategy to recover the bus voltages. During the optimization, we set the lower bound of all bus voltages to be 0.95 p.u. and the upper bound of load bus voltages to be 1.05 p.u. For generator buses, we set the maximum voltage magnitude to be 1.08 p.u., which is slightly higher than load buses. These settings are practical. Figure 4.22 shows the bus voltages after MPC based control was implemented. From the figure, we can see that all the bus voltages were restored to be above 0.95 p.u.

The control strategy is shown in Table 4.4. The first row has the time information of the 5 control sampling points, i.e. 20 seconds, 30 seconds, 40 seconds, 50 seconds, and 60 seconds. Each column corresponding to the control sampling point has the information of the control actions. For example, at time 20 second, both under load tap changers increase their tap ratios

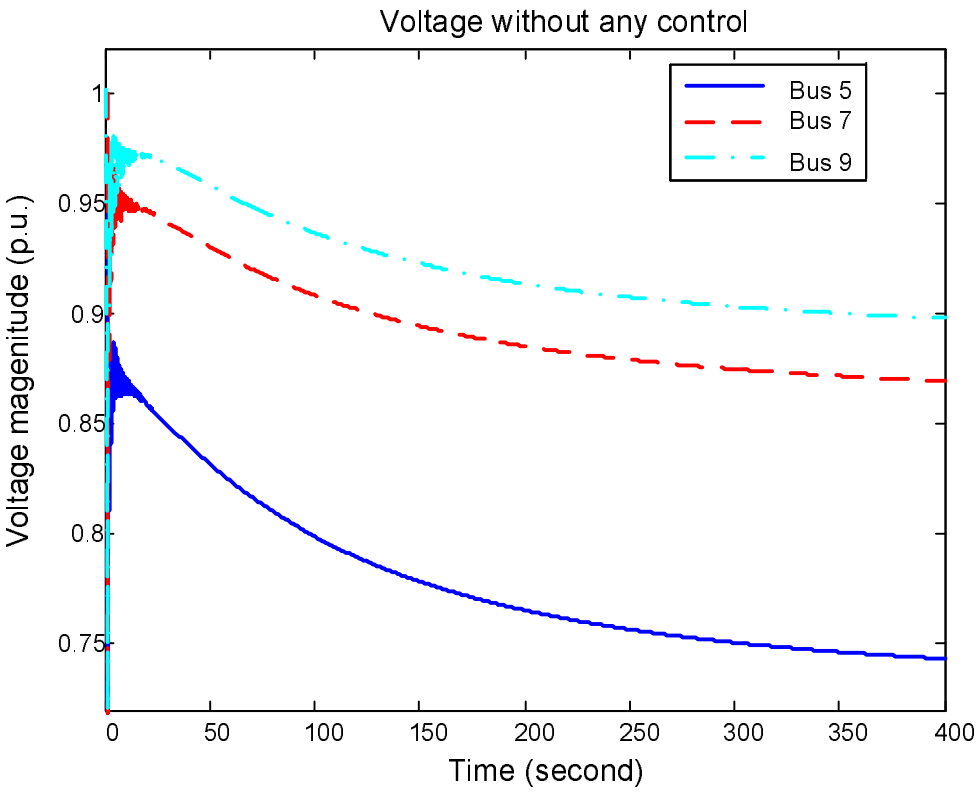

Figure 4.21 Voltage behavior of the modified WECC case without MPC control

by 3 steps, which is 0.018 p.u.. No load shedding has been taken. All the existing three SVCs increase their susceptance output by 0.1 p.u..

4.5.5 Modified New England 9-Generator 39-Bus Test System

4.5.5.1 System description

Figure 4.23 shows the modified New England 9-generator 39-bus system. There are totally 41 buses and 9 generators. Two transformer banks with under load tap changers are added between bus 8 and bus 40, bus 4 and bus 41. A fourth-order generator model is used. The exception is that a third-order model is used for the generator at bus 39. In addition, all generators excluding those at bus 34 and bus 37 have automatic voltage regulators (AVRs), which are represented by fourth-order models. The loads are represented by the exponential recovery dynamic models. The control variables are as follows:

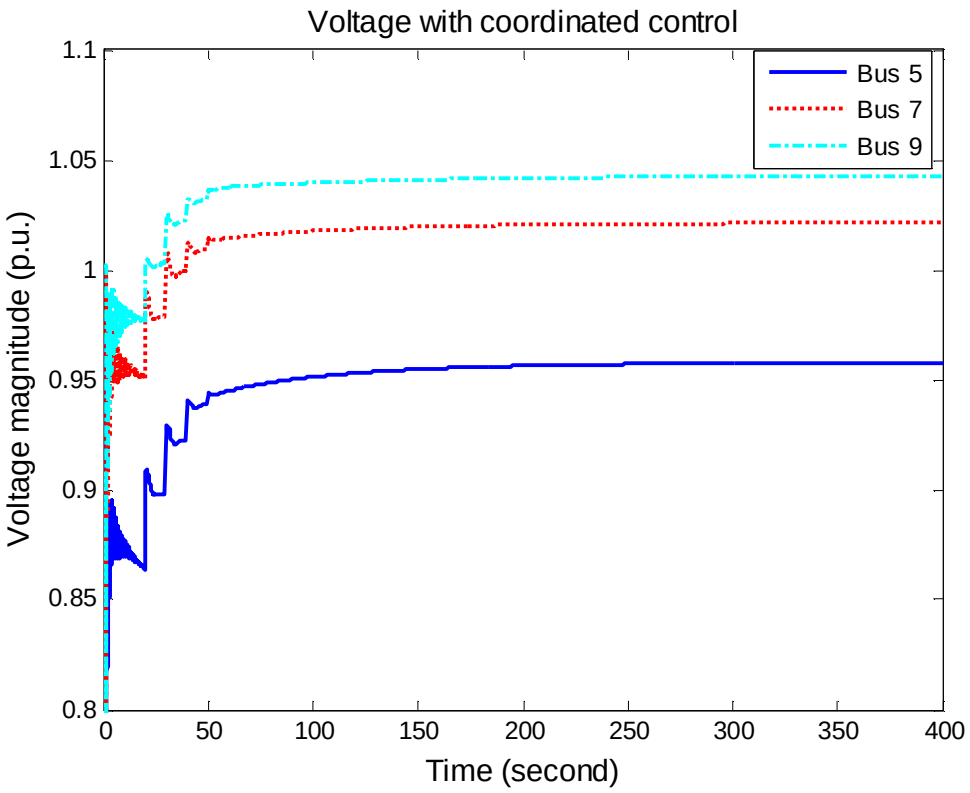

Figure 4.22 Voltage behavior of the modified WECC with MPC control

- The SVCs at buses 1, 6, 14, and 28;
- The under load tap changers at the transformer banks between bus 8 and bus 40, bus 4 and bus 41;
- The load shedding at bus 15 and bus 16.

4.5.5.2 Fault scenario

The contingency considered here is a three-phase-to-ground fault at bus 21 at $t = 1.0$ second, which is cleared at $t = 1.2$ seconds by the tripping of the transmission line between bus 21 and bus 22. Bus voltages drop dramatically when the fault occurs as shown in Figure 4.24. After the fault is cleared at 1.2 seconds, the voltages recover greatly whereas some oscillations follow. About 20 seconds later, the oscillations are damped out, but the voltages start to decline slowly because of the exponential recovery of the loads. Around 2 minutes

Time(second)	20	30	40	50	60
LTC between bus 6 and 10 (step)	3	3	3	3	0
LTC between bus 6 and 10 (step)	3	3	0	0	0
Load shedding at bus 5(%)	0	0	0	0	0
Load shedding at bus 10 (%)	0	0	0	0	0
Load shedding at bus 11(%)	0	0	0	0	0
SVC capacitor change at bus 5 (p.u.)	0.1	0.1	0.1	0	0
SVC capacitor change at bus 7 (p.u.)	0.1	0 .1	0.0221	0.0248	0.0005
SVC capacitor change at bus 8 (p.u.)	0.1	0.0587	0	0	0

Table 4.4 The resulting control strategy for the modified WECC system

later, the voltages collapse.

4.5.5.3 Simulation result with only SVC control

In this test case, there are three types of voltage control options. They are ULTCs, SVCs and load shedding. This subsection studies the effect of SVCs on the restoration of the voltage behavior. There are four SVCs, which locate at bus 1, bus 6, bus 14 and bus 28. The upper limit of these SVCs is 0.3 p.u.. The control strategy is to switch all the available capacity of SVCs at 20 seconds. The voltage behavior is presented in Figure 4.25. From the Figure 4.25, we find that even if all the SVCs are put into use, the voltage can not be stabilized following the contingency.

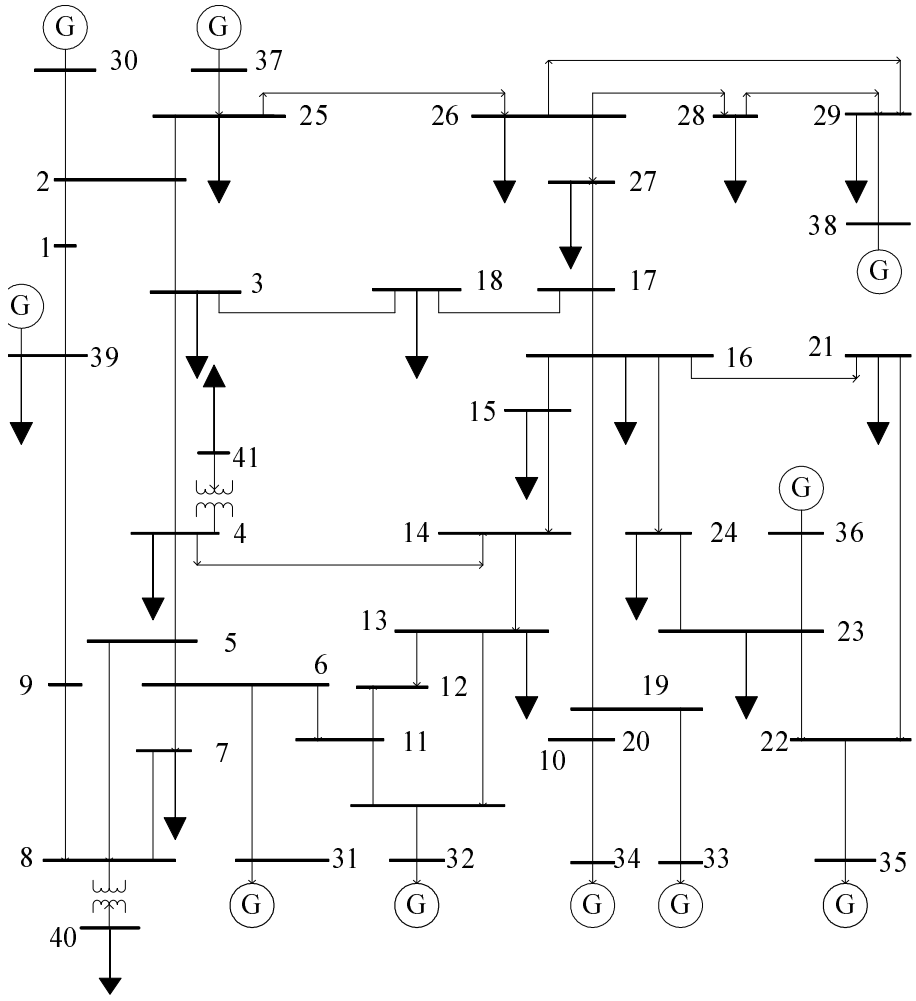

Figure 4.23 Modified New England 10-generator 39-bus test system

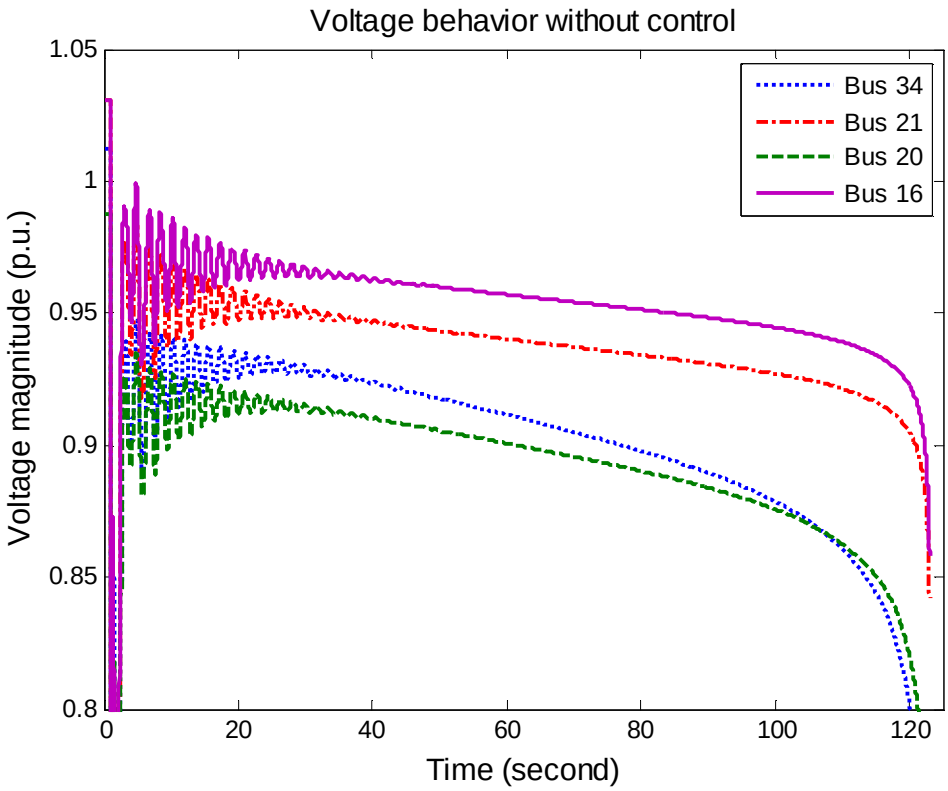

Figure 4.24 Voltage behavior of the modified New England system without MPC control

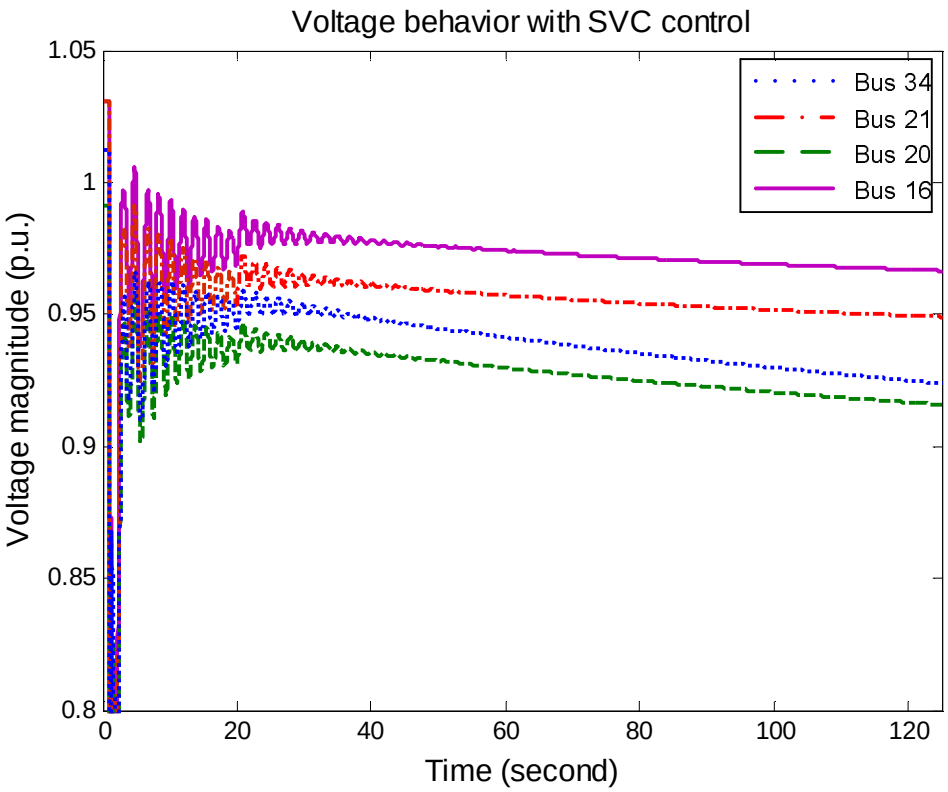

Figure 4.25 Voltage behavior of the modified New England system with only SVC control

4.5.5.4 Simulation result with coordinated control strategy

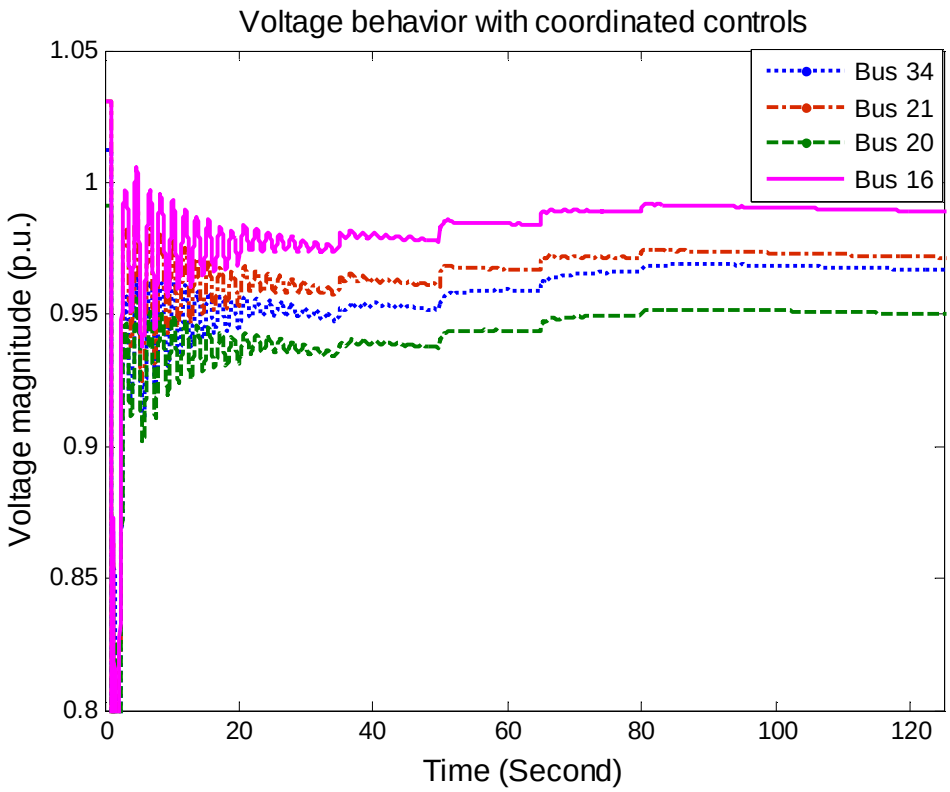

Figure 4.26 Voltage behavior of the modified New England system with coordinated voltage control

In this example, we have chosen prediction horizon T_p to be 90 seconds (the time in which voltage drops by nearly 12% at bus 20). T_c has been chosen to be 75 seconds. We found that a sample duration of $T_s = 15$ seconds works well for this example, and so we have the number of control steps: $N = \frac{T_c}{T_s} = \frac{75}{15} = 5$. The control action determined by the MPC based algorithm starts around 20 seconds to recover voltage. The system response with MPC in place is shown in Fig. 4.26. With the MPC implemented, the voltages are stabilized at a value between [0.95, 1.05] p.u.. The corresponding control strategy is shown in Table 4.5. From that table, we find that the under load tap changers are at the maximum change steps at each sampling point. Load shedding is also used to stabilize the system. The table shows a coordinated control strategy between under load tap changer, static var compensators as well as load shedding.

Time(second)	20	35	50	65	75
SVC at bus 1 (p.u.)	0	0	0	0	0
SVC at bus 6 (p.u.)	0	0	0.1	0	0.0544
SVC at bus 14 (p.u.)	0	0.0806	0.1	0.0274	0.092
SVC at bus 28 (p.u.)	0	0	0.1	0	0
LTC between buses 8 and 40 (steps)	3	3	3	3	3
LTC between buses 4 and bus 41 (steps)	3	3	3	3	3
Load shedding at bus 15 (%)	5	10	10	10	0
Load shedding at bus 16 (%)	0	0	0	0	0

Table 4.5 The control strategy for the modified New England system

4.5.6 Security Constrained Coordinated Dynamic Voltage Stabilization

Equations (4.36)-(4.43) consist of the optimization formulation to determine a coordinated voltage control strategy. In this section, security constraint (4.44) is added to find a coordinated voltage control strategy which not only stabilizes voltage but also maintains a desired security margin.

$$SM^{k-1} + \sum_{m=1}^{M_c} SM^k_{C_m}(\sum_{n=1}^{N-k} \Delta C^k_{mn}) + \sum_{m=M_c+1}^{M_c+M_d} SM^k_{D_m}(\sum_{n=1}^{N-k} S^k_{mn}\Delta D^k_{mn}) \geq SM_D \quad (4.44)$$

Here,

- SM^{k-1} is the voltage stability margin at time $t_k - T_s$.
- $SM^k_{C_m}$ is the stability margin sensitivity with respect to continuous control m added at time t_k.
- $SM^k_{D_m}$ is the stability margin sensitivity with respect to discrete control m added at time t_k.
- SM_D is the desirable stability margin for the system.

A brief summary of the procedure to determine the control strategy at time t_k based on MPC is as follows:

(1.) At time t_k (i.e. the $(k+1)^{th}$ sampling instant), an estimate of the current state $x(t_k)$ is obtained. At the same time, the trajectory sensitivities of bus voltages with respect to the continuous and discrete controls to be added at instants $t_k+(n-1)T_s, n = 1 \ldots N-k$ are obtained. Voltage stability margin sensitivities with respect to continuous and discrete controls are obtained based on a continuation power flow program. They are denoted as $SM^k_{C_m}$ and $SM^k_{D_m}$ respectively.

(2.) At time t_k, the mixed integer quadratic programming (MIQP) optimization problem (4.36)-(4.43) and (4.44) is solved, we get the security constrained coordinated voltage control strategy and implement the first step.

(3.) Increase k to $k+1$ and repeat steps (1)-(3) until $k = N-1$

4.5.6.1 Test case

System description The proposed method is illustrated using a modified New England 39-bus system as shown in Fig. 4.27. There are totally 41 buses and 9 generators. Two transformer banks with load tap changers are added between bus 8 and bus 40, bus 4 and bus 41. The loading condition is 10% more than that of the original New England testing case. Generator 37 is removed in base case. A fourth-order generator model is used. The exception is that a third-order model is used for the generator at bus 39. In addition, all generators excluding those at bus 34 have automatic voltage regulators (AVRs), which are represented by fourth-order models.

The loads are represented by the exponential recovery dynamic models. The parameters of the load model are $T_P = T_Q = 30, \alpha_s = 0, \alpha_t = 1, \beta_s = 0, \beta_t = 4.5$. The control variables are as follows:

- SVCs at buses 1, 6, 14, and 28;
- Load tap changers at the transformer banks between bus 8 and bus 40, bus 4 and bus 41;
- Load shedding at bus 15 and bus 16.

Load shedding is an emergency voltage control action. A higher cost weight should be used to make sure that load shedding is trigged only when other control actions are not sufficient. To avoid over-voltage problems, the maximum amount of the controls is limited at each sampling point. For SVCs, the maximum control amount is 0.1 p.u., the maximum number of load tap changer steps is 3 and the maximum load shedding at one sampling point is 10%. The step size of LTCs is 0.006 p.u.. The step size of load shedding is 5%. The desirable post-fault voltage stability margin is set to be 35%.

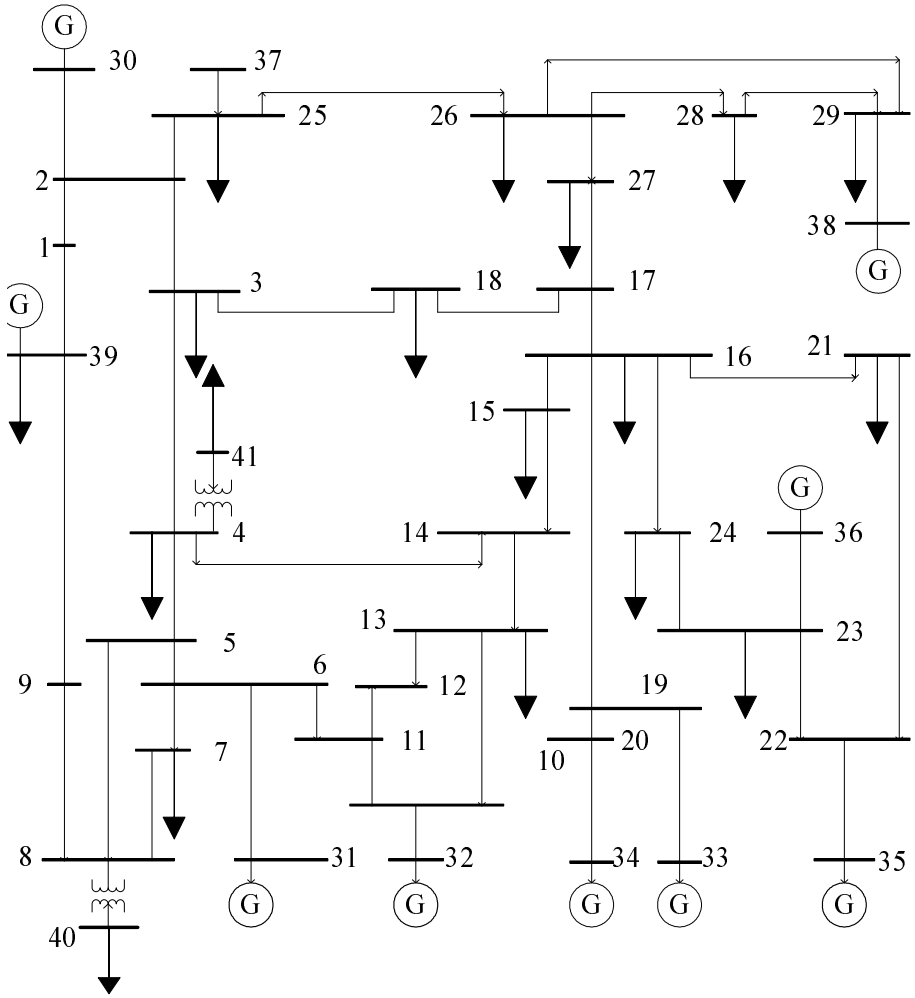

Figure 4.27 9-generator 41-bus test system

Fault scenario The contingency considered here is a three-phase-to-ground fault at bus 21 at $t = 1.0$ second, which is cleared at $t = 1.2$ seconds by the tripping of the transmission line

between bus 21 and bus 22. Voltage behavior of the modified New England system is shown in Fig. 4.28. From $t = 0$ second to $t = 1.0$ second, voltages are constant representing that they are in steady state. At time $t = 1.0$ second, voltages drop dramatically when the fault occurs. After the fault is cleared at 1.2 seconds, the voltages recover greatly whereas some oscillations follow. About 20 seconds later, the oscillations are damped out, but the voltages start to decline slowly because of the exponential recovery of the loads. Around 4 minutes later, the voltages collapse. The post-fault voltage stability margin is 31.1%.

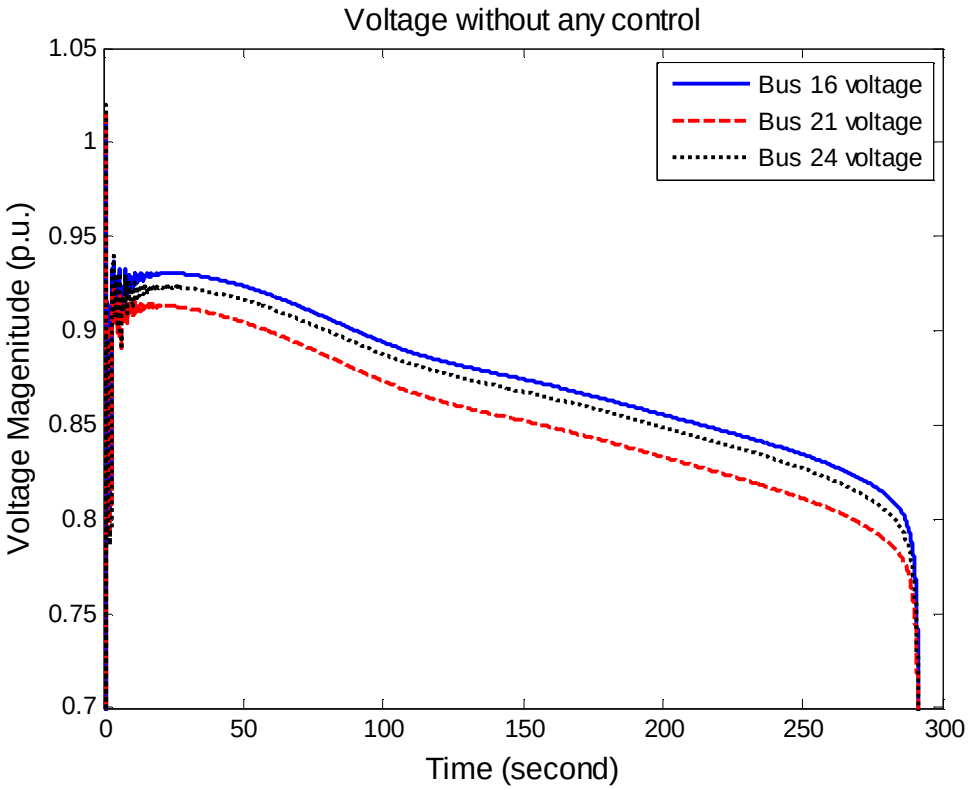

Figure 4.28 Voltage behavior of the 9-generator 41-bus test system without MPC control

Simulation result In this example, we have chosen prediction horizon T_p to be 75 seconds (the time in which voltage drops by nearly 12% at bus 21). T_c has been chosen to be 50 seconds. We found that a sample duration of $T_s = 10$ seconds works well for this example, and so we have the number of control steps: $N = \frac{T_c}{T_s} = \frac{50}{10} = 5$. The control action determined by the MPC based algorithm starts around 20 seconds to recover voltage. The system

Time(second)	20	35	50	65	75
SVC at bus 1 (p.u.)	0	0	0	0	0
SVC at bus 6 (p.u.)	0	0.0215	0	0	0
SVC at bus 14 (p.u.)	0.0065	0.1	0.1	0.094	0
SVC at bus 28 (p.u.)	0	0	0.013	0.093	0
LTC between buses 8 and 40 (steps)	3	3	3	3	0
LTC between buses 4 and bus 41 (steps)	3	3	3	3	0
Load shedding at bus 15 (%)	10	10	10	5	5
Load shedding at bus 16 (%)	10	10	0	0	0

Table 4.6 The control strategy for the 9-generator 41-bus test system

response with MPC in place is shown in Fig. 4.29. With the MPC implemented, the voltages are stabilized at a value between [0.95, 1.05] p.u.. The voltage stability margin is 35.1%. The corresponding control strategy is shown in Table 4.6. It can be noted in the table that the load tap changers are applied to the maximum allowed at each sampling point. Load shedding is also used to stabilize the system. The table shows a coordinated control strategy among load tap changers, static var compensators and load shedding is utilized for voltage stabilization with a guaranteed stability margin. As shown in simulations, MPC is applied after a fault has occurred, and it is not required that MPC be used before the occurrence of a fault. Also since MPC is applied after a fault, the initial condition is arbitrary in all our simulations, i.e., the MPC-based control is successful independently of the initial conditions.

4.6 Implementation Issues

Figure 1.3 presents a general architecture for the implementation a real time SPS. The functional structure of implementing the MPC based coordinated voltage control proposed above is shown in Figure 4.30. Line flow measurements, bus voltage information, switch status measured by phase measurement units (PMUs) and collected by Phasor Data Concentrators (PDCs) are sent to a control center through communication channels. These measurements plus a network model are used by the state estimator (SE) for filtering out the noise and estimating the auxiliary (also known as static state) variables. The results from the state

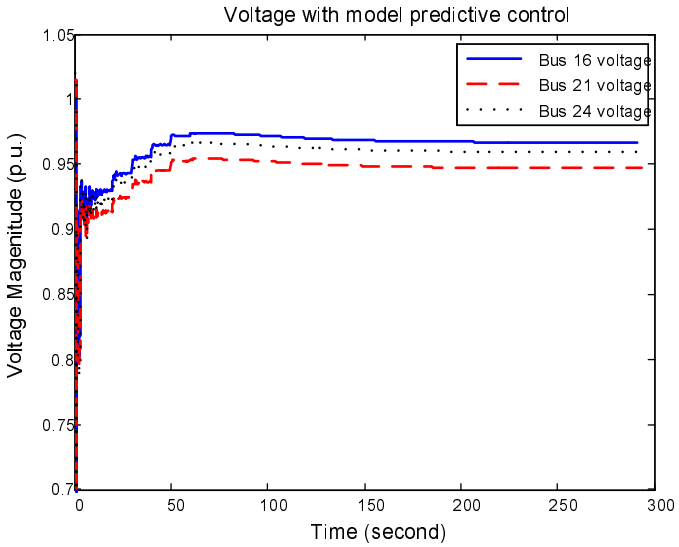

Figure 4.29 Voltage behavior of the modified New England system with MPC-based coordinated voltage control

estimator are used for power flow analysis. A power flow solution is then used by an on-line dynamic security assessment program to initialize the state variables of the dynamic models. Further, it uses system models and disturbance information to perform the contingency analysis to evaluate the security margin of the power system. If a contingency is identified where the system will become unstable, MPC based computation gets triggered at the time an identified critical contingency occurs. A final step is to implement the computed control to improve the security of the power system.

The steps of the MPC computation in the k^{th} iteration include:

- Estimate static variables $y(t_k)$ such as voltage magnitudes and angles at time t_k as well as the dynamic variables $x(t_k)$ such as generator angles, velocities and real and reactive load recovery. The values of the static variables is provided by the state-estimator. As far as the dynamic variables are concerned, they can be classified into short-term dynamic variables (such as generator angles and velocities) and long-term dynamic variables (such as real and reactive load recovery). The values of the long-term dynamic variables can be directly measured and hence are known, whereas the short-term dynamic variables are in quasi steady-state (QSS) with respect to the long-term voltage/frequency stability

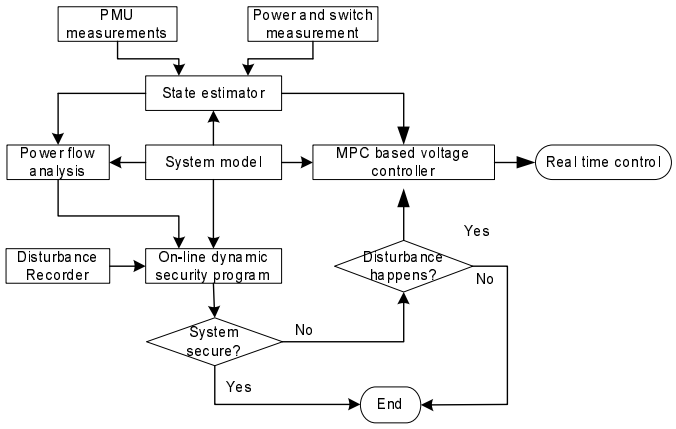

Figure 4.30 Structure of implementing a MPC based Voltage stabilization

phenomenon investigated in this paper. Thus the values of the short-term dynamic variables can be obtained by solving an equilibrium equation of the form:

$$0\ (=\dot{x}_s) = f_s(x_s, x_l, y, u), \tag{4.45}$$

where x_s is the short-term dynamic variable vector (to be computed by solving (4.45)), x_l is long-term dynamic variable vector (which is measured and hence known), y is the static variable vector (which is provided by the state-estimator and hence known), and u is the input variable vector (which is of course known). Then in equation (4.45), the number of unknowns (dimension of x_s) is the same as the number of equations (dimension of f_s), and so the short-term dynamic variables can be computed by solving (4.45).

- Run time-domain simulation to compute the system trajectory given the current state.
- Obtain trajectory sensitivities of voltage with respect to the control variables as a by-product of the time-domain simulation performed in the previous step.
- Obtain voltage stability margin with respect to the control variables based on a continuation power flow program.
- Solve the quadratic programming optimization problem and implement the first step of the control.

For all the work that has been done in this chapter, all the required algorithms have been developed in Matlab. For optimization, existing packages such as CPLEX has been used. For the WECC test case in section 4.3, the total computation time is around 7 minutes. The 99 percent of the computation time is used for time domain simulation. For a potential practical application of the proposed approach, a commercial grade programming should be used to improve the computation performance (time, numerical accuracy, etc.).

The proposed approach is model-based, and so it requires the availability of accurate models. Such models are already available and are being used for state-estimation and dynamic security assessment. Thus no new models will be required for the proposed approach. For those power system applications where accurate models are not available, there is no choice but to continue using the rules based predefined SPSs. We also realize that the measurements can be noisy as well as delayed. The "MPC based voltage controller" block however does not directly deal with the measurements. These are input to the "State Estimator" or "Dynamic Security Assessment" blocks, and these blocks are designed to cope with noisy/delayed measurements.

4.7 Summary

This chapter studies voltage control strategies based on a modified model predictive control with decreasing control horizon. The proposed MPC approach involves a *dynamic* analysis for the computation of a desired control. This chapter mainly includes the following work:

- This chapter proposes a formulation of a model predictive control based system protection scheme for maintaining voltage stability under contingencies. The stabilizing control is achieved through the economic use of shunt capacitors.

- This chapter provides a formulation of a control strategy not only prevents voltage instability, but also maintains a desired amount of post-transient voltage stability margin. Voltage stability margin sensitivities are used to characterize the effect of control variables on voltage stability margin enhancement. Prior work involving dynamic analysis for voltage stabilization did not include voltage stability margin as part of the control objective.

- This chapter provides a formulation of an optimal coordination of static var compensators, transformer load tap changers and load shedding to improve voltage performance following large disturbances.

The distinguishing features of our MPC formulation are as follows:

- Use of trajectory sensitivities for determining the effect of control on voltage stabilization, which is a more accurate way of determining the effectiveness of control (as opposed to the less accurate linearization around a single state or more time-consuming computations based on numerical simulations).

- Optimization is performed repeatedly at each sampling instant. Only the first control step is implemented. This feature corrects the errors brought by model approximation, such as a linearized relationship between the voltages and the control variables.

- A decreasing horizon MPC is used. The control horizon decreases from one iteration to the next. This modification not only reduces the computation time, but also helps the convergence of the optimization process. This feature of MPC has not been explored in prior work on stabilization of power systems.

- Optimization performed at each step involves a quadratic cost function together with linear constraints, which makes the formulation scalable to large-sized practical systems (as demonstrated by the application to the 39 bus New England system).

CHAPTER 5. Software Development

5.1 Overview

Power System Analysis Toolbox (PSAT) is developed and maintained by F. Milano (75). It is a Matlab toolbox for electric power system analysis. The main functions of this toolbox include: power flow analysis, optimal power flow analysis, small signal stability analysis, time domain simulation, etc.

The power flow and time domain simulation functions are used in our simulation. We extended the time domain simulation part to include the trajectory sensitivity calculation and do the MPC optimization. Figure 5.1 shows the overall flowchart of our simulation work.

Data file contains the model and contingency information. It is the input to a power flow analysis. After that, time domain simulation is initialized by the power flow result and runs until the end of the prediction horizon of the first control sampling point. At iteration 1, voltage stability margin and its sensitivity with respect to controls are calculated. Trajectory sensitivity matrix calculation provides sensitivities with respect to control variables at the first control sampling point. Then the optimization program starts to run to get the control actions at each control step. After that, the first step of control actions is implemented and the control parameters of the system are updated in the control update step. Then time domain simulation for the next control sampling point is initialized. Time domain simulation runs until the next control sampling point. Iteration number is increased by 1. Then the program will check if the iteration number has reached the number of control steps. If yes, simulation ends. Otherwise, at the current control sampling point *iter*, repeat the sensitivity calculation, optimization, control update, etc.

The files related with the implementation of MPC based voltage control are listed in Table

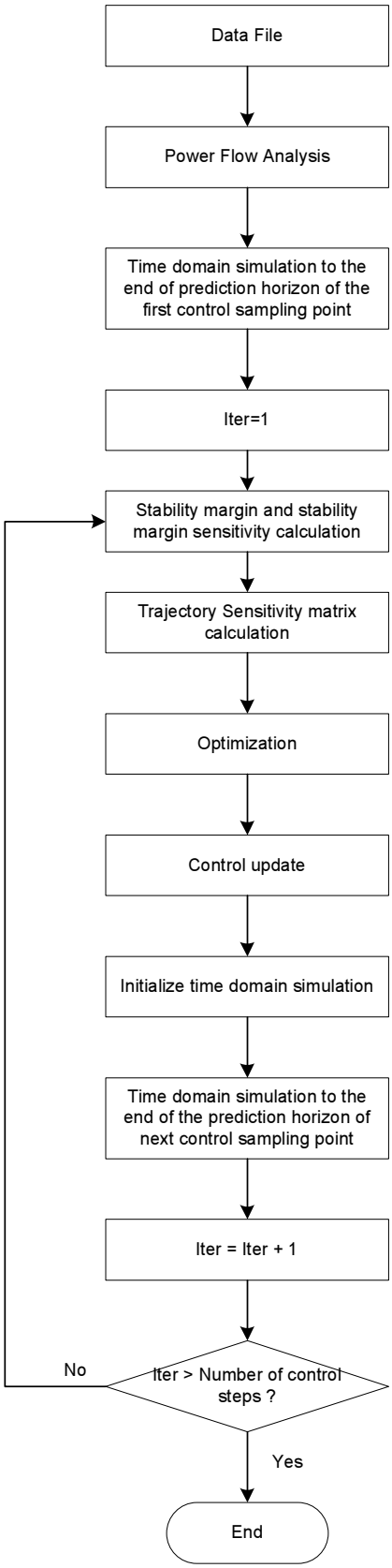

Figure 5.1 The flow chart of the MPC based control simulation

5.1. This table contains 2 columns. The first column lists the function of the files. The second column contains the file names used in our MPC based voltage stabilization design.

Function	Files
Data File	WECC_Data.m, NewEngland_Data.m
Power Flow Analysis	runpsat.m
Time Domain Simulation	runpsat.m
Sensitivity Calculation	SenAtCs.m
Optimization	MPCOpt.m
Initialize time domain simulation	InitializeTD.m
Main program	WECC_MPC.m, NewEngland.m,

Table 5.1 The function and the associated file names in MPC implementation

5.2 Data file

The data file contains all the data used in power flow analysis and time domain simulation. It includes bus, transmission line, transformers, slack bus, PV bus, PQ bus, shunt, generator, load model, fault information, breaker, etc. Detailed information of these models can be find in (75). The following subsection introduces the data format used in the Data file.

5.2.1 Bus

Bus data is defined in Bus.con. Bus data format is in Table 5.2.

Column	Description	Unit
1	Bus number	int
2	Voltage base	kV
3	Voltage amplitude initial guess	p.u.
4	Voltage phase initial guess	p.u.
5	Area number	int
6	Region number	int

Table 5.2 Bus data format

5.2.2 Transmission line and transformer

Transmission line and transformer information are stored in Line.con. The data format is in Table 5.3.

Column	Description	Unit
1	From bus	int
2	To bus	int
3	Power rating	MVA
4	Voltage rating	kV
5	Frequency rating	Hz
6	Line length	km
7	Primary and secondary voltage ratio	kV/kV
8	Resistance	p.u.
9	Reactance	p.u.
10	*not used*	-
11	Fixed tap ratio	p.u./p.u.
12	Fixed phase shift	deg
13	Current limit	p.u.
14	Active power limit	p.u.
15	Apparent power limit	p.u.

Note: Column 6 only valid for transmission lines.
Column 7 only valid for transformers.

Table 5.3 Line data format

5.2.3 Slack bus

Slack bus is a bus used to balance the real and reactive power in the system. It is a bus with fixed voltage magnitude and phase. The slack bus information is stored in SW.con. The data format is shown in Table 5.4.

5.2.4 PV bus

PV bus has fixed voltage magnitude and real power injection. The PV bus data information is stored in PV.con. The data format is shown in Table 5.5.

Column	Description	Unit
1	Bus number	int
2	Power rating	MVA
3	Voltage base	kV
4	Voltage magnitude	p.u.
5	Reference angle	p.u.
6	Maximum reactive power	int
7	Minimum reactive power	int
8	Maximum voltage	p.u.
9	Minimum voltage	p.u.
10	Active power guess	p.u.
11	Loss participation coefficient	-

Table 5.4 Slack bus data format

Column	Description	Unit
1	Bus number	int
2	Power rating	MVA
3	Voltage base	kV
4	Active power	p.u.
5	Voltage magnitude	p.u.
6	Maximum reactive power	int
7	Minimum reactive power	int
8	Maximum voltage	p.u.
9	Minimum voltage	p.u.
11	Loss participation coefficient	-

Table 5.5 PV bus data format

5.2.5 PQ load

PQ bus has a fixed real and reactive power injection. The PQ bus data information is stored in PQ.con. The data format is shown in Table 5.6.

Column	Description	Unit
1	Bus number	int
2	Power rating	MVA
3	Voltage base	kV
4	Active power	p.u.
5	Reactive power	p.u.
6	Maximum voltage	p.u.
7	Minimum voltage	p.u.
8	Allow conversion to impedance	boolean

Table 5.6 PQ bus data format

5.2.6 Shunt

Shunt data is stored in Shunt.con. The data format is shown in Table 5.7.

Column	Description	Unit
1	Bus number	int
2	Power rating	MVA
3	Voltage base	kV
4	Frequency rating	Hz
5	Conductance	p.u.
6	Susceptance	p.u.

Table 5.7 Shunt data format

5.2.7 Synchronous machine

Synchronous machine data is stored in Syn.con. The data format is shown in Table 5.8.

Column	Description	Unit
1	Bus number	int
2	Power rating	MVA
3	Voltage base	kV
4	Frequency rating	Hz
5	Machine model	-
6	Leakage reactance	p.u.
7	Armature resistance	p.u.
8	d-axis synchronous reactance	p.u.
9	d-axis transient reactance	p.u.
10	d-axis sub-transient reactance	p.u.
11	d-axis open circuit transient time constant	s
12	d-axis open circuit sub-transient time constant	s
13	q-axis synchronous reactance	p.u.
14	q-axis transient reactance	p.u.
15	q-axis sub-transient reactance	p.u.
16	q-axis open circuit transient time constant	s
17	q-axis open circuit sub-transient time constant	s
18	Mechanical starting time (2*inertia constant)	kWs/kVA
19	Damping coefficient	p.u.
20	Speed feedback gain	gain
21	Active power feedback gain	gain
22	Active power ratio at node	[0,1]
23	Reactive power ratio at node	[0,1]
24	d-axis additional leakage time constant	s

Table 5.8 Synchronous machine data format

5.2.8 Exponential Load model

Exponential load model is introduced in chapter 2. The data related with this component is stored in Exload.con. The data format is shown in Table 5.9.

Column	Description	Unit
1	Bus number	int
2	Power rating	MVA
3	Active power voltage coefficient	kV
4	Active power frequency coefficient	Hz
5	Real power time constant	s
6	Reactive power time constant	s
7	Static real power exponent	-
8	Dynamic real power exponent	-
9	Static reactive power exponent	-
10	Dynamic reactive power exponent	-

Table 5.9 Exponential Recovery Load Data Format

5.2.9 Fault

Table 5.10 shows data for a three-phase fault. The data is contained in Fault.con.

Column	Description	Unit
1	Bus number	int
2	Power rating	MVA
3	Voltage base	kV
4	Frequency rating	Hz
5	Fault time	p.u.
6	Clearance time	p.u.
7	Fault resistance	p.u.
8	Fault reactance	p.u.

Table 5.10 Fault data format

5.3 Power flow

The power flow problem is formulated as the solution of a nonlinear set of equations as follows:

$$\begin{aligned} \dot{x} = 0 &= f(x, y) \\ 0 &= g(x, y) \end{aligned} \tag{5.1}$$

where y are the algebraic variables, i.e. voltage magnitudes and phase angles. x are the state variables, such as generator electrical rotor angle, rotor speed, etc. Newton-Raphson method is used to solve the power flow problem. At each iteration, the Jacobian matrix of Equation (5.1) is updated and linear equation (5.2) is solved until Δx^i and Δy^i is less than the tolerance or the iteration number reaches maximum (the latter case indicates that power flow can not converge).

$$\begin{aligned} \begin{bmatrix} \Delta x^i \\ \Delta y^i \end{bmatrix} &= - \begin{bmatrix} F_x^i & -F_y^i \\ G_x^i & G_y^i \end{bmatrix}^{-1} \begin{bmatrix} f^i \\ g^i \end{bmatrix}, \\ \begin{bmatrix} x^{i+1} \\ y^{i+1} \end{bmatrix} &= \begin{bmatrix} x^i \\ y^i \end{bmatrix} + \begin{bmatrix} \Delta x^i \\ \Delta y^i \end{bmatrix} \end{aligned} \tag{5.2}$$

5.4 Time domain simulation

Time domain simulation is a commonly used way to study dynamic behavior of power systems. Consider the DAE model

$$\dot{x} = f(x, y) \tag{5.3}$$

$$0 = g(x, y) \tag{5.4}$$

Trapezoidal approach is used to approximate Equation (5.3) with a set of algebraic difference equations coupled to the original algebraic Equation (5.4). The evolution of the states x, and y from time instant t_i to the next time instant t_{i+1} can be described as

$$x^{i+1} = x^i + \frac{\eta}{2}(f(x^{i+1}, y^{i+1}) + f(x^i, y^i)) \tag{5.5}$$

$$0 = g(x^{i+1}, y^{i+1}) \tag{5.6}$$

where superscript i is the time instant t_i, $i+1$ is the time instant t_{i+1} and $\eta = t_{i+1} - t_i$ is the integration time step. Rearrange Equation (5.5) and Equation (5.6) as follows:

$$F = \begin{bmatrix} \frac{\eta}{2} f(x^{i+1}, y^{i+1}) - x^{i+1} + \frac{\eta}{2} f(x^i, y^i) + x^i \\ g(x^{i+1}, y^{i+1}) \end{bmatrix} = 0 \tag{5.7}$$

Equation (5.7) is a set of implicit nonlinear algebraic equations. The Newton iterative technique is commonly used to solve for x^{i+1} and y^{i+1}, given x^i and y^i

$$\begin{bmatrix} x^{i+1} \\ y^{i+1} \end{bmatrix} = \begin{bmatrix} x^i \\ y^i \end{bmatrix} - F_\chi^{-1} F$$

where, F_χ is the Jacobian of F with respect to x, y.

$$F_\chi = \begin{bmatrix} \frac{\eta}{2} f_x - I & \frac{\eta}{2} f_y \\ g_x & g_y \end{bmatrix} \tag{5.8}$$

5.5 Trajectory sensitivity

The basic concept of trajectory sensitivity has been introduced in Chapter 4. Here, we introduce the numerical realization of trajectory sensitivities. Differentiating Equations (5.3) and (5.4) with respect to the initial conditions x_0 results in the DAEs of trajectory sensitivities

$$\dot{x}_{x_0} = f_x x_{x_0} + f_y y_{x_0} \tag{5.9}$$

$$0 = g_x x_{x_0} + g_y y_{x_0} \tag{5.10}$$

The trajectory sensitivity can be approximated by trapezoidal integration as follows:

$$\begin{aligned} x_{x_0}^{i+1} &= x_{x_0}^i + \frac{\eta}{2}(f_x^i x_{x_0}^i + f_y^i y_{x_0}^i + f_x^{i+1} x_{x_0}^{i+1} + \bar{f}_y^{i+1} y_{x_0}^{i+1}) \\ 0 &= g_x^{i+1} x_{x_0}^{i+1} + g_y^{i+1} y_{x_0}^{i+1} \end{aligned}$$

Rearranging the above equation results in

$$\begin{bmatrix} \frac{\eta}{2} f_x^{i+1} - I & \frac{\eta}{2} f_y^{i+1} \\ g_x^{i+1} & g_y^{i+1} \end{bmatrix} \begin{bmatrix} x_{x_0}^{i+1} \\ y_{x_0}^{i+1} \end{bmatrix} = \begin{bmatrix} -\frac{\eta}{2}(f_x^i x_{x_0}^i, + f_y^i y_{x_0}^i) - x_{x_0}^i \\ 0 \end{bmatrix} \tag{5.11}$$

Therefore, the sensitivity matrix $\begin{bmatrix} x_{x_0}^{i+1} \\ y_{x_0}^{i+1} \end{bmatrix}$ can be obtained as a solution of a linear matrix equation. Notice that the coefficient matrix of Equation (5.11) is exactly the same as Jacobian matrix F_χ (in Equation (5.8)) in solving for x^{i+1} and y^{i+1} in time domain simulation.

5.6 Voltage stability margin

For the security constrained voltage control design, voltage stability margin and sensitivities of voltage stability margin with respect to control need to be calculated at each iteration. The mathematical formulation is in Chapter 4 Section 4.4.2. We make use of current available continuation program of Dr. Ajjarapu (Iowa State University) to do the calculation.

5.7 Optimization

The optimization problem solved in each sampling point of MPC is actually a quadratic programming as follows:

Minimize

$$x^T Q x + f' x$$

subject to

$$Ax <= B$$

$$l \leq x \leq u$$

where Q and f' are parameters of the cost function, A, B are parameters defining the inequality constraints and l,u are upper and lower limits of variable x.

5.8 Initialize time domain simulation

Time domain simulation needs a starting point, i.e. x_0 and y_0. When time domain simulation starts from normal condition, a power flow result is used to initialize it. However, when it starts from any control sampling point, a snapshot of the system is used to initialize the time

domain simulation. Therefore, this step initializes a time domain simulation with a system snapshot and necessary parameters.

5.9 Main program

Main program realizes the function shown in Figure 5.1 by calling different modules introduced above. The output of a main program is the control matrix as well as system behavior with the designed controls.

5.10 Summary

This chapter mainly introduces the software realization of the work in our dissertation. The source codes related with the simulation can be found in Appendix.

CHAPTER 6. Conclusion and Future Work

6.1 Summary of the dissertation

The overall research objective is to develop advanced control strategies that can be used to prevent power system instability following contingencies. The contribution of the proposed work is following:

- Propose a method to compute the stability region of a stable equilibrium point with the purpose of power system stability analysis based on reachability analysis. The validity of a discrete control strategy in transient stability design is determined by examining the stability region of the power system with the control strategies on. The advantages of the proposed method include:
  - The stability region is computed accurately. In addition, it's easy to implement. We only need to form the mathematic model of the post-fault power system and identify the stable equilibrium point. After that, level set methods are employed to compute the stability region as a backward reachable set.
  - The control strategies proposed guarantee the stability of the post-fault system.
- Propose an approach to determine a control strategy for maintaining voltage stability following the occurrence of a contingency by means of model predictive control. The contribution includes:
  - Propose an effective method to find the sequence as well as the amounts of the shunt capacitors to be added after a contingency to improve the performance of voltages as well as prevent voltage collapse following disturbances.

- Propose a formulation to find the sequence as well as the amounts of the shunt capacitors not only to improve the voltage behavior of a post-fault system, but also to account for the system security. Voltage stability margin is adopted to indicate the security degree of a post fault system.
- Propose a formulation to determine an optimal coordinated control strategy consisting of continuous and discrete power system controls to improve voltage performance and prevent voltage instability. The coordination includes static var compensation, load tap changer and load shedding.

6.2 Directions of future research

Based on the proposed research work in the dissertation, future research might be done in a variety of directions. Potential research focus could include the following areas:

- Dynamic state estimation. Current state estimation is based on static analysis. The inputs to a state estimator are status of circuit breakers, voltage magnitudes, real and reactive power consumption of loads, transmission line and transformer flow and generator outputs. The outputs include all real and reactive power consumption of loads, generator real power outputs and voltage magnitudes of generator buses. Variables related with power flow analysis are estimated. Since currently we don't have short term dynamic state variable measurements. The implementation discussed in Chapter 4 is based on QSS model. In the future, we need focus on the dynamic state estimation to solve the problem.

- Time delay issue. To implement the MPC based control strategy, we need send the signal to substations. This communication involves time delay. In the future, we need investigate the effect of time delay on the effectiveness of MPC based control schemes.

- We studied the robustness of the MPC based control schemes by time domain simulation. Another direction is to develop a systematic way to do the robustness study.

APPENDIX

Source Code for MPC Based Optimization

This chapter provides a sample of source codes that has been used in design MPC based voltage stabilization control strategy.

.1 WECC Data

```
Bus.con = [ ...
1 16.5 1.05 0 4 1;
3 13.8 1    0 3 1;
4 230  1    0 2 1;
5 230  1    0 2 1;
6 230  1    0 2 1;
7 230  1    0 2 1;
8 230  1    0 2 1;
2 18   1    0 5 1;
9 230  1    0 2 1];
Line.con = [ ...
9   8  100   230 60 0 0     0.00595  0.0504  0.1045 0 0 0 0 0;
7   8  100   230 60 0 0     0.00425  0.036   0.0745 0 0 0 0 0;
9   6  100   230 60 0 0     0.0185   0.085   0.149  0 0 0 0 0;
7   5  100   230 60 0 0     0.016    0.0805  0.153  0 0 0 0 0;
5   4  100   230 60 0 0     0.005    0.0425  0.088  0 0 0 0 0;
6   4  100   230 60 0 0     0.0085   0.046   0.079  0 0 0 0 0;
```

```
2   7  100    18 60 0 0.078 0        0.0625  0      0 0 0 0 0;
3   9  100  13.8 60 0 0.06  0        0.0586  0      0 0 0 0 0;
1   4  100  16.5 60 0 0.072 0        0.0576  0      0 0 0 0 0];
SW.con = [ ...
1  100 16.5  1.04 0  99  -99  1.1 0.9  0.8  1 ];
PV.con = [ ...
2  100    18 1.63 1.025  99  -99 1.1  0.9  1;
3  100  13.8 0.85 1.025  99  -99 1.1  0.9  1 ];
PQ.con = [ ...
6  100  230  0.9 0.3  1.2  0.8  0;
8  100  230    1 0.35 1.2  0.8  0;
5  100  230 1.75 0.7  1.2  0.8  0 ];
Syn.con = [ ...
2 100   18 60 4 0 0 0.89 0.12 0   6 0 0.86 0.19 0 0.535 0  12.8 0 0 0 1 1 0.002;
3 100 13.8 60 4 0 0 1.31 0.18 0 5.8 0 1.25 0.25 0   0.6 0  6.02 0 0 0 1 1 0.002;
1 100 16.5 60 4 0 0 0.15 0.06 0 8.9 0 0.09 0.09 0  0.31 0 47.28 0 0 0 1 1 0.002];

Exc.con = [ ...
1  2  5  -5  20  0.2  0.063  0.35  0.01  0.314 0.001  0.0039   1.555];
Exload.con = [6 100 230 60 30 30 0 1.0 0 4.5;
              8 100 230 60 30 30 0 1.0 0 4.5;
              5 100 230 60 30 30 0 1.0 0 4.5];
Fault.con = [5  100  230  60  1  1.2  0  0.001 ];
Breaker.con = [5 4 100 230 60 1 1.2 10000];
Shunt.con = [5 100 230 60 0 0;
             7 100 230 60 0 0;
             8 100 230 60 0 0
             ];
```

```
Varname.bus = {...
'Bus 1'; 'Bus 2'; 'Bus 3'; 'Bus 4'; 'Bus 5';
'Bus 6'; 'Bus 7'; 'Bus 8'; 'Bus 9'};
```

.2 Sensitivity Calculation

```
function [Sen] = SenAtCs(snap_i)
global Snapshot Varout Sensitivity
fm_var;
snap_i = snap_i + 1;
Line.Y = Snapshot(snap_i).Y;
t0 = Snapshot(snap_i).time;
tidx = find(Varout.t == t0);
% The length of the sensitivity matrix cell (:, snap_i-1)
L= length(Varout.t(tidx:end));
[row, col, pg] = size(Sensitivity);
firstIdx = pg-L+1;
h = Varout.t(tidx+1) - Varout.t(tidx);
 DAE.V = Varout.V(tidx,:)';
 DAE.a = Varout.ang(tidx,:)';
 DAE.x = Varout.x(tidx,:)';
 if Syn.n > 0
  Syn.pm = Varout.Pm(tidx,:)';
  Syn.vf = Varout.Vf(tidx,:)';
 end
  fm_call('i');
  %%%%%%%%%%----------------------------------------------------------------
  %%%%%%%%%%----------------------------------------------------------------
  %Initialization of Trajectory sensitivity calculation.
```

```
  %name rule: trajectory sensitivity of xbar
  %(state varialbe as well as B variable) to xbar
  % is tsxbar2xbar, a
  tsxbar2xbara = speye(DAE.n);
  tsy2xbara = -(DAE.Jlfv\DAE.Gx)*tsxbar2xbara;
  tsmatrixa = [tsxbar2xbara;tsy2xbara];
  tsfa = [0.5*h*(DAE.Fx*tsxbar2xbara + DAE.Fy * tsy2xbara) +
           tsxbar2xbara; zeros(2*Bus.n,DAE.n)];
  Sensitivity(:,:,firstIdx)= tsmatrixa(DAE.n+Bus.n+1:end,DAE.n-Shunt.n+1:end);
  %%%%%%%%%%----------------------------------------------------------------
  %%%%%%%%%%----------------------------------------------------------------
for iteri = 1:(L-1)
   %fprintf('\n iteration = % 5d', iteri);
   varidx = iteri + tidx ;
   DAE.V = Varout.V(varidx,:)';
   DAE.a = Varout.ang(varidx,:)';
   DAE.x = Varout.x(varidx,:)';
   if Syn.n > 0
    Syn.pm = Varout.Pm(varidx,:)';
    Syn.vf = Varout.Vf(varidx,:)';
   end
   h = Varout.t(varidx)-Varout.t(varidx-1);
   Dn = DAE.n;
   identica = speye(max(Dn,1));
%-----------------------------------
%%%%%%%%----------------------------
%Trajectory sensitivity calculation
fm_call('i');
```

```
for i = 1:SW.n
  DAE.Fy(:,SW.bus(i)) = 0;
  DAE.Gx(SW.bus(i),:) = 0;
  DAE.Fy(:,Bus.n+SW.bus(i)) = 0;
  DAE.Gx(Bus.n+SW.bus(i),:) = 0;
end
for i = 1:PV.n
  DAE.Fy(:,Bus.n+PV.bus(i)) = 0;
  DAE.Gx(Bus.n+PV.bus(i),:) = 0;
end
% check for islanded buses
if ~isempty(Bus.island)
  kkk = Bus.island;
  DAE.Jlfv(kkk,:) = 0;
  DAE.Jlfv(:,kkk) = 0;
  DAE.Jlfv(:,kkk+Bus.n) = 0;
  DAE.Jlfv(kkk+Bus.n,:) = 0;
  if Settings.octave
    DAE.Jlfv(kkk,kkk) = eye(length(kkk));
    DAE.Jlfv(kkk+Bus.n,kkk+Bus.n) = eye(length(kkk));
  else
    DAE.Jlfv(kkk,kkk) = speye(length(kkk));
    DAE.Jlfv(kkk+Bus.n,kkk+Bus.n) = speye(length(kkk));
  end
  DAE.g(kkk) = 0;
  DAE.g(kkk+Bus.n) = 0;
  DAE.V(kkk) = 1e-6;
  DAE.a(kkk) = 0;
```

```
end
DAE.Ac = [identica - h*0.5*DAE.Fx, -h*0.5*DAE.Fy; DAE.Gx, DAE.Jlfv];
tsmatrix = DAE.Ac\tsfa;
%sensitivity{k-1} = num2cell(tsmatrix);
tsxbar2xbara = tsmatrix(1:DAE.n,:);
tsy2xbara = tsmatrix(DAE.n+1:DAE.n+2*Bus.n,1:DAE.n);
tsmatrixa = tsmatrix;
Sensitivity(:,:,iteri+firstIdx) = tsmatrix(DAE.n+Bus.n+1:end,DAE.n-Shunt.n+1:end);
tsfa = [0.5*h*(DAE.Fx*tsxbar2xbara + DAE.Fy * tsy2xbara) +
      tsxbar2xbara; zeros(2*Bus.n,DAE.n)];
end
  Sen = Sensitivity;
```

.3 Optimization

```
%Input parameter:
%    sensitivity: a cell stroed the sensitivity (dV/dB)
%    bmax: The upper limit of capacitor
%    f: cost function vector
%    Vmax: voltage upper limit
%    Vmin: voltage lower limit
%    LB: lower boundary for capacitor
%    UB: Upper boundary for capacitor
%
%Output parameter:
%DeltaB: The vector of the first step control
function [deltaB] = MPCOpt(bmax,Vmax,Vmin, LB,UB)
global Bus Shunt Snapshot SenArray m RemainC
```

```
%Set up the constraints for the limit of capacitor. That means
%  u+deltau <=Umax
%row and column is used to form the index of the state variable in the sparse matrix.
row = [];
%A1 is the matrix, row is the capacitor i, column is the number of state variable.
for i = 1:Shunt.n
    row = [row; i*ones(RemainC,1)];
end
column =[];
for i = 1:Shunt.n
    for j = 1:RemainC
     column = [column; i + (j-1)*Shunt.n];
    end
end
n = length(row);
A1 = sparse(row,column,ones(n,1), Shunt.n,RemainC*Shunt.n);
B1 = bmax - Shunt.b(Shunt.bus);
%Set up the constraints for voltage magnitude, that is
% Vmin=<V + s*deltaU<= Vmax. The voltage we care is the last point of the
% prediction horizon.
V = Snapshot(end).V;
A2 = SenArray(:,:,end);
B2 = Vmax - V;
A3 = - A2;
B3 = -(Vmin - V);
A = [A1;A2;A3];
B = [B1;B2;B3];
%Solve the optimization problem
```

```
DeltaB0 = 0.05*ones(Shunt.n,1);
DeltaB0 = repmat(DeltaB0,RemainC,1);
options = optimset('LargeScale','off');
x = fmincon(@objfun,DeltaB0,A,B,[],[],LB,UB,[],options);
%Get the first step action
deltaB = x(1:Shunt.n);
```

.4 Initialize Time domain simulation

```
function InitializeTd(m,cs,pt,pterm)
global Snapshot Line Bus DAE Syn Settings RemainC
  Line.Y = Snapshot(2).Y;
  Bus.Pg = Snapshot(2).Pg;
  Bus.Qg = Snapshot(2).Qg;
  Bus.Pl = Snapshot(2).Pl;
  Bus.Ql = Snapshot(2).Ql;
  DAE.V = Snapshot(2).V;
  DAE.a = Snapshot(2).ang;
  DAE.x = Snapshot(2).x;
  DAE.Jlf = Snapshot(2).Jlf;
  DAE.Jlfv = Snapshot(2).Jlfv;
  DAE.Fx = Snapshot(2).Fx;
  DAE.Fy = Snapshot(2).Fy;
  DAE.Gx = Snapshot(2).Gx;
  if Syn.n > 0
    Syn.pm = Snapshot(2).pmech;
    Syn.vf = Snapshot(2).vfd;
  end
  Settings.t0 = Snapshot(2).time;
```

```
  if (RemainC>1)
  Settings.tf = Settings.t0 + cs + pt;
  end
  if (RemainC==1)
  Settings.tf = pterm;
  end
  InitialTime = Settings.t0 + cs;
  for i = 1:m
  Snapshot(i+1).time = InitialTime + (i-1)*cs;
  end
  Snapshot(i+2).time = InitialTime + pt;
```

.5 Main program

```
global Sensitivity SenArray m RemainC
pt = 40;  %prediction horizon.
cs = 7;   %sampling time 4s. Every 4s put on new control;
m = 5;  % control horizon is 3*4 = 12 s.
pterm = 100; %simulation time
VarMpcOut = struct('t',[], ...
                'x',[], ...
                'V',[], ...
                'ang',[] );
run('AddPathToPsat');
initpsat;
runpsat('WECC_Data.m','U:\Aug 08\psat\MPCSimulation\VoltageControl','data');
runpsat('pf');
bmax = 1*ones(Shunt.n,1);
Vmax = 1.05*ones(Bus.n,1);
```

```
Vmin = 0.95*ones(Bus.n,1);
Settings.fixt = 1;
Settings.tstep = 0.01;
InitialTime = 1.2;
Settings.tf = pt + InitialTime;
clpsat.refresh = 0;
for i = 1:m
    Snapshot(i+1).time = InitialTime + (i-1)*cs;
end
Snapshot(i+2).time = InitialTime + pt;
runpsat('td');
criticalt = min(abs(Varout.t - InitialTime));
nfaultclear = find(abs(Varout.t - InitialTime)==criticalt);
VarMpcOut.t = Varout.t(1:nfaultclear,:);
VarMpcOut.x = Varout.x(1:nfaultclear,:);
VarMpcOut.V = Varout.V(1:nfaultclear,:);
VarMpcOut.ang = Varout.ang(1:nfaultclear,:);
Umatrix = [];
for controli = 1:m
    fprintf('\n control sampling point %5d', controli);
    SenArray=[];   %Sensitivity matrix for each sampling point.
    criticalt = min(abs(Varout.t - Snapshot(2).time));
    nCurrentIdx = find(abs(Varout.t - Snapshot(2).time)==criticalt);
    nTotalIdx = length(Varout.t);
    Row = Bus.n;
    Column = Shunt.n;
    Page = nTotalIdx-nCurrentIdx + 1;
    Sensitivity = zeros(Row,Column,Page);
```

```
    RemainC = m - controli + 1;
   for i = 1:RemainC
        SenCsi = SenAtCs(i);
        Sensitivity = zeros(Row,Column,Page);
        SenArray =[SenArray, SenCsi];
   end
       LB = zeros(Shunt.n,1);
       LB = repmat(LB,RemainC,1);
       UB = [0.1;0.1;0.1];
       UB = repmat(UB,RemainC,1);
    deltaB = MPCOpt(bmax,Vmax,Vmin,LB,UB);
    Umatrix = [Umatrix, deltaB];
    Shunt.con(:,6) = Shunt.con(:,6) + deltaB;
    InitializeTd(RemainC,cs,pt,pterm);
    runpsat('td');
    criticalt = min(abs(Varout.t - Snapshot(2).time));
    nCurrentIdx = find(abs(Varout.t - Snapshot(2).time)==criticalt);
    VarMpcOut.t = [VarMpcOut.t; Varout.t(1:nCurrentIdx,:)];
    VarMpcOut.x = [VarMpcOut.x; Varout.x(1:nCurrentIdx,:)];
    VarMpcOut.V = [VarMpcOut.V; Varout.V(1:nCurrentIdx,:)];
    VarMpcOut.ang = [VarMpcOut.ang; Varout.ang(1:nfaultclear,:)];
end
    VarMpcOut.t = [VarMpcOut.t; Varout.t(nCurrentIdx+1 : end,:)];
    VarMpcOut.x = [VarMpcOut.x; Varout.x(nCurrentIdx+1 : end,:)];
    VarMpcOut.V = [VarMpcOut.V; Varout.V(nCurrentIdx+1 : end,:)];
    VarMpcOut.ang = [VarMpcOut.ang; Varout.ang(nCurrentIdx+1 : end,:)];
```

BIBLIOGRAPHY

[1] Agreira, C. I. F., Ferreira, C. M. M., Pinto, J. A. D., and Barbosa, F. P. M. (2003). Contingency screening and ranking algorithm using two different sets of security performance indices. In *Proceedings of 2003 IEEE Bologna PowerTech Conference*, volume 4, pages 1–5.

[2] Agreira, C. I. F., Ferreira, C. M. M., Pinto, J. A. D., and Barbosa, F. P. M. (2006). The performance indices to contingencies screening. In *International Conference on Probabilistic Methods Applied to Power Systems 2006*, pages 1–8.

[3] Ajjarapu, V. and Christy, C. (1992). The continuation power flow: a tool for steady state voltage stability analysis. *IEEE Transactions on Power Systems*, 7(1):416–423.

[4] Anthony, N. M., Fouad, A. A., and Vittal, V. (1983). Power system transient stability using individual machine energy functions. *IEEE Transactions on Circuits and Systems*, 30:266–276.

[5] Atic, N., Rerkpreedapong, D., Hasanovic, A., and Feliachi, A. (2003). NERC compliant decentralized load frequency control design using model predictive control. In *2003 IEEE Power Engineering Society General Meeting*, pages 554–559, Toronto,Canada.

[6] Bergen, A. and Vittal, V. (1999). *Power system analysis*. Prentice Hall, Inc.

[7] Bernard, S., Trudel, G., and Scott, G. (1996). A 735 kv shunt reactors automatic switching system for hydro-quebec network. *IEEE Transactions on Power Systems*, 11(4):2024 C 2030.

[8] Canizares, C. A. and Alvarado, F. L. (1993). Point of collapse and continuation methods for large AC/DC systems. *IEEE Transactions on Power Systems*, 8(1):1–8.

[9] Chang, J. and Chow, J. H. (1997). Time-optimal series capacitor control for damping inter-area modes in interconnected power systems. *IEEE Transactions on Power Systems*, 12(1):215 – 221.

[10] Chang, S. K., Marks, G. E., and Kato, K. (1990). Optimal real time voltage control. *IEEE Transactions on Power Systems*, 5(3):750–758.

[11] Chen, S. and Glavitsch, H. (1993). Stabilizing switching. *IEEE Transactions on Power Systems*, 8(4):1511 – 1517.

[12] Chen, Y. L. (1996). Weak bus-oriented optimal multi-objective VAr planning. *IEEE Transactions on Power Systems*, 11(4):1885–1890.

[13] Cheng, D. and Ma, J. (2003). Calculation of stability region. In *Proceedings of the 42-nd IEEE conference on decision and control*, volume 6, pages 5615–5620, maui, Hawaii,USA.

[14] Chiang, H. and Chu, C. (1995). Theoretical foundation of the bcu method for direct stability analysis of network-reduction power system models with samll transfer conductances. *IEEE Transactions on Power Systems*, 42:252–262.

[15] Chiang, H., Wu, F., and Varaiya, P. (1994). A BCU method for direct analysis of power system transient stability. *IEEE Transactions Power Systems*, 9:1194–1208.

[16] Chiang, H. D., Flueck, A. J., Shah, K. S., and Balu, N. (1995). CPFLOW: a practical tool for tracing power system steady-state stationary behavior due to load and generation variations. *IEEE Transactions on Power Systems*, 10(2):623–634.

[17] Chiang, H. D., Hirch, M. W., and Wu, F. F. (1988). Stability regions of nonlinear autonomous dynamic systems. *IEEE Transactions on Automatic Control*, 33:16–27.

[18] Chiang, H. D. and Thorp, J. S. (1989). The closest unstable equilibrium point method for power system dynamic security assessment. *IEEE Transactions on Circuits and Systems*, 36:1187–1199.

[19] Chiang, H. D. and Wu, F. F. (1988). Foundations of the potential energy boundary surface method for power system transient stability analysis. *IEEE Transactions on Circuits and Systems*, 35:712–728.

[20] Chow, Q. B., Kundur, P., Acchione, P. N., and Lautsch, B. (1989). Improving nuclear generating station response for electrical grid islanding. *IEEE Transactions on Energy Conversion*, EC-4:406–413.

[21] CIGRE Task Force 38.01.07 on Power System Oscillations (1996). Analysis and control of power system oscillations. CIGRE Technical Brochure.

[22] CIGRE Task Force 38.02.14 Rep. (1999). Analysis and modeling needs of power system under major frequency disturbances.

[23] Corsi, S., Pozzi, M., Sabelli, C., and Serrani, A. (2004a). The coordinated automatic voltage control of the Italian transmission grid-part I: reasons of the choice and overview of the consolidated hierarchical system. *IEEE Transactions on Power Systems*, 19(4):1723–1732.

[24] Corsi, S., Pozzi, M., Sabelli, C., and Serrani, A. (2004b). The coordinated automatic voltage control of the Italian transmission grid-part II: control apparatuses and field performance of the consolidated hierarchical system. *IEEE Transactions on Power Systems*, 19(4):1733–1741.

[25] Crandall, M. G. and Lions, P. L. (1984). Two approximations of solutions of Hamilton-Jacobi equations. *Mathematics of Computation*, 43(167):1–19.

[26] Crow, M. (2003). Infrastructure roots. evolution of electric power in the United States. *Power and Energy Magazine, IEEE*, 1(2):20–21.

[27] Cutsem, T. V. (2000). Voltage instability: phenomenon, countermeasures and analysis methods. *Proceedings of the IEEE*, 88:208–227.

[28] Debs, A. S. (1988). *Modern Power Systems Control and Operation*. Kluwer Academic, Maryland.

[29] Doudna, J. H. (1988). Application and implementation of fast valving and generator tripping schemes at Gerald Gentleman station. *IEEE Transactions on Power Systems*, 3(3):1155–1166.

[30] El-Kady, M. A., Bell, B. D., Carvalho, V. F., Burchett, R., Happ, H. H., and Vierath, D. R. (1986). Assessment of real - time optimal voltage control. *IEEE Transactions on Power Systems*, PWRS-1(2):98–105.

[31] Evans, L. C. (1998). *Partial differential equations*. American Mathematical Society.

[32] Fouad, A. A., Aboytes, F., Carvalho, V., Corey, S., Dhir, K., and Vieera, R. (1988). Dynamic security assessment practices in North America. *IEEE Transactions on Power Systems*, 3(3):1310–1321.

[33] Fourlas, G. K., Kyriakopoulos, K. J., and Vournas, C. D. (2004). Hybrid systems modeling for power system. *IEEE Circuits and Systems Magazine*, 4(3):16–23.

[34] Fu, C. and Bose, A. (1999). Contingency ranking based on severity indices in dynamic security analysis. *IEEE Transactions on Power Systems*, 14(3):980–986.

[35] Gao, B., Morison, G. K., and Kundur, P. (1996). Toward the development of a systematic approach for voltage stability assessment of large-scale power systems. *IEEE Transactions on Power systems*, 11:1314–1324.

[36] Godart, T. F. and Puttgen, H. B. (1991). A reactive path concept applied within a voltage control expert system. *IEEE Transactions on Power Systems*, 6(2):787–793.

[37] Granville, S. and Lima, M. C. A. (1994). Application of decomposition techniques to VAr planning: methodological and computational aspects. *IEEE Transcations on Power Systems*, 9(4):1780–1787.

[38] Grijalva, S. and Hiskens, I. (2000). Hybrid system modeling of frequency control and load shedding. In *32nd North American Power Symposium*, Waterloo, Canada.

[39] Haque, M. H. (2004). Improvement of first swing stability limit by utilizing full benefit of shunt FACTS devices. *IEEE Transactions on Power Systems*, 19(4):1894 – 1902.

[40] Hecke, J. V., Janssens, N., Deuse, J., and Promel, F. (2000). Coordinated voltage control experience in Belgium. Technical report, CIGRE Task Force 38-111.

[41] Hein, J. T. (2003). An essential industry at the crossroad: deregulation,restructuring nad a new model for the united states' bulk power system. Master's thesis, University of Colorado at Denver.

[42] Hill, D. (1993). Nonlinear dynamic load models with recovery for voltage stability studies. *IEEE Transactions on Power Systems*, 8(1):166–176.

[43] Hill, D. J., Lof, P. A., and Anderson, G. (1990). Analysis of long-term voltage stability. In *Proceedings of the 10th Power System Computation Conference*, pages 1252–1259.

[44] Hiskens, I. A. (2004). Power system modeling for inverse problems. *IEEE Transactions on Circuits and Systems*, 51(3):539–551.

[45] Hiskens, I. A. and Gong, B. (2005). MPC-based load shedding for voltage stability enhancement. In *44th IEEE Conference on Decision and Control*, pages 4463–4468, Seville,Spain.

[46] Hiskens, I. A. and Pai, M. A. (2000). Trajectory sensitivity analysis of hybrid systems. *IEEE Transactions on Circuits and Systems*, 47(2):204–220.

[47] IEEE Committee Report (1968). Computer representation of excitation systems. *IEEE Transactions on Power Apparatus and Systems*, PAS-87(6):1460–1464.

[48] IEEE Committee Report (1978). Description of discrete supplemental control for stability. *IEEE Transactions on Power Apparatus and Systems*, 97(1):149–165.

[49] IEEE Committee Report (1981). Excitation system models for power system stability studies. *IEEE Transactions on Power Apparatus and Systems*, PAS-100(5):494–509.

[50] IEEE PES Working Group on System Oscillations (1995). Power system oscillations. IEEE Special Publication 95-TP-101.

[51] Jing, Z., Jia, Z., and Gao, Y. (2003). Research on the stability region in a power system. *IEEE Transactions on Circuits and Systems*, 50:298–304.

[52] Karlsson, D. and Hill, D. (1994). Modeling and identification of nonlinear dynamic loads in power systems. *IEEE Transactions on Power Systems*, 9(1):157–166.

[53] Karlsson, D. and Waymel, X. (2001). System protection schemes in power networks. Technical report, CIGRE Task Force 38.02.19.

[54] Khalil, H. K. (2002). *Nonlinear System (Third Edition)*. Prentice Hall, New Jeasey.

[55] Kim, G. and Lee, K. (2005). Coordination control of ULTC transformer and STATCOM based on an artificial neural network. *IEEE Transactions on Power Systems*, 2(2):580–586.

[56] Kimbark, E. W. (1966). Improvement of system stability by switched series capacitors. *IEEE Transactions on Power Apparatus and Systems*, 85(2):180–188.

[57] Kimbark, E. W. (1969). Improvement of power system stability by changes in the network. *IEEE Transactions on Power Apparatus and Systems*, 88(5):773–781.

[58] Kosterev, D. N. and Kolodziej, W. J. (1995). Bang-bang series capacitor transient stability control. *IEEE Transactions on Power Systems*, 10(2):915 – 924.

[59] Kundur, P. (1981). A survey of utility experiences with power plant response during partial load rejections and system disturbances. *IEEE Transactions on Power Apparatus and Systems*, PAS-100:2471–2475.

[60] Kundur, P. (1994). *Power System Stability and Control*. McGraw Hill, New York.

[61] Kundur, P., Paserba, J., Ajjarapu, V., Andersson, G., Bose, A., and etc. (2004). Definition and classification of power system stability. *IEEE Transactions on Power Systems*, 15:1387–1401.

[62] Kurihara, I., Takahashi, K., and Kermanshahi, B. (1995). A new method of evaluating system margin under various system constraints. *IEEE Transactions on Power Systems*, 10(4):1904–1910.

[63] Larsson, M., Hill, D. J., and Olsson, G. (2002). Emergency voltage control using search and predictive control. *International Journal of Power and Energy Systems*, 24(2):121–130.

[64] Larsson, M. and Karlsson, D. (2003). Coordinated system protection scheme against voltage collapse using heuristic search and predictive control. *IEEE Transactions on Power Systems*, 18(3):1001–1006.

[65] Liacco, T. E. D. (1967). The adaptive reliability control system. *IEEE Transactions on Power Apparatus and Systems*, PAS-86(5):517–531.

[66] Liu, C. and Thorp, J. (2000). New methods for computing power system dynamic response for real-time transient stability prediction. *IEEE Transactions on Circuits and Systems I: Fundamental Theory and Applications*, 47:324–337.

[67] Liu, C. and Vu, K. (1989). Analysis of tap-changer dynamics and construction of voltage stability region. *IEEE Transactions on Circuits and Systems*, 36:271–289.

[68] Liu, C. C. and Tomsovic, K. (1986). An expert system assisting decision-making. *IEEE Transactions on Power Systems*, PWRS-1(3):195–201.

[69] Liu, H., Jin, L., McCalley, J. D., Kumar, R., and Ajjarapu, V. (2005). Linear complexity search algorithm to locate shunt and series compensation for enhancing voltage stability. In *Proceedings of the 37th Annual North American Power Symposium*, pages 344–350.

[70] Liu, H., Jin, L., McCalley, J. D., Kumar, R., and Ajjarapu, V. (2006). Planning minimum reactive compensation to mitigate voltage instability. In *Proceedings of 2006 IEEE Power Engineering Society General Meeting*, pages 4452–4456, Montreal, Canada.

[71] Liu, X. D., Osher, S., and Chan, T. (1996). Weighted essentially non-oscillatory schemes. *Journal of Computational Physics*, 126:202–212.

[72] Machias, A. V., Souflies, J. L., and Dialynas, E. N. (1989). A fuzzy transient stability index in power system security evaluation. *IEEE Transactions on Automatic Control*, 34(6):662–666.

[73] Marques, A. B., Taranto, G. N., and Falcao, D. M. (2005). A knowledge-based system for supervision and control of regional voltage profile and security. *IEEE Transactions on Power Systems*, 20(1):400–407.

[74] Matsuda, S., Ogi, H., Nishimura, K., Okataku, Y., and Tamura, S. (1990). Power system voltage control by distributed expert systems. *IEEE Transactions on Power Systems*, 37(3):236–240.

[75] Milano, F. (2005). An open source power system analysis toolbox. *IEEE Transactions on Power Systems*, 20(3):1199–1206.

[Mitchell] Mitchell, I. M. *A toolbox of level set methods version 1.0 [online].* Available: http://www.cs.ubc.ca/ mitchell/ToolboxLS/index.html.

[76] Mitchell, I. M. (2002). *Application of level set methods to control and reachability problems in continuous and hybrid systems.* PhD dissertation, Stanford University, Stanford.

[77] Morison, G. K., Gao, B., and Kundur, P. (1993). Voltage stability analysis using static and dynamic approaches. *IEEE Transactions on Power Systems*, 8:1159–1171.

[78] Osher, S. and Fedkiw, R. (2003). *Level set methods and dynamic implicit surfaces.* Springer-Verlag New York, Inc.

[79] Osher, S. and Sethian, J. A. (1988). Fronts propagating with curvature dependent speed: algorithms based on Hamilton-Jacobi formulations. *Journal of Computational Physics*, 79:12–49.

[80] Pai, M. A. (1998). *Power system dynamics and stability*. Prentice Hall, Inc.

[81] Park, J. Y., Nam, S. R., and Park, J. K. (2007). Control of a ULTC considering the dispatch schedule of capacitors in a distribution system. *IEEE Transactions on Power Systems*, 22(2):755–761.

[82] Paserba, J., Leonard, D., Miller, N., Naumann, S., Lauby, M., and Sener, F. (1994). Coordination of a distribution level continuously controlled compensation device with existing substation equipment for long term var management. *IEEE Transactions on Power Delivery*, 20(2):1034–1040.

[83] Pavella, M. R. and Evans, F. J. (1985). Direct methods for studying dynamics of large scale power system - a survey. *Automatica*, 32:1–21.

[84] Qi, R., Cook, D., Kliemann, W., and Vittal, V. (2000). Visualization of stable manifolds and multidimensional surfaces in the analysis of power system dynamics. *Journal of Nonlinear Science*, 10:175–195.

[85] Qin, S. and Song, Y. (2001). The theory of hybrid control systems and its application perspective in electric power systems. In *2001 International Conferences on Info-tech and Info-net*, pages 85–94, Beijing, China.

[86] Rahimi, F. A., Lauby, M. G., Wrubel, J. N., and Lee, K. L. (1993). Evaluation of the transient energy function method for on-line dynamic security analysis. *IEEE Transactions on Power Systems*, 8(2):497–507.

[87] Rawlings, J. (2000). Tutorial overview of model predictive control. *IEEE Control Systems Magazine*, 20(3):38–52.

[88] Saha, S., Fouad, A. A., Kliemamm, W. H., and Vittal, V. (1997). Stability boundary approximation of a power system using the real normal form of vector fields. *IEEE Transactions on Power Systems*, 12:797–802.

[89] Sancha, J. L., Fernandez, J. L., Cortes, A., and Abarca, J. T. (1996). Secondary voltage control: analysis, solutions and simulation results for the Spanish transmission system. *IEEE Transactions on Power Systems*, 11(2):630–638.

[90] Shu, C. W. and Osher, S. (1988). Efficient implementation of essentially non-oscillatory shock-capturing schemes. *Journal of Computational Physics*, 77(2):439–471.

[91] Smed, T. (1993). Feasible eigenvalue sensitivity for large power systems. *IEEE Transactions on Power systems*, 8(2):555–563.

[92] Song, H. and Kezunovic, M. (2005). Static security analysis based on vulnerability index and network contribution factor method. In *Proceedings of 2005 IEEE/PES Transmission and Distribution Conference and Exhibition: Asia and Pacific*, pages 1–8.

[93] Taranto, G., Martins, N., Martins, A. C. B., Falcao, D. M., and Santos, M. G. D. (2000). Benefits of applying secondary voltage control scheme to the Brazilian system. In *Proceedings of Power Engineering Society Summer Meeting*, pages 937–942.

[94] Varaiya, P. V., Wu, F. F., and Chen, R. (1985). Direct methods for transient stability analysis of power systems: recent results. In *Proceedings of IEEE*, volume 73, pages 1703–1715.

[95] Venkatasubramanian, V. and Ji, W. (1997). Numerical approximation of (n-1)-dimensional stable manifolds in large systems such as power system. *Automatica*, 33:1877–1883.

[96] Vu, H., Pruvot, P., Launay, C., and Harmand, Y. (1996). An improved voltage control on large-scale power system. *IEEE Transactions on Power Systems*, 11(3):1295–1303.

[97] Vu, K. and Liu, C. (1992). Shrinking stability regions and voltage collapse in power systems. *IEEE Transactions on Circuits and Systems*, 39:271–289.

[98] Wagner, W. R., Keyhani, A., Hao, S., and Wong, T. C. (1990). A rule based approach to decentralized voltage control. *IEEE Transactions on Power Systems*, 5(2):643–651.

[99] Wen, J. Y. and Wu, Q. H. (2004). Optimal coordinated voltage control for power system voltage stability. *IEEE Transactions on Power Systems*, 19(2):1115–1122.

[100] Yorino, N., El-Araby, E. E., Sasaki, H., and Harada, S. (2003). A new formulation for FACTS allocation for security enhancement against voltage collapse. *IEEE Transactions on Power Systems*, 18(1):3–10.

[101] Zaborszky, J. G., Huang, J. G., Zheng, B., and Leung, T. C. (1988). On the phase portraits of a class of large nonlinear dynamic systems such as the power systems. *IEEE Transactions on Automatic Control*, 33:4–15.

[102] Zima, M. and Andersson, G. (2003). Stability assessment and emergency control method using trajectory sensitivies. In *Proceedings of 2003 IEEE Bologna Power Tech Conference*, page 7, Bologna.

[103] Zima, M. and Andersson, G. (2005). Model predictive control employing trajectory sensitivities for power systems applications. In *Proceedings of the 44-nd IEEE Conference on Decision and Control*, pages 4452–4456, Seville,Spain.

[104] Zima, M., Korba, P., and Andersson, G. (2003). Power systems voltage emergency control approach using trajectory sensitivities. In *Proceedings of 2003 IEEE Conference on Control Applications*, pages 189–194, Istanbul, Turkey.

ACKNOWLEDGEMENTS

First, I would like to thank my advisor, Dr. Ratnesh Kumar, for his support, understanding and encouragement during the whole work of this dissertation. His advice played an important role in the completion of this work. He not only taught me valuable insights on conducting academic research but also gave me good instructions on career and life.

I also want to express my gratitude to the rest of my program of study committee: Dr. Nicola Elia, Dr. Chen-Ching Liu, Dr. Venkataramana Ajjarapu, and Dr. Ron M. Nelson. I greatly appreciate their valuable comments and advice on this work. Thank you very much for your contributions as members of my committee and efforts to help me improve my work.

Next, I would like to thank the alumni and graduate students in the control group at Iowa State University, Dr. Wenbing Qiu, Jing Huang, Qin Wen, Songyan Xu and Saayan Mitra. I appreciate all their helps and friendships.

Last but not least, I would like to thank my husband, my parents and my two dear sisters. Their endless love and encouragement helped me through all these years.